# Acoustic Treatment Design Scaling Methods

Volume 2: *Advanced Treatment Impedance Models for High Frequency Ranges*

R. E. Kraft
General Electric Aircraft Engines, Cincinnati, Ohio

J. Yu and H. W. Kwan
Rohr, Inc., Chula Vista, California

Abstract

The primary purpose of the study presented in this volume of the Task Order 25 Final Report is to develop improved models for the acoustic impedance of treatment panels at high frequencies, for application to sub-scale treatment designs. Effects that cause significant deviation of the impedance from simple geometric scaling are examined in detail, an improved high frequency impedance model is developed, and the improved model is correlated with high frequency impedance measurements.

Only single-degree-of-freedom honeycomb sandwich resonator panels with either perforated sheet or "linear" wiremesh faceplates are considered here. The objective is to understand those effects that cause the simple single-degree-of-freedom resonator panels to deviate at the higher scaled frequency from the impedance that would be obtained at the corresponding full scale frequency. This will allow the sub-scale panel to be designed to achieve a specified impedance spectrum over at least a limited range of frequencies. As long as the impedance achieved in the scale model is known with a sufficient degree of accuracy, it can be reliably translated to the full scale design.

An advanced impedance prediction model has been developed that accounts for some of the known effects at high frequency that have previously been ignored as a small source of error for full scale frequency ranges. The model has been implemented in a computer program and used to compare with predicted data from the currently-used impedance model and with measured data for a number of treatment configurations of various scale. Based on this study, the outlook on ability to use scaled perforate facesheet single-degree-of-freedom resonator liners to represent full scale is encouraging. Care must be taken to make the proper adjustments in porosity and cavity depth of the scaled liner to best fit the full scale impedance.

Table of Contents

1. Introduction

1.1 Purpose and Problems of Treatment Scaling

The noise suppression provided by acoustic treatment liners in aircraft engine ducts is essential to being able to meet aircraft flyover noise regulations. Testing to validate the performance of acoustic treatment design concepts is an integral part of the design process. The cost of building and testing treatment designs on full scale engines, however, is prohibitive, and designers are seldom afforded the luxury of more than one attempt at designing and testing the final design that will be used in production.

The ability to design, build, and test miniaturized acoustic treatment panels on scale model fan rigs representative of the full scale engine provides not only a cost-saving but an opportunity to optimize the treatment by allowing tests of different designs. To be able to use scale model treatment as a full scale design tool, it is necessary that the designer be able to reliably translate the scale model design and performance to an equivalent full scale design.

The key to this accomplishment is the acoustic treatment impedance parameter. The suppression obtained at a full scale frequency for a given treatment impedance value should be the same as that obtained with the same impedance value at the corresponding scaled frequency in the scale model. At that frequency, at least, the impedance design parameter transfers directly from sub-scale to full scale.

When testing acoustic treatment on sub-scale model vehicles, it would be desirable to achieve the same treatment suppression as a function of scaled frequency that would be obtained on the full scale engine. This requires that the source generation characteristics, the engine geometry, and the acoustic impedance scale directly with frequency over the full frequency range of interest. Although sub-scale fan rigs are believed to represent the source characteristics and duct geometry with adequate validity, the treatment impedance representation presents unique problems.

The acoustic impedance for conventionally designed acoustic treatment panels does not scale directly with geometric length and frequency, due to second-order effects. One cannot simply "shrink" a full scale treatment design and expect the impedance at the scaled frequency to be the same as that at full scale. While the sub-scale treatment can be designed to achieve any impedance at a single frequency, it may not have the same impedance spectrum over the scaled frequency range as the equivalent full scale liner does over its corresponding range.

Thus, the particular impedance characteristics of the sub-scale liner under its particular operating conditions must be accommodated for treatment scaling to be a successful design tool. The key is being able to know what acoustic impedance has been obtained as a function of frequency in the scale model with sufficient assurance that the impedance values can be transferred to the full scale design, if not the physical treatment design parameters. To achieve this, improved impedance models and measurement methods are needed to be able to determine acoustic impedance accurately at high frequencies.

1.2 Objectives and Limitations of Study

The primary purpose of the study presented in this volume of the Task Order 25 Final Report is to develop improved models for the acoustic impedance of treatment panels at high frequencies. Effects that cause significant deviation of the impedance from simple geometric scaling are examined in detail, an improved high frequency impedance model is developed, and the improved model is correlated with high frequency impedance measurements.

Only the simplest acoustic treatment panel designs are considered here. These are single-degree-of-freedom honeycomb sandwich resonator panels with either perforated sheet or "linear" wiremesh faceplates. The perforated sheet resonators are defined in terms of the panel geometric parameters. The perforations are assumed to be straight, square-edged holes. The wiremesh liners are defined in terms of DC flow resistance coefficients and cavity depth. All treatment panels are assumed to be locally reacting.

Double layer liners (designated by 2DOF or DDOF) are a natural extension of single layer liners (SDOF). DDOF liners are not considered explicitly in this report, but the items pertaining to resistance and mass reactance of SDOF facesheets are directly applicable to DDOF counterparts, either facesheet or septum. The septum of a DDOF liner, of course, has no grazing flow effect contribution. A model for calculating the impedance of a DDOF liner, given the facesheet and septum properties, can be found in Reference 1 and is also discussed briefly in Volume 3 of this Final Report.

Bulk absorber liners might find use in scaled treatment designs, but cost limitations precluded their examination in this Contract. Bulk absorber liners are currently a topic of investigation in NASA Contract NAS1-20102, Task 4, which involves both impedance model development and impedance measurement.

This limitation to simple panel types is based on the assumption that it is more appropriate to use the treatment scaling tool by designing and building the simplest, cheapest, and most easily controlled treatment panels for testing in the scale model, as opposed to attempting to represent the frequency-dependent impedance variation of complex designs such as two-degree-of-freedom honeycomb sandwich panels or bulk absorbers. The potential application of treatment scaling to more advanced treatment designs is considered in a separate volume.

The objective, then, is to understand those effects that cause the simple single-degree-of-freedom resonator panels to deviate at the higher scaled frequency from the impedance that would be obtained at the corresponding full scale frequency. This will allow the sub-scale panel to be designed to achieve a specified impedance spectrum over at least a limited range of frequencies. As long as the impedance achieved in the scale model is known with a sufficient degree of accuracy, it can be reliably translated to the full scale design.

---

[1]   Motsinger, R. E. and Kraft, R. E., "Design and Performance of Duct Acoustic Treatment", in Hubbard, H. H. ed., *Aeroacoustics of Flight Vehicles: Theory and Practice*, Vol. 2: Noise Control, NASA Ref. Pub. 1248, Vol. 2, August 1991, p.177.

In this study, we exclusively consider frequency-domain impedance models. The development and application of time-domain impedance models is the subject of a separate volume of the Final Report. A comparison of the advantages and limitations of frequency-domain models and time-domain models will be discussed briefly below.

An original intent of the study was to include the effects of grazing flow on the impedance of treatment panels at high frequency. Difficulties encountered in the laboratory experiments to measure the impedance with grazing flow at high frequencies have significantly proscribed the progress made toward this objective, since we are not able to evaluate the accuracy of current models in the high frequency regime with flow. Thus, this study is limited to the case of normal incidence impedance without grazing flow, and the problems of measuring impedance in the presence of grazing flow and recommendations for overcoming these problems in the future are presented in a separate volume.

1.3 Treatment Scaling Philosophy

1.3.1 Geometric Scaling

Scaling is based on the assumption of similarity of physical phenomena under changes in length scale. Scaling of aircraft engines for noise studies assumes similarity in fluid flow and acoustic generation and propagation phenomena. We consider those scaling parameters that are particularly relevant to acoustic propagation phenomena, assuming that the noise generation mechanisms and the flow field maintain perfect similarity with scaling.

A useful approximation for aircraft engine acoustic scaling is that the engine fan rpm at any particular operating condition varies inversely with fan diameter, maintaining a constant fan tip speed. This rule applies even for fan designs with different numbers of fan blades, as the blade loading generally increases as the blade number decreases while the fan rpm remains constant.

The fan blade tip speed is proportional to the fan rpm times the fan diameter,

$$V_T = \frac{2\pi\Omega}{60}\frac{D}{2} \tag{1-1}$$

where V_T is the tip speed, Ω is the fan rpm, and D is the fan diameter. The blade-passing-frequency, f_{bp} is given by

$$f_{bp} = \frac{N_B\Omega}{60} \tag{1-2}$$

where N_B is the number of fan blades. Using these two relations, the constant tip speed relation can be expressed as

3

$$f_{bp}D \approx cnst \tag{1-3}$$

The constant is proportional to the number of fan blades, but these must be the same in the scale model and full scale engine to maintain performance and acoustic generation similarity.

The fundamental non-dimensionalized frequency scaling parameter can be defined as

$$\eta \equiv \frac{fD}{c} \tag{1-4}$$

where c is the speed of sound and D must be interpreted as the fan diameter in the cylindrical inlet duct and be replaced by the duct height H in the annular exhaust duct. The acoustic scaling rule is that, at a minimum, the value of η must be the same in the scale model and full scale fan:

$$\eta_{fs} = \frac{D_{fs}f_{fs}}{c} = \eta_{sm} = \frac{D_{sm}f_{sm}}{c} \tag{1-5}$$

where the subscript fs indicates full scale and the subscript sm indicates scale model.

If the temperatures of the scale model and full scale are the same, the speed of sound will be the same in both cases, and this means that the scale model frequency is related to the full scale frequency by

$$f_{sm} = \frac{D_{fs}}{D_{sm}} f_{fs} \tag{1-6}$$

Thus the frequency scales inversely with model length scale.

Further justification for treatment scaling can be obtained in terms of the mode content of the source. Similarity in source generation requires that the same duct modes be generated at the corresponding scale model and full scale frequencies. The propagation of these modes can be non-dimensionalized by use of the parameter η.

The duct mode eigenvalues can be non-dimensionalized by the duct radius, such that the eigenvalue, denoted by γ, is the same for any size duct. The mode cut-off frequency, which is the frequency below which the mode attenuates exponentially and above which it propagates unattenuated in a hardwall duct, is given in terms of γ as

$$f_{c/o} = \frac{\gamma c}{\pi D} \tag{1-7}$$

The η-value at cut-off is then simply

4

$$\eta_{c/o} = \frac{\gamma}{\pi} = \text{cnst} \tag{1-8}$$

Thus, mode cut-off is independent of duct scale. We will consider the implications of duct modal propagation on treatment scaling in greater detail below.

1.3.2 Expected Scaling Ranges

The scale factor relating scale model to full scale can be expressed as the ratio of scale model fan diameter to full scale fan diameter:

$$SF = \frac{D_{sm}}{D_{fs}} \tag{1-9}$$

The frequency, of course, goes inversely as scale factor, such that a 1/5 scale model, for instance, would run at 5 times the full scale frequency.

To get an idea of what the range of scale factor that might be encountered in practice might be, assume the following:

Maximum full scale fan diameter	=	120 inches
Minimum full scale fan diameter	=	60 inches
Maximum scale model fan diameter	=	24 inches
Minimum scale model fan diameter	=	12 inches

Then the minimum scale factor encountered would be 1/10, and the maximum value would be 1/2.5.

Assuming that 10,000 Hz. is the highest full scale frequency of interest, then the upper limit of scaled frequencies would be from 25,000 Hz. to 100,000 Hz. These upper frequencies are beyond the range of hearing and are well above those normally dealt with in aircraft noise measurements, extending into the ultrasonic range. As an aside, it should be noted that frequencies in this range may lead to difficulties in the farfield measurement of the noise levels, since the atmospheric absorption correction for propagation to the farfield may not be known accurately.

Consider also that a 1/2.5 scale model applied to a large 120 inch turbofan gives a 48 inch diameter scale model, which is as large as some small full scale fans used in commuter aircraft. On the other hand, consider that a one inch deep treatment tuned to about 2000 Hz. on the 120 inch fan would have to be scaled to only 0.10 inches deep for a 1/10 scale model, a formidable fabrication task considering the required precision.

The objective is to determine a range of scale factor for a given full scale fan size for which treatment scaling is a practical undertaking. This will be bounded by the cost factor for the

5

largest diameter scale model fan obtainable and the precision/constructability factor for the thinnest depth acoustic treatment panel that can achieve the desired impedance components.

1.3.3 Impedance Scaling Parameters

The fundamental acoustic treatment design and scaling parameter is the acoustic impedance, Z, defined as the ratio of acoustic pressure to normal component of acoustic velocity at the treatment surface. The impedance is a frequency-domain parameter, defined to have a certain value at each frequency. As a frequency-domain parameter, the impedance must account for differences in phasing between the acoustic pressure and velocity, and is therefore represented as a complex number,

$$Z = R + iX \tag{1-10}$$

where $i = \sqrt{-1}$, R, the real part of the impedance, is the acoustic resistance, and X, the imaginary part of the acoustic impedance, is the acoustic reactance.

The units of acoustic impedance in the cgs system are $g/(cm^2 \, sec)$ or cgs Rayls. The acoustic impedance is usually non-dimensionalized by the characteristic acoustic impedance of air (free space), which is given at a pressure of 1 atmosphere and 20° C by $\rho_0 c = 41.5$ cgs Rayls, where ρ_0 is the ambient atmospheric density.

The fundamental law of acoustic treatment scaling is that the scaled treatment impedance at the scaled frequency must equal the full scale treatment impedance at the corresponding full scale frequency:

$$\frac{Z_{fs}(f_{fs})}{\rho_0 c} = \frac{Z_{sm}(f_{sm})}{\rho_0 c} \quad \text{where } f_{sm} = SF \cdot f_{fs} \tag{1-11}$$

This is a direct consequence of the modal theory of duct propagation, which shall be described in detail below.

The design parameters for a perforated plate single-degree-of-freedom treatment panel are the perforate porosity (open area ratio), the orifice hole diameter, the faceplate thickness, and the cavity depth. Environmental effects on impedance include the mean flow Mach number, the boundary layer thickness, and the incident sound intensity. How the impedance depends on each of these parameters and their consequences regarding treatment impedance scaling is the subject of this report.

6

1.3.4 Phenemona Preventing Simple Impedance Scaling

It will be shown in what follows that certain components of the acoustic resistance and reactance scale geometrically without a problem, but that other components include secondary effects that do not scale. Effects that are functions of the orifice Reynolds number, in particular, the orifice mass reactance, will be shown to cause scaling problems. It will also be demonstrated how these non-scaleable effects can be minimized and accommodated, resulting in a positive perspective regarding the feasibility of treatment scaling.

1.4 Prior Work in Treatment Impedance Modeling

An extensive literature exists on the study of the impedance of resonators with orifices, dating back to the middle of the last century, if one includes the work of Kirchoff, Helmholtz, and Raleigh. Important work on the impedance of orifices and perforates was done in this century by Sivian in the 1930's and by Ingard and associates in the 1950's. Effort on this problem accelerated rapidly toward the end of the 1960's, when it became apparent that perforated honeycomb sandwich liners were highly practical and effective noise suppressers when applied as linings to the walls of aircraft engine ducts.

It is not the purpose of this study to present an extensive literature review of this work, as this has been accomplished within the past 25 years by a number of authors, very notably by Melling[2] in 1973. A comprehensive bibliography of references used in this study will be provided at the end of Section 3.0.

This study builds on the prior effort of many researchers, but is oriented to attempt to discover those effects that might have special relevance to impedance of scaled treatment at high frequencies. In order to obtain models of treatment impedance that were appropriate for full scale engines at frequencies below 10,000 Hz, prior researchers often made simplifying assumptions that caused small errors in the range of interest, but may lead to significant discrepancies for scaled treatment conditions. The objective of this study is to identify and re-examine some of these assumptions.

1.5 Approach

The first step in this study was to examine existing acoustic impedance models and the assumptions upon which they were based. Simplifying assumptions that may have some relevance to high frequencies were identified. Investigations to attempt to quantify the effects that were potential contributors to impedance at high frequencies were made.

---

[2]   Melling, T. H., "The Acoustic Impedance of Perforates at Medium and High Sound Pressure Levels", J. of Sound and Vibration, 29(1), 1973, pp. 1-65.

An advanced impedance prediction model that includes high frequency effects was developed. The model was compared to results of the current impedance model and to measured data using normal incidence impedance tube measurements that were conducted as part of this contract. Predictions and measurements cover a frequency range up to 12,000 Hz., about twice the highest frequency of measurement available prior to the study.

Results of the predictions and measurements were analyzed for their implications on the feasibility of acoustic treatment scaling as a design tool. A preliminary assessment is made, and recommendations are made for both analytical and experimental improvements that are needed before a final decision on the feasibility on treatment scaling and the proper method for its implementation can be made.

1.6 Summary of Results

An advanced impedance prediction model has been developed that accounts for some of the known effects at high frequency that have previously been ignored as a small source of error for full scale frequency ranges. The model has been implemented in a computer program and used to compare with predicted data from the currently-used impedance model and with measured data for a number of treatment configurations of various scale.

For broadband pressure excitation at high SPL levels such as will be experienced in an aircraft engine duct, the nonlinear effect on resistance tends to give a flat resistance spectrum over the full range of excitation frequencies. This appears to be verified by measurement for both full scale and sub-scale perforated plate treatment panels up to about 13,000 Hz.

The biggest problem encountered was accounting for the effects of the end correction on resistance and mass reactance. No comprehensive model was found that fit all cases, as the end correction has been found to vary in a complex manner with orifice Reynolds number, orifice geometry, and porosity. An extensive set of parametric measurements and concurrent theoretical investigations is needed if it is desired to develop a more universally-applicable model

Good agreement between predicted and measured impedance was found in the linear facesheet case when the DC flow resistance values are used to determine resistance, at least up to 13,000 Hz. The mass reactance issue is not so clear, but the mass reactance of a wiremesh facesheet is small.

Based on this study, the outlook on ability to use scaled perforate facesheet single-degree-of-freedom resonator liners to represent full scale is encouraging. Care must be taken to make the proper adjustments in porosity and cavity depth of the scaled liner to best fit the full scale impedance.

A safer solution at this point is probably to use a linear wiremesh facesheet bonded directly to the honeycomb with no supporting perforate. Predicted and measured impedance for the linear single-degree-of-freedom panels agree quite well up to 13,000 Hz. The use of the

wiremesh with no perforate support requires a small honeycomb cell size and may present bonding problems.

The conclusions in this study are restricted by the upper limit to the measurement frequency of 13,000 Hz. Extending to higher frequencies will require advanced measurement techniques both with and without grazing flow that are not yet available. It is highly recommended that any further effort include development of advanced impedance measurement methods.

2. Current Full-Scale Impedance Models

2.1 Acoustic Suppression Due to Treatment

2.1.1 Analytical Suppression Prediction Models

To understand the importance of acoustic impedance as a design parameter in determining the performance of acoustic treatment as a noise suppression concept, it is useful to review briefly the modal solution to acoustic wave propagation in a duct. Readers interested in a more detailed formulation of wave propagation in aircraft engine ducts are directed to the early papers by Rice[3,4] or the more recent survey article by Eversman[5].

The partial differential equation for the acoustic pressure in a duct with uniform mean flow is given by

$$\left(\frac{\partial}{\partial t} + U\frac{\partial}{\partial z}\right)^2 p = c^2 \nabla^2 p \tag{2-1}$$

where

t	=	time
z	=	axial variable
p	=	acoustic pressure
c	=	speed of sound
U	=	mean flow velocity

The solution to this equation in cylindrical coordinates for the mth order spinning mode in an inlet duct is given by

$$p(r,\theta,z,t) = \sum_{j=1}^{\infty} A_{mj} J_m\left(\gamma_{mj}\frac{r}{R}\right)e^{im\theta}e^{i\left(\kappa_{mj}z - \omega t\right)} \tag{2-2}$$

where

j	=	radial mode index
A_{mj}	=	(m,j) mode coefficient
J_m	=	m^{th} order Bessel function of the first kind

[3] Rice, Edward J., "Attenuation of Sound in Soft Walled Circular Ducts", NASA TM X-52443, May, 1968.

[4] Rice, Edward J., "Spinning Mode Sound Propagation in Ducts with Acoustic Treatment and Sheared Flow", NASA TM X-71672, March 1975.

[5] Eversman, Walter, "Theoretical Models for Duct Acoustic Propagation and Radiation", Chapter 13 in Hubbard, H. H., ed., *Aeroacoustics of Flight Vehicles: Theory and Practice, Volume 2: Noise Control*, NASA Reference Publication 1258, Vol. 2, 1991, pp. 101-163. (Currently published by and available from the Acoustical Society of America.)

10

γ_{mj}	=	eigenvalue for (m,j) mode
R	=	duct radius
θ	=	circumferential variable
ω	=	circular frequency, $= 2\,\pi\,f$

and κ_{mj} is the axial propagation constant, given by

$$\kappa_{mj}R = \frac{-kRM \pm \sqrt{(kR)^2 - \left(1 - M^2\right)\gamma_{mj}^2}}{1 - M^2} \qquad (2\text{-}3)$$

The $e^{-i\omega t}$ time convention has arbitrarily been used for the propagation equation. It should be noted that it is customary in treatment design to use the $e^{+i\omega t}$ convention, which requires taking the complex conjugate of the impedance values when shifting conventions. (This difference between theoreticians and designers has been unresolved for 30 years.)

The boundary condition that the solution must satisfy is that the pressure divided by the normal component of acoustic velocity must equal the wall impedance, or,

$$Z = \frac{p}{v_w} \qquad (2\text{-}4)$$

For continuity of particle displacement at the wall, assuming an infinitely thin boundary layer, it can be shown that the normal component of acoustic velocity at the wall, v_w, is related to the radial derivative of acoustic pressure by[6]

$$v_w = -i\,\frac{k}{\rho c}\,\frac{\partial p/\partial r}{\left(k - M\kappa_{mj}\right)^2} \qquad (2\text{-}5)$$

The previous two equations can be combined to give the boundary condition that the acoustic pressure must satisfy at the duct wall,

$$\frac{Z}{\rho c} = \frac{ip\left(k - M\kappa_{mj}\right)^2}{k\,\partial p/\partial r} \qquad (2\text{-}6)$$

When the pressure modal expansion in Equation (2-2) is substituted into this expression, we obtain

---

[6]   Eversman, Walter, "Theoretical Models for Duct Acoustic Propagation and Radiation", Chapter 13 in Hubbard, H., ed., *Aeroacoustics of Flight Vehicles: Theory and Practice. Volume 2.* NASA Reference Publication 1258, August, 1991, p. 112 (currently published by ASA).

$$J_m(\gamma_{mj}) + i\frac{Z}{\rho c}\frac{\gamma_{mj}}{kR}\frac{J'_m(\gamma_{mj})}{\left(1 - M\frac{\kappa_{mj}R}{kR}\right)^2} = 0 \qquad (2\text{-}7)$$

where the prime denotes the derivative of the Bessel function with respect to r. This is a complex, nonlinear, transcendental equation for the roots γ_{mj}, which must be solved by nonlinear equation root extraction techniques.

The modal suppression rate, in terms of dB per normalized axial distance (axial length divided by duct radius) is given by

$$dB_{per\,R} = -8.686\,Im(\kappa_{mj}R) \qquad (2\text{-}8)$$

where Im( ) implies the imaginary part. From Equation (2-3) and Equation (1-4) we see that $\kappa_{mj}R$ can be written in terms of the frequency parameter η as

$$\kappa_{mj}R = \frac{-\pi\eta M \pm \sqrt{(\pi\eta)^2 - (1 - M^2)\gamma_{mj}^2}}{1 - M^2} \qquad (2\text{-}9)$$

Thus, $\kappa_{mj}R$ is a function of η, M, and γ_{mj}. Also, from Equation (1-4), we have

$$kR = \frac{2\pi f R}{c} = \frac{\pi f D}{c} = \pi\eta \qquad (2\text{-}10)$$

Then Equation (2-7) can be written

$$J_m(\gamma_{mj}) + i\frac{Z}{\rho c}\frac{\gamma_{mj}}{\pi\eta}\frac{J'_m(\gamma_{mj})}{\left(1 - M\frac{\kappa_{mj}R}{\pi\eta}\right)^2} = 0 \qquad (2\text{-}11)$$

and, since η is invariant with respect to scaling, we can conclude that the eigenvalue γ_{mj} is invariant with scale factor.

Since both η and γ_{mj} are invariant in scaling, this indicates that the axial modal suppression per unit radius is the same for both sub-scale model and full scale. Further, since the total suppression of any pressure source can be completely described as a linear superposition of modes, the overall suppression rate will be the same in sub-scale and full scale ducts. The argument holds equally well for annular ducts, where the only difference is that the radial modes

12

must be replaced by eigenfunctions given by a combination of Bessel functions of the first and second kinds.

The key point is that the suppression at a given η value depends only on the wall impedance boundary condition, and this is independent of the duct scale factor. This is true whether an idealized modal solution is used or whether the acoustic propagation is determined by a numerical solution method such as the finite element method, which could be used for a non-uniform duct. All methods require that the wall boundary condition be given in terms of acoustic impedance.

The actual duct suppression obtained will also depend upon the particular combination of modes that is generated by the fan noise source. For successful treatment scaling, the scale model must generate the same set of modes as the full scale fan. This will be the case if close attention is paid to obtaining flow and geometry similarity between the scale model rotor/stator and the corresponding full scale case.

2.1.2 Acoustic Impedance as a Design Parameter

At a given η-value in a uniformly-treated segment of duct, there is a particular value of acoustic impedance that maximizes the attenuation rate of a given mode[7,8]. Each mode will have a different optimum impedance value. Any linear weighted combination of modes will have an optimum impedance value that may not be the same as the optimum value for any of the component modes.

The job of the treatment designer is to estimate the impedance that will maximize the suppression over a desirable range of frequencies and then design a treatment panel concept that will achieve these impedance values as closely as possible over as wide a frequency range as possible.

This job requires accurate prediction models to relate the physical parameters of the treatment panel to the acoustic impedance. Accurate methods of measuring acoustic impedance, particularly under aircraft engine duct environmental conditions are necessary to validate the prediction models. Suppression performance of treatment designs measured in scale model or full scale engine tests then provide proof of the design concept.

Due to the cost of full scale engine testing, the designer may not have the ability to test the design until the actual engine noise certification test. Not only is this test costly, but the cost of a noise certification failure, in both financial and time terms, would be devastating to an engine program. This leads to conservatism in treatment design, which may not optimize engine weight.

---

[7]   Rice, Edward J., "Attenuation of Sound in Ducts with Acoustic Treatment - A Generalized Approximate Equation", NASA TM X-71830, November, 1975.

[8]   Rice, Edward J., "Acoustic Liner Optimum Impedance for Spinning Modes with Mode Cut-Off Ratio as the Design Criterion", NASA TM X-73411, 1976.

13

This is the justification for running preliminary scale model tests to determine treatment performance in a cost effective and timely fashion.

If it weren't for the acoustic impedance, which incorporates two design parameters (resistance and reactance), the treatment designer would be forced to determine optimum designs in terms of the physical parameters of the liner. Even for a simple single-degree-of-freedom liner, this would include porosity, hole diameter, faceplate thickness, and cavity depth—four parameters (although porosity and cavity depth are the most important).

To design a more complex two-degree-of-freedom panel to achieve suppression bandwidth, at least three additional parameters must be added (two DC flow resistance coefficients and a percent immersion for a wiremesh septum). Thus, adequate models to relate the physical parameters to impedance and reliable impedance measurement methods to validate the models are necessary tools for efficient liner design.

2.2 Basic Impedance Prediction Models

2.2.1 Single-Degree-of-Freedom Treatment Panel

Figure (2-1). shows a drawing of a perforated plate honeycomb sandwich single-degree-of-freedom treatment panel that is the focus of this study. Figure (2-2). defines the geometric parameters for the treatment panel design. The open area ratio (or porosity), σ, is defined as the area of one hole times the number of holes per unit area of surface (assuming that all holes have equal area or that an average hole area is known).

PERFORATED
FACESHEET

HONEYCOMB
CELLS

RIGID
BACKPLATE
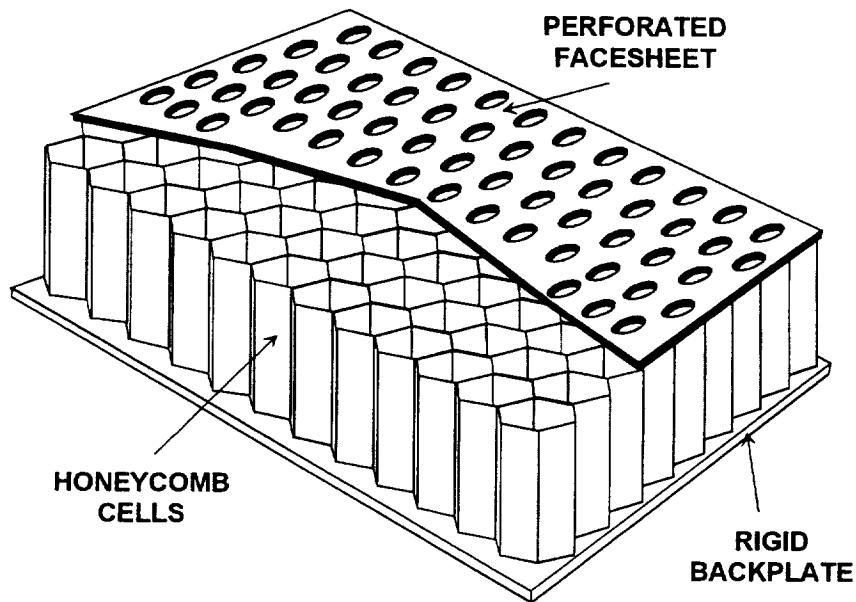
Figure (2-1)   Illustration of perforated plate honeycomb sandwich single-degree-of-freedom treatment panel.
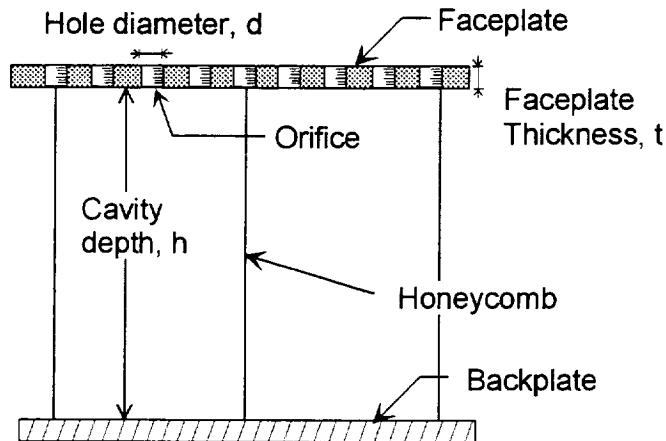
Figure (2-2)   Geometric definition of single-degree-of-freedom resonator panel.

The design and impedance models for a perforated plate single-degree-of-freedom liner are discussed in detail in an article by Motsinger and Kraft[9], which includes an extensive list of references. Since this article fairly completely describes the currently-used impedance model, it will be used as the basis for the discussion which follows. The results and a description of the models are presented here, for reference. For details of the model derivations, refer to Motsinger and Kraft.

The purpose of the discussion of the current impedance model is to provide a frame of reference for the extensions and amplifications of the model which follows. This model has been used with success for aircraft engine treatment design for many years, and is probably adequate for use at frequencies below 10,000 Hz.

2.2.2   Acoustic Resistance

2.2.2.1   Components of resistance

There are three components of resistance for a perforated facesheet:

9   Motsinger, R. E. and Kraft, R. E., "Design and Performance of Duct Acoustic Treatment", Chapter 14 in Hubbard, H. H., ed., *Aeroacoustics of Flight Vehicles: Theory and Practice, Volume 2: Noise Control*, NASA Reference Publication 1258, Vol. 2, 1991, pp. 165-206. (Currently published by and available from the Acoustical Society of America.)

1. Linear viscous resistance component
2. Nonlinear turbulent jet resistance component
3. Grazing flow contribution

Linearity refers to the dependence of the resistance component on the intensity level of the incident sound—linear components are independent of the incident sound level while nonlinear components increase as incident sound level increases. We can write

$$\frac{R}{\rho c} = A + BU + R_{gf} \tag{2-12}$$

where

$$A = \frac{32\mu t}{\rho c \sigma C_D d^2}, \tag{2-13}$$

is the linear viscous resistance component,

$$B = \frac{1}{2c(\sigma C_D)^2}, \tag{2-14}$$

is the nonlinear turbulent jet resistance component, and

$$R_{gf} = \frac{M}{\left(2. + 1.256\frac{\delta^*}{d}\right)\sigma} \tag{2-15}$$

is the linear grazing flow resistance component. For these formulas, we define

U	=	rms value of overall acoustic velocity incident on liner
μ	=	absolute coefficient of viscosity of air
t	=	faceplate thickness
d	=	orifice hole diameter
C_D	=	orifice discharge coefficient
σ	=	faceplate porosity
c	=	speed of sound
δ^*	=	boundary layer displacement thickness

For an explanation of why one coefficient of a linear relationship in velocity is called the "linear term" and the other coefficient is called the "nonlinear" term, see Motsinger and Kraft[9] , pp. 179-180. Essentially, it is because the pressure drop across a resistive sheet is proportional to the

16

square of the instantaneous velocity through the sheet. Dividing the pressure drop by the velocity to get resistance makes the nonlinear pressure drop a linear resistance relationship.

The rms value of overall acoustic velocity, U, depends on the incident SPL and the impedance of the liner at each frequency. It is defined as

$$U = \sqrt{\sum v_i^2}$$

(2-16)

where v_i^2 is the mean square velocity in the ith frequency band and the sum is over all participating frequency bands. The mean square velocity in the ith band is determined from the impedance relation,

$$\left(v_i\right)_{rms} = \frac{(p_{rms})_i}{Z_i}$$

(2-17)

where p_{rms} is the rms value of acoustic pressure in the ith frequency band, obtained from the given SPL at the ith frequency. The acoustic velocity is not known until liner impedance is determined, and vice-versa, requiring an iterative procedure for their determination. Generally, the iteration converges quite rapidly.

The grazing flow resistance contribution is an empirical formulation due to Heidelberg, Rice, and Homyak[10], and is based on the pioneering work of Rice[11,12]. Note that it is constant with frequency. The coefficients A and B are also independent of frequency. Since U is the rms value of acoustic velocity integrated over all frequencies, U is also independent of frequency, making the nonlinear term and therefore this entire model for the resistance totally frequency-independent. Later, looking at more advanced models, we shall see that this is a first approximation, and that there are higher-order resistance terms that are frequency-dependent.

Under typical aircraft engine operating conditions, with a flow Mach number around Mach 0.4, an overall SPL of about 140-150 dB, and a porosity of around 10%, the linear grazing flow resistance, R_{gf}, is usually the dominant contributor. The second highest contribution to resistance comes from the nonlinear term, BU. The linear viscous resistance A is normally negligible.

[10]   Heidelberg, Laurence J., Rice, Edward J., and Homyak, Leonard, "Experimental Evaluation of a Spinning-Mode Acoustic Treatment Design Concept for Aircraft Inlets", NASA Technical Paper 1613, 1980.

[11]   Rice, Edward J., "A Model for the Acoustic Impedance of a Perforated Plate Liner with Multiple Frequency Excitation", NASA TM X-67950, October, 1971.

[12]   Rice, Edward J., "A Model for the Pressure Excitation Spectrum and Acoustic Impedance of Sound Absorbers in the Presence of Grazing Flow", AIAA Paper 73-995, October, 1973.

2.2.2.2 DC flow resistance of perforated plate

It was noted in Motsinger and Kraft[9] that the coefficient A in Equation (2-12) is due to the the pipe flow friction for flow in a hole and that the coefficient B is due to dynamic head loss due to turbulence associated with entrance and exit losses. It has been noted that both of these coefficients are independent of frequency. In fact, they can be identified as the DC flow resistance coefficients for a resistive sheet, where DC implies Direct Current (adapted from the electrical nomenclature for current with no fluctuating component).

A DC flow resistance measurement is an attempt to determine the A and B coefficients experimentally[13]. The pressure drop Δp across a resistive sheet sample and the incident constant velocity U_{DC} associated with this pressure drop are measured for several different values of pressure drop and corresponding velocities (corrected as required). The measured DC flow resistance is then given by

$$R_{DC} = \frac{\Delta p}{U_{DC}} \qquad (2\text{-}18)$$

The measured R_{DC} points are plotted as a function of U_{DC} (usually in cgs Rayls versus cm/sec), and the A and B coefficients are determined by a linear least squares curve fit.

Figure (2-3) is an example of a DC flow measurement for an 8.5% porosity perforated facesheet with hole diameter of 0.062 inches and thickness of 0.024 inches. Note that the assumption of linearity of DC flow resistance in velocity is quite good. As can be noted from the statistical data from the curve fit, the DC flow A-value is 0.01279 cgs Rayls and the B-value is 0.1654 cgs Rayls per cm/sec.

---

[13] Motsinger, R. E., Syed, A. A., Manley, M. B., "The Measurement of the Steady Flow Resistance of Porous Materials", AIAA-83-0779, April, 1983.
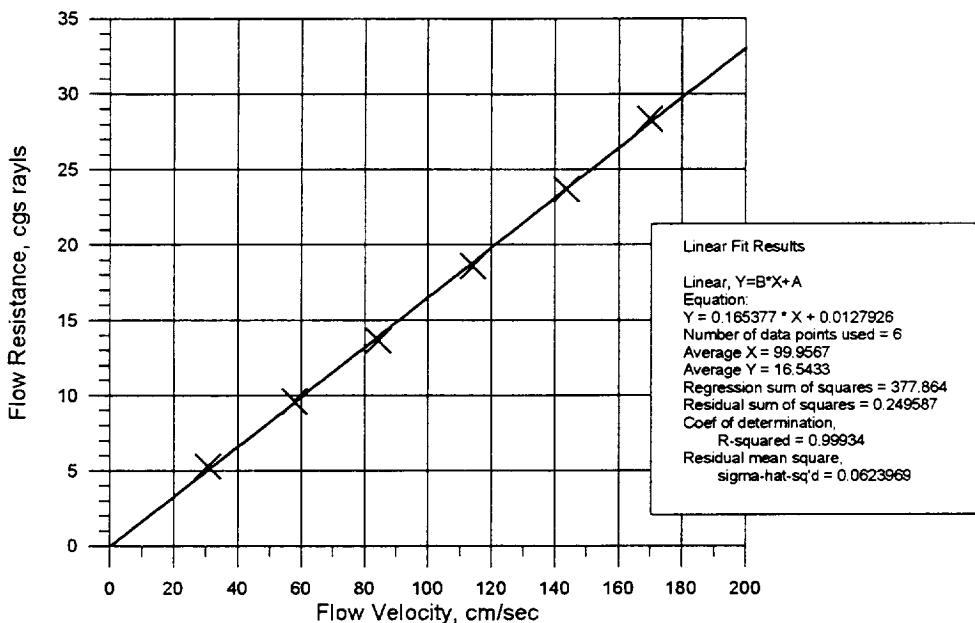
Figure (2-3)   Example of DC flow resistance measurement with linear curve fit for 8.5% porosity facesheet.

In practice, the DC flow resistance values are often expressed in a different form. The DC flow resistance is given as its value at a specified flow velocity, say 105 cm/sec:

$$R_{105} = A + 105 \cdot B \tag{2-19}$$

and the Nonlinear Factor is given as the ratio of the DC flow resistance at a high flow rate to that at a low flow rate, say 200 cm/sec and 20 cm/sec:

$$NLF_{200/20} = \frac{A + 200 \cdot B}{A + 20 \cdot B} \tag{2-20}$$

Unfortunately, there is no standardization as to the particular flow values at which to define R or NLF, so that one must always be careful to specify the flow rates and, conversely, to check the flow rates at which the values were measured if receiving the data. The A and B values, which are not subject to the same inconsistency as long as the units are specified, can always be obtained by inverting the R and NLF formulas.

The DC flow resistance coefficients are extremely useful for characterizing the resistance of a faceplate, particularly under the assumption that the resistance is not a function of frequency. For resistive facesheets such as wiremesh, this is the only way of characterizing the sheet resistive properties, because analytical models for these types of liners are generally not available. In what

19

follows, we shall examine correlations between the analytical models for A and B and the measured DC flow values.

The major limitation of the DC flow resistance measurement is that it provides no information about possible higher frequency effects on facesheet resistance, since the measurements are made at zero frequency. This does not seem to have been a serious deficiency in normal practice for either perforated plates or wiremesh type facesheets, but may be a problem at sub-scale treatment frequencies.

2.2.2.3 Issues with resistance

The assumed dependence of the nonlinear resistance component on the overall rms acoustic velocity means that the resistance becomes independent of the spectral shape of the applied sound pressure. This appears to be a good approximation when the applied spectrum has a flat broadband shape over the frequency range of interest, but little work has been done to determine whether the shape of the pressure spectrum has any effect on the frequency dependence of the impedance in cases where it might have a skewed or peaked shape. One might also question whether the assumption is good at very high frequency ranges where the second-order frequency-dependent effects increase in magnitude.

The empirical models for grazing flow effects are based primarily on in-situ impedance measurements made using the two-microphone method of Dean[14]. This method is very difficult to implement in practice, and is subject to precision requirements that compounds the difficulty of its application to the high frequency case. Better, less demanding measurement methods are required to provide advancements in this area.

In the advanced model development below, we shall consider higher order frequency-dependent effects that arise from the consideration of a more exact model of oscillating flow through an orifice. Previously neglected effects such as the end correction to the linear part of the resistance will be introduced. Effects such as the contribution from the radiation resistance, negligible under current conditions, will be re-examined for potential contribution at higher frequencies.

---

[14] Dean, P. D., "An In-Situ Method of Wall Acoustic Impedance Measurement in Flow Ducts", J. Sound & Vib., Vol 34, No. 1, May 8, 1974, pp. 97-130.

2.2.3 Acoustic Reactance

2.2.3.1 Components of reactance

The reactance of a perforated plate single-degree-of-freedom liner can be separated into three distinct components:

1. The mass reactance contributions from the air mass within the orifice tube core.
2. The mass reactance contributions from the end corrections just outside each end of the orifice tubes.
3. The reactive contribution from the standing wave in the finite length cavity.

We can write this as

$$\frac{X}{\rho c} = \frac{X_{mt}}{\rho c} + \frac{X_{mec}}{\rho c} + \frac{X_{cav}}{\rho c} \tag{2-21}$$

where the meaning of the subscripts is obvious.

The simplest contribution is the reactance of the cavity, which can be written as

$$\frac{X_{cav}}{\rho c} = -\cot(kh) \tag{2-22}$$

where h is the cavity depth. It should be noted that we are using the $e^{+i\omega t}$ convention for the reactance, and this requires the negative sign before the cotangent and gives a positive mass reactance.

The cavity reactance can easily be derived by solving the forward-traveling and backward-traveling wave solution in a tube with one end open and the other closed for the ratio of pressure to velocity at the open end of the tube with an applied pressure at the open end. Inherent in this formulation is the assumption that the cross-dimension of the cavity is much smaller than a wavelength (only plane waves propagate in the cavity) and that the effects of viscosity at the cavity walls on the acoustic propagation in the cavity can be neglected.

The form of the mass reactance that is currently in use as standard practice[9] for the core mass reactance is:

$$\frac{X_{mt}}{\rho c} = \frac{kt}{\sigma C_D}, \tag{2-23}$$

and the expression for the end correction is

21

$$\frac{X_{mec}}{\rho c} = \frac{k\varepsilon d}{\sigma C_D}, \qquad\qquad (2\text{-}24)$$

where the semi-empirically-determined end coefficient ε is

$$\varepsilon = \frac{0.85\left(1.-0.7\sqrt{\sigma}\right)}{1+305\cdot M^3} \qquad\qquad (2\text{-}25)$$

These equations can be combined to include both the core mass reactance and the end correction in one expression for the overall mass reactance, X_m,

$$\frac{X_m}{\rho c} = \frac{k(t+\varepsilon d)}{\sigma C_D} \qquad\qquad (2\text{-}26)$$

The above formulas differ from those presented in Reference 9 in two respects. First, the discharge coefficient is not shown in the denominator of the mass reactance in Reference 9. The literature has been inconsistent in the presence of C_D in the denominator of the mass reactance, but, as will be shown in the formal theoretical derivation below, it should appear. Possibly the absence of the discharge coefficient in the denominator is compensated by the empiricism in the end correction factor, but this is not the proper way to formulate the problem.

Second, the Mach-number-dependent factor in the denominator of the mass reactance end correction factor was omitted in Motsinger and Kraft. The reduction in end correction factor with Mach number (the end correction on the flow side of the faceplate is at least partially "blown away" by the grazing flow) should be included to increase the accuracy of the model.

2.2.3.2 Measurement of reactance

No information on mass reactance is obtained from the DC flow resistance measurement. The usual method for obtaining measurements of reactance is a normal incidence impedance measurement using a normal incidence impedance tube apparatus (see discussion and list of references in Motsinger and Kraft[9]). Modern implementations of the normal incidence impedance tube that use the multiple-microphone measurement method can obtain the entire impedance spectrum rapidly using a broadband sound source[15]. The source SPL spectrum at the faceplate surface can be obtained as output of the measurement.

This measurement provides the impedance of the entire single-degree-of-freedom resonator at each frequency, so that the reactance is the combined mass reactance and cavity reactance. Since the cavity reactance is felt to be reliably predicted with the cotangent function,

---

[15]   Seybert, A. F. and Parrott, T. L., "Impedance Measurement Using a Two-Microphone, Random Excitation Method", NASA TM-78785, 1978.

the mass reactance can be extracted by subtracting the cavity reactance from the measured reactance,

$$X_m = X_{meas} - X_{cav} = X_{meas} + \cot(kh) \qquad (2\text{-}27)$$

If the capability of easily varying the cavity depth of the treatment sample in the normal incidence impedance tube is provided, the depth at any frequency could be set to make cot(kh) = 0, in which case the mass reactance would be measured directly at that frequency.

There is no direct method of separating the mass reactance end correction from the core mass reactance. Effects of incident sound intensity on the end effect must be intuited from parametric measurements with the impedance tube.

2.2.3.3 Issues with mass reactance

As will be discussed in the next Section, the current model for the mass reactance ignores higher order frequency-dependent terms. It is essentially the low frequency approximation to the exact model. These high frequency effects may be very important to treatment scaling.

Current models for the mass reactance include an empirical model for the loss in end correction with grazing flow, but generally ignore the effect of sound intensity on the decrease in mass reactance. Measurements to be presented in this study indicate that this is an important effect (this is not a new discovery—it has been known for decades!).

Historically, the mass reactance has been known to be the least accurately correlated component between prediction and measurement, in some cases being over-predicted and in other cases under-predicted. The effects have been relatively minor, however, and have largely been ignored. It appears that through the happy circumstance of two wrongs making a right, the lack of frequency dependence in the model has approximately compensated the end correction loss effect at higher SPL levels. This situation may no longer be acceptable, however, in the case of sub-scale treatment.

23

3. High Frequency Impedance Implications of Prior Research

3.1 Objective of Research Review

The objective of reviewing prior research on acoustic impedance of single-degree-of-freedom panels with perforated facesheets was to identify effects that researchers may have ignored under the assumption that their contributions were negligible under ordinary treatment operating conditions. These effects were examined for potential implications to impedance at high frequencies.

Some of the possible effects identified to be investigated were:

1. Higher order effects on resistance and mass reactance, including end effects, that are frequency-dependent and nonlinear.
2. The radiation resistance
3. The dependence of orifice discharge coefficient on orifice acoustic Reynold's number.

These effects are evaluated in this study, particularly in terms of the fluid mechanics of fluid flow through an orifice, both in isolation and when affected by neighboring orifice flow.

A universal assumption of almost all researchers is that the dimensions of the facesheet hole diameter and thickness and the cavity cross-dimension are all much smaller than a wavelength (this is not a restriction for the cavity depth). For treatment scaling, we do not violate this assumption. We assume that as the frequency goes up and the wavelength goes down, the relevant treatment dimensions all scale such that they remain small compared to a wavelength.

The subject of this Section is to provide a brief historical discussion of selected instances of prior work that have implication to treatment scaling. An extensive Historical Bibliography of papers discussed and others that were omitted from the discussion is included as Appendix B.

3.2 Discussion of the Review by Melling

Probably one of the most comprehensive discussions of the impedance of perforated plate single-degree-of-freedom resonators is that of Melling[15]. Much of the development in this study is based on the material presented in this article.

Melling considers both the linear and nonlinear regimes of resistance and mass reactance. He develops expressions for the impedance of an orifice from the exact theory of flow in a capillary tube including effects of viscosity, commonly referred to as the Crandall model (but traceable to Kirchoff and Raleigh in the last century). It is demonstrated that the current model

---

[15]   Melling, T. H., "The Acoustic Impedance of Perforates at Medium and High Sound Pressure Levels", J. Sound & Vib., 29(1), 1973, pp. 1-65.

for resistance and mass reactance is the zero frequency approximation of the exact Crandall model, referred to as the Poiseuille model.

Melling considers the contributions of both Sivian and Ingard to the determination of the end corrections for resistance and mass reactance. The issue of a final "best" model for end correction is not fully resolved, but Melling recommends a final model.

Melling mentions the effect of radiation resistance, but assumes that it is negligible. A correction for the effects of interaction among the orifices due to Fok has been included as part of the resistance and mass reactance end correction.

The nonlinear resistance term is the subject of an extensive investigation. As part of this study, Melling notes the importance and variability of the orifice discharge coefficient and its dependence on orifice Reynolds number and orifice geometry. The form derived by Melling for the nonlinear resistance coefficient B is very close to the standard value. Melling's recommended value is

$$B_M = 1.2 \frac{1}{2c} \frac{1-\sigma^2}{(\sigma C_D)^2} \tag{3-1}$$

This differs from Equation (2-12) by a factor of 1.2 and by the presence of a σ^2 term in the numerator. The omission of the σ^2 term in the standard model is an approximation, and it should be included for completeness.

The validity of the theoretical analysis is assessed by an extensive set of measurements of perforated sheets of varying porosities. The frequencies in the measurements are limited to about 3400 Hz upper value.

Thus, Melling has identified all the issues that were identified as having potential impact on the impedance of sub-scale treatment liners at high frequencies. The high frequency implications of the foundation laid by Melling will be examined in the next Section. It should be noted that there may yet be improvements to the standard impedance model at full scale frequencies to be afforded by re-examining some of Melling's conclusions, combined with further validation through a more comprehensive and precise set of measurements.

3.3 Contributions of Sivian and Ingard

From the 1930's through the 1950's several researchers considered the problem of the impedance of an isolated orifice. Sivian[16] derived an expression for the end corrections for

---

[16]   Sivian, L. J., "Acoustic Impedance of Small Orifices", J. Acoustic Society of America, Volume 7, October, 1935, pp. 94-101.

resistance and mass reactance that are still being used today. Ingard[17] derived a slightly different empirical correlation for end correction. Both of these cases are considered in detail in Melling.

Ingard and his associates have made extensive theoretical and experimental investigations into the nonlinearity in the resistance of orifices[18]. Ingard and Labate[19] noted the four regimes of orifice flow behavior, which are classified depending on intensity and frequency of the incident sound and the geometry of the orifice:

1. Low intensity, stationary circulation, flow along the axis out from the orifice, symmetric.
2. Stationary circulation, but flow along axis toward the orifice, symmetric.
3. Medium intensity, pulsations superimposed on circulation, not always symmetric.
4. High intensity, predominant pulsations, jets and vortex rings formed once each cycle, very sudden onset, symmetric.

The region of circulation increases from the edges of the flow to the center as the intensity increases. Ingard and Labate also noted that the orifice Reynold's number was not a very accurate predictor of onset of nonlinearity since the nonlinearity is not due to turbulence alone, but also depends on frequency and geometry. Many subsequent studies are confirmations or amplifications of these observations.

3.4 Contributions of Rice and Hersh

In the 1970's, Edward Rice and his colleagues at NASA Lewis examined the effects of multiple-frequency excitation and the effects of grazing flow on perforated plate resonators. Rice noted that the overall rms acoustic velocity was the appropriate value to use in the nonlinear resistance term, as opposed to the narrowband acoustic velocity, when the incident SPL spectrum is relatively flat[20]. Rice also noted that nonuniformities in the incident SPL spectrum, such as multiple protruding tones, may have effects on the measured impedance not fully explained by the overall rms velocity model.

Rice has also studied the effect of grazing flow on impedance, and examined the effects of combined grazing flow and broadband pressure excitation[21]. Rice noted the similarity in the grazing flow and multiple frequency excitation effects, and postulated that there may be physical interactions between the phenomena. Rice's correlation for the effects of grazing flow on resistance is widely used in current practice.

17   Ingard, Uno, "On the Theory and Design of Acoustic Resonators", J. Acoustical Society of America, Vol. 25, No. 6, November, 1953, pp. 1037-1061.

18   Ingard, Uno and Ising, Hartmut, "Acoustic Nonlinearity of an Orifice", J. Acoustic Society of America, Vol. 42, No. 1, 1967, pp. 6-17.

19   Ingard, U. and Labate, S., "Acoustic Circulation Effects and the Nonlinear Impedance of Orifices", J. Acoustic Society of America, Volume 22, No. 2, March 1950.

20   Rice, Edward J., "A Model for the Acoustic Impedance of a Perforated Plate Liner with Multiple Frequency Excitation", NASA TM X-67950, October, 1971.

21   Rice, Edward J., "A Model for the Pressure Excitation Spectrum and Acoustic Impedance of Sound Absorbers in the Presence of Grazing Flow", AIAA 73-995, October 1973.

Alan Hersh, Bruce Walker, and T. Rogers have been studying the behavior of Helmholtz resonators for many years. They have used numerical integration techniques to solve a fluid mechanical model, deriving an advanced model for mass reactance of an orifice[22,23,24]. The model establishes distinct nonlinear effects on mass reactance for sufficiently high orifice velocity levels, and indicates that the effective orifice discharge coefficient is a function of orifice velocity, hole diameter, and frequency.

Hersh and his associates have also done extensive studies on the effects of grazing flow on the impedance of single and clustered orifices[25,26,27,28]. They have examined the effects of the grazing flow on the fluid mechanics of the orifice, and developed analytical models that correlate both resistance and reactance with grazing flow. Their studies indicate a complex dependence on frequency, grazing flow boundary layer thickness, and orifice discharge coefficient, which itself varies in a complex manner. For grazing flow Mach numbers typical of aircraft engine ducts, they find a resistance relationship quite close to the Heidelberg model, and note that the effects of grazing flow and high sound pressure levels appear to eliminate the end correction on the mass reactance quite effectively.

The models of Hersh, Walker, and Rogers are fairly complex in form, and require the determination of some empirical constants. Due to their complexity, probably not as much attention was paid to these models as might be warranted for the current study. It would be worthwhile to revisit the Hersh impedance models at a future date in light of the analytical results and measured data to be presented below.

3.5 Other Contributions

Other authors have made significant contributions to specific aspects of the problem. Tijdeman[29], for instance, presents an extensive theoretical study of sound propagation in rigid cylindrical tubes, including numerical analysis solutions, but does not consider the effects of the

[22] Hersh, A. S. and Rogers, T., "Fluid Mechanical Model of the Acoustic Impedance of Small Orifices", AIAA 75-495, March, 1975.

[23] Hersh, Alan S. and Walker, Bruce, "Fluid Mechanical Model of the Helmholtz Resonator", NASA CR-2904, September, 1977.

[24] Hersh, A. S., "Nonlinear Behavior of Helmholtz Resonators", AIAA 90-4020, October 1990.

[25] Hersh, A. S. and Walker, B., "The Acoustic Behavior of Helmholtz Resonators Exposed to High Speed Grazing Flows", AIAA 76-536, July, 1976.

[26] Hersh, A. S. and Walker, B., "Effect of Grazing Flow on the Acoustic Impedance of Interacting Cavity-Backed Orifices", AIAA 77-1336, October, 1977.

[27] Hersh, A. S., Walker, B., and Bucka, M., "Effect of Grazing Flow on the Acoustic Impedance of Helmholtz Resonators Consisting of Single and Clustered Orifices", AIAA 78-1124, July, 1978.

[28] Walker, B. E., Charwat, A. F., "Correlation of the Effects of Grazing Flow on the Impedance of Helmholtz Resonators", J. Acoustical Soc America, 72(2), August, 1982.

[29] Tijdeman, H., "On the Propagation of Sound Waves in Cylindrical Tubes", J. Sound & Vibration, 39(1), 1975, pp. 1-33.

end correction. In his monograph[30], Allard focuses on propagation of sound in bulk absorber type materials, but includes chapters on propagation in tubes and effects of perforated facesheets.

Kooi and Sarin[31] develop an empirical model for grazing flow effects on resistance and mass reactance end correction for a perforated faceplate resonator. Their correlations are a function of frequency, Mach number, hole geometry, and a quantity they call skin friction velocity, which depends on the Mach number, viscosity, and boundary layer thickness and profile. As with the Hersh impedance model, the Kooi and Sarin formulation is worthy of further examination in light of the results of this study, but was not examined any further as part of this effort.

There are many other worthy research efforts that have not been mentioned here. Some of this work will be referenced specifically in the analysis section that follows. It is hoped the reader has gained at least a rough perspective of the work on impedance of Helmholtz resonators that has been conducted in the past. The results of this historical study is the focus of the current analysis on the research objectives listed at the beginning of this section. The interested reader is referred to the Historical Bibliography in Appendix B for further guidance.

One recurring theme in these research projects is the variability of the orifice discharge coefficient with flow conditions. Another is the empiricism associated with the resistance and mass reactance end corrections. At times, it is felt that the two effects become empirically entwined, and what may be a variation in end correction should be interpreted as a variation of discharge coefficient, or vice-versa.

We have a good understanding of the fluid mechanical physical phenomena associated with the orifice flow, but we need a more unified fluid mechanics theory to resolve these empirical anomalies. Then we need accurate and reliable measurements to support the theory. Further examination of some of these subjects could lead to improved full scale impedance models, as well as provide enlightenment for treatment scaling.

The empirically-derived results are of limited value for the current effort because they were generally measured at low frequencies (or under steady flow conditions) and may not apply to sub-scale frequency regimes. Of more use are the discussions of theoretical models that investigate fundamental physical phenomena that can be extended into the high frequency regime.

---

[30]   Allard, J. F., *Propagation of Sound in Porous Media: Modelling Sound Absorbing Materials*, Elsevier Applied Science, 1993.

[31]   Kooi, J. W., and Sarin, S. L., "An Experimental Study of the Acoustic Impedance of Helmholtz Resonator Arrays Under a Turbulent Boundary Layer", AIAA 81-1998, October, 1981.

4. Examination of High Frequency Effects on Impedance

4.1 Advanced Impedance Model Development

4.1.1 Crandall Model for Impedance of a Tube

The solution for the propagation of an acoustic plane wave in a capillary tube including the effects of viscosity has been derived by a number of authors[32,33], and will not be repeated here. The following assumptions are invoked for the analysis:

1. All orifice dimensions are small compared to a wavelength.
2. The fluctuating flow through the orifice due to the acoustic excitation can be assumed to be hydrodynamically incompressible.
3. The flow velocity profile across the hole diameter, while not uniform, can be replaced by its averaged value.
4. The pressure gradient along the hole (in the thickness direction), $\partial p/\partial x$, can be replaced by $\Delta p/t$, where t is the thickness of the plate (orifice length).

The basic solution is for an infinite length tube, that is, it includes only the mass of air in the tube core. The end effects are added on as a separate component.

$$\frac{Z}{\rho c} = \frac{1}{c \cdot \sigma \cdot C_D} \left[\frac{i \cdot \omega \cdot t}{F(k_s' r)} \right] \tag{4-1}$$

where c is the speed of sound, σ is the porosity, C_D is the orifice discharge coefficient, $\omega = 2\pi f$ is the circular frequency, r is the orifice radius,

$$k_s' \equiv \sqrt{-\frac{i\omega}{v'}} \tag{4-2}$$

is the Stokes wave number in the hole,

$$v' = \frac{\mu'}{\rho} \tag{4-3}$$

is the effective kinematic viscosity under isothermal conditions near a highly conducting wall, μ' is the effective absolute viscosity, ρ is the air density, and

---

[32] Allard, J. F., *Propagation of Sound in Porous Media: Modelling Sound Absorbing Materials*, Elsevier Applied Science, 1993, Chapter 4.

[33] Melling, T. H., "The Acoustic Impedance of Perforates at Medium and High Sound Pressure Levels", J. Sound and Vibration, 29(1), 1973, pp. 9-12.

$$F(k_s'r) \equiv 1 - \frac{2 \cdot J_1(k_s'r)}{k_s'r J_0(k_s'r)} \tag{4-4}$$

where J_0 and J_1 are Bessel Functions of the first kind.

The expression for the impedance has been divided by the porosity times the orifice discharge coefficient to convert from the lumped impedance of an isolated orifice to the lumped surface impedance due to the facesheet for an array of holes in a perforated plate. For the perforate, it is assumed that there is no interaction among the holes.

The argument of the Bessel functions is complex. In the past, this made the $F(k_sr)$ function very difficult to compute, leading researchers to develop approximate forms or use numerical integration solutions. With modern computers, subroutines are available to compute the Bessel functions of complex argument with no problem.

The viscosity coefficient used in Equation (4-2) is not the usual absolute viscosity coefficient of air. We will define μ as the absolute coefficient of viscosity coefficient of air, for an adiabatic process. The coefficient μ', however, is an effective value that arises out of the acoustic wave process along a highly conducting wall, where the process is assumed to be isothermal. Sivian[34] noted the difference between the two viscosities, and gave the following formulation for μ', but did not indicate its origin:

$$\mu' = \mu\left[1 + \frac{\gamma - 1}{\sqrt{Pr}}\right]^2 \tag{4-5}$$

where γ is the ratio of specific heats in air and Pr is the Prandtl number in air. We are using the prime convention from the original nomenclature of Sivian and note that convention was switched in Melling[33].

In air $\gamma = 1.4$ is a constant and the Prandtl number, defined as

$$Pr \equiv \frac{c_p\mu}{K_T} \tag{4-6}$$

where c_p is the specific heat of air at constant pressure, and K_T is the thermal conductivity of air. In air, Pr is a constant equal to 0.706 over a wide range of temperatures, so that we can set

$$\mu' = 2.179\mu \tag{4-7}$$

---

[34]   Sivian, L. J., "Acoustic Impedance of Small Orifices", J. Acoustical Soc America, Vol. 7, October 1935, pp.94-101.

A useful expression for the standard absolute viscosity of air as a function of temperature, known as the Sutherland Law, is[35]

$$\mu(T) = \mu_r \frac{T_r + 111}{T + 111} \left(\frac{T}{T_r} \right)^{1.5}$$

(4-8)

where T is the temperature in degrees Kelvin, and, in cgs units, the reference viscosity μ_r is 1.796E-4 g/(cm-sec) at the reference temperature of $T_r = 293$ K.

A complete derivation of the expression for effective viscosity in terms of acoustic vorticity and entropy modes can be found in either Pierce[36] or Morse and Ingard[37]. The condition under which the effective viscosity coefficient should be used is that the orifice walls are good heat conductors and that the circumference of the orifice is large compared to a thermal wavelength. The thermal wavelength, λ_T is given by

$$\lambda_T = 2\pi \sqrt{\frac{2K_T}{\rho \omega c_p}}$$

(4-9)

For a typical full-scale treatment 0.05 inch hole, this would require that the frequency be much greater than about 15 Hz. For a sub-scale (or millipore) 0.005 inch hole, this would require that the frequency be much greater than 1500 Hz. Thus, there are normal operating frequency ranges where it is not clear which manifestation of the viscosity coefficient should be used.

This model results in both a real (resistance) and imaginary (mass reactance) term, both of which are functions of frequency. These are, respectively, the linear viscous resistance term and the mass reactance term that can be ascribed to the lumped slug of mass in the core of the orifice. As yet, no end corrections have been applied. Note also that this is the linear contribution to the resistance and mass reactance. There are strong velocity-dependent terms for the resistance and nonlinear effects on reactance that are yet to be included.

One disadvantage of this form is that the resistance and mass reactance terms do not separate explicitly, they must be determined as the real and imaginary parts of Equation (4-1). The low frequency and high frequency approximations of this form, which shall be examined later, are easier to compute and do provide this separation.

[35]   Sherman, Frederick S., *Viscous Flow*, McGraw-Hill, 1990, p. 70.
[36]   Pierce, Allan D., *Acoustics: An Introduction to Its Physical Principles and Applications*, McGraw-Hill, 1981, pp.523-529.
[37]   Morse, Philip M., and Ingard, K. Uno, *Theoretical Acoustics*, McGraw-Hill, 1968, pp. 291-292.

31

4.1.2 End Effects on Resistance and Mass Reactance

While the contribution of the core slug in the orifice can be derived from purely theoretical considerations, the contribution of the end correction, except possibly for very low orifice flow velocities, is mostly empirically derived. Melling[33] describes the contributions of Sivian and Ingard to the determination of the end correction in great detail, and this will not be repeated here.

The final expression for the exact solution to the lumped facesheet resistance and mass reactance of an array of orifices, including the end corrections, is given by Melling as

$$\frac{Z}{\rho c} = \frac{i\omega}{c \cdot \sigma \cdot C_d} \left[\frac{t}{F(k_s'r)} + \frac{8d}{3\pi F(k_s r) \cdot \psi'(\xi)} \right] \tag{4-10}$$

where the second term in brackets is that due to the end correction,

$$k_s \equiv \sqrt{-\frac{i\omega}{\nu}} \tag{4-11}$$

is the Stokes wave number for an adiabatic medium (non-thermally-conducting region external to the hole). $\psi'(\xi)$ is the Fok function, which accounts for interactions among neighboring holes[38], where

$$\xi \equiv \sqrt{\sigma} \tag{4-12}$$

A computational expression for the Fok function is

$$\psi'(\xi) = \sum_{n=0}^{8} a_n \xi^n \tag{4-13}$$

where

$a_0 = 1.0$	$a_1 = -1.4092$	$a_2 = 0.0$
$a_3 = +0.33818$	$a_4 = 0.0$	$a_5 = +0.06793$
$a_6 = -0.02287$	$a_7 - +.003015$	$a_8 = -0.01614$

The Fok function starts from one when porosity is zero and increases monotonically to about 3.0 when porosity reaches 25%. Thus, its effect is to decrease the end correction with increasing porosity.

---

[38]   Melling, T. H., "The Acoustic Impedance of Perforates at Medium and High Sound Pressure Levels", J. Sound and Vibration, 29(1), 1973, pp. 16-17.

The second term in the brackets in Equation (4-10) is an end correction term due to Sivian[34]. Equation (4-10) is the form recommended by Melling to predict the lumped mass reactance of a perforated facesheet, and the form that will be adopted in the advanced impedance prediction model below.

4.1.3 Approximations of Poiseuille and Helmholtz Regimes

The derivation and rationalization behind the low and high frequency approximations are discussed in detail in Melling[33]. Only the resulting equations will be presented here.

The Poiseuille model is the low frequency approximation to the exact model of Equation (4-10). The Poiseuille form for the facesheet impedance is

$$\frac{Z_P}{\rho c} = \frac{32vt}{c\sigma C_d d^2} + i\frac{k}{\sigma C_D}\left(\frac{4}{3}t + \frac{8}{3\pi}\frac{d}{\psi'}\right) \tag{4-14}$$

where the real part is the resistance and the imaginary part is the mass reactance. The orifice interaction effect is included as part of the end correction. Note that the resistance is just the DC flow A-value. The Poiseuille model is valid when

$$\frac{d}{2}\left(\frac{2\pi f}{v}\right)^{1/2} \langle 1 \tag{4-15}$$

For full-scale engines at low frequencies, the linear resistance term is usually assumed to be small enough to ignore.

The high frequency approximation to the facesheet impedance is known as the Helmholtz model. This is derived from the exact equation as

$$\frac{Z_H}{\rho c} = \frac{\sqrt{8\omega v}\cdot t}{c\sigma C_D d} + \frac{16vt}{c\sigma C_D d^2} + i\left(\frac{kt}{\sigma C_D} + \frac{\sqrt{8\omega v}}{c\sigma C_D}\frac{t}{d} + \frac{8}{3\pi}\frac{d}{\psi'}\right) \tag{4-16}$$

The real part of the Helmholtz model is the high frequency approximation for the linear contribution of viscous resistance of orifices in a perforate. A second order term has been added to the resistance. This second order correction to the Helmholtz model resistance is important for matching the exact model at intermediate frequencies. As in the Poiseuille model, the orifice interaction effect has been included in the mass reactance. The Helmholtz model is valid when

$$\frac{d}{2}\left(\frac{2\pi f}{v}\right)^{1/2} \rangle 10 \tag{4-17}$$

Currently, it is often standard practice to use the Poiseuille model at all frequencies, regardless of the predicted frequency dependence of the linear resistance term. This has been acceptable only because the error is small at lower frequencies, due to small contribution of the linear resistance term compared to the nonlinear term and the effects of grazing flow. This may not be acceptable when considering sub-scale treatment frequency ranges.

Assuming c, C_d, σ, and ν are the same at full and sub-scale, the Helmholtz resistance increases as $\sqrt{f}$ and t/d. Although Poiseuille resistance is not a function of frequency, it scales as t/d^2. In the Helmholtz model, there is also seen to be an additional term proportional to $\sqrt{f}$ in the mass reactance. The issue of a variable discharge coefficient will be discussed later.

4.1.4 Radiation Resistance Contribution

A contribution to the resistance that has been assumed to be negligible under low frequency conditions is the radiation resistance. If we assume that the radiation resistance of a vibrating slug of air in the orifice of a perforated plate is the same as that of a piston vibrating in an infinite baffle, ignoring interaction effects, the radiation resistance for an array of orifices in a perforated plate will be[39]

$$\frac{R_{rad}}{\rho c} = \frac{1}{\sigma}\left[1 - \frac{J_1(2ka)}{ka}\right]$$

(4-18)

where a is the radius of the holes in the perforated sheet. For very small values of ka, this can be approximated by

$$\frac{R_{rad}}{\rho c} = \frac{1}{2\sigma}(ka)^2$$

(4-19)

For full scale treatment, assuming the maximum frequency is 10,000 Hz. the largest hole size is 0.08 inches, and the minimum porosity is 5%, the radiation resistance contribution would be $R_{rad}/\rho c$ = 0.34, which is a small but not a negligible contribution. A more typical 10% porosity facesheet would have half this value, and it will drop rapidly with frequency.

Since ka is invariant with scaling, we can expect the same values for scaled acoustic treatment, as long as the hole diameter is reduced by the appropriate scaling factor. If the hole diameter for the scaled treatment is made larger than the value dictated by the scaling factor, the radiation resistance will increase rapidly.

---

[39]   Morse, Philip M., and Ingard, K. Uno, *Theoretical Acoustics*, McGraw-Hill, 1968, pp. 383-387.

34

Figure (4-1) is a plot of the normalized radiation resistance as a function of ka for a porosity of 5%. The exact form of the radiation resistance contribution is included in the final model for acoustic impedance.
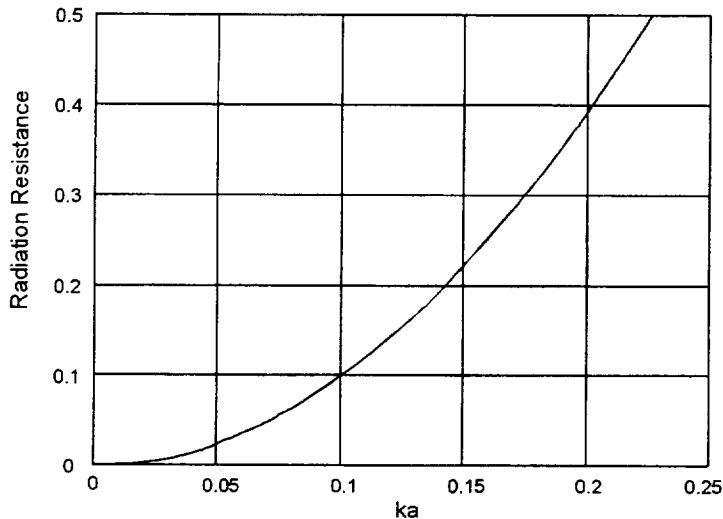

Figure (4-1)   **Predicted radiation resistance normalized by ρc for a 5% facesheet as a function of ka.**

4.1.5 Nonlinear Resistance Contribution

Melling[40] presents a detailed discussion of the development of the nonlinear contributions to the resistance and reactance. By nonlinear, it should be noted, is meant that the resistance or reactance depends on the acoustic velocity in the orifice, and therefore on the incident SPL of the pressure wave. Since, given the incident SPL, the acoustic velocity depends on the impedance and the impedance is a function of the acoustic velocity, an iterative procedure must be followed to determine the acoustic impedance.

The theoretical derivation of the nonlinear terms in the impedance of a facesheet is based on the linear momentum equation, under the following set of assumptions:

1. The fluid obeys the Stokes law for viscous shear.
2. Entropy variations are negligible.
3. The diffusion of acoustic momentum in the viscous medium is negligible.
4. The radial component of acoustic velocity outside the hole is compensated by an end effect.
5. The acoustic parameters can be replaced by their values averaged over the hole.

---

[40]   Melling, T. H., "The Acoustic Impedance of Perforates at Medium and High Sound Pressure Levels", J. Sound and Vibration, 29(1), 1973, pp. 44-59.

35

6. The square of the acoustic velocity averaged over the hole area is approximately equal to the square of the average velocity. This limits the analysis to relatively flat flow profiles in the hole.

7. The acoustic velocity has simple harmonic time dependence.

8. The gradient is constant along the hole, that is, we can replace $\partial/\partial x$ with $1/t$ ($t \ll \lambda$), where t is the length of the hole.

9. The orifice is square-edged.

10. The steady-state and the instantaneous acoustic behavior are equivalent.

The last assumption, that of quasi-steady motion for the flowfield due to the acoustic perturbation around the hole, will be shown to be questionable under some operating conditions.

Under these assumptions, Melling derives the following form for the nonlinear resistance contribution:

$$\frac{R_{NL}}{\rho c} = \frac{1.2}{2c} \frac{1 - \sigma^2}{(\sigma C_D)^2} V_{rms} \qquad (4\text{-}20)$$

The nonlinear resistance term arises from the loss of kinetic energy in the flow through the hole, with a correction added for the effects of radial flow just outside both sides of the hole. By invoking the quasi-steady flow condition, Melling then identifies this term with the standard form for the nonlinear part of the DC flow resistance through a perforate. This form is a factor of 1.2 greater than the currently used impedance prediction form. This is somewhat compensated by the reduction from σ^2 in the numerator of the Melling version, which is usually not included in the standard impedance prediction model.

The linear part of the orifice mass reactance and resistance also arise from the momentum equation derivation, but no corresponding nonlinear contribution to mass reactance appears. Melling notes that the major velocity-dependent effect on mass reactance is that due to the loss of the end effects as the flow through the orifice transforms from laminar to turbulent. The key to determining the mass reactance effect is through knowledge of the axial location of the *vena contracta*, which moves away from the orifice with increasing flow rate, but little is quantitatively known about this behavior.

Melling notes that the quasi-steady flow assumption hinges on the relative size of the first term in the Euler equation for the acoustic field perturbing the flow through the orifice, which must be small compared to the other two terms[41]. The Euler equation is

$$\bar{\rho}\frac{\partial u'}{\partial t} + \bar{\rho}u'\frac{\partial u'}{\partial x} + \frac{\partial p'}{\partial x} = 0 \qquad (4\text{-}21)$$

[41] Melling, T. H., "The Acoustic Impedance of Perforates at Medium and High Sound Pressure Levels", J. Sound and Vibration, 29(1), 1973, p. 47.

36

where the bars denote ambient average values and the primes denote fluctuating quantities. The inverse of the time scale is represented by a frequency, f, the length scale by an effective orifice length t_{eff}, and the velocity in the hole is related to the incident acoustic velocity by

$$u' = \frac{v'}{\sigma} \qquad (4\text{-}22)$$

where the incident velocity is estimated from the incident pressure and assumed surface impedance by

$$u' = \frac{p}{\sigma Z} \qquad (4\text{-}23)$$

Using these scales as estimates of the magnitude of each term in the equation, we can write the ratio of term one to term two as

$$\frac{T1}{T2} = \frac{\sigma ckt_{eff}}{2\pi(7.68E-7)10^{SPL/20}} \qquad (4\text{-}24)$$

and the ratio of the first term to the third term as

$$\frac{T1}{T3} = \frac{kt_{eff}}{\sigma} \qquad (4\text{-}25)$$

If we assume that the maximum frequency of interest is 10,000 Hz. and that the maximum value of t_{eff} is 0.25 cm., then the maximum value of kt_{eff} will be about 0.46. If we assume a minimum SPL of 130 dB and a maximum porosity of $\sigma = 0.15$, then the ratio of the first term over the second term is given by

$$\frac{T1}{T2} = 154.8 \qquad (4\text{-}26)$$

If we assume a minimum porosity of 5%, then the ratio of the first term to the third term is

$$\frac{T1}{T3} = 9.2 \qquad (4\text{-}27)$$

Neither of these ratios could be considered small—in fact, the frequency would have to be reduced by more than two orders of magnitude before T1/T2 becomes small. This makes the question of quasi-steady flow questionable, which makes the assumption that the DC flow measured parameters can be applied to the resistance terms as empirical parameters questionable, at least at the higher frequencies. Since kt_{eff} is invariant with scaling, this is a potential problem both at full scale and sub-scale.

4.1.6 Advanced Impedance Prediction Model

To construct the advanced impedance prediction model, a number of elements of the development from the previous section were adapted to the current impedance model as revisions or options. In particular, the revisions were:

1. Incorporation of the exact Crandall model to compute the linear resistance and mass reactance options. This replaces the Poiseuille model, which formed the basis of the existing model.
2. Addition of the radiation resistance term.
3. Incorporation of the Fok function for neighboring hole coupling effects on the end correction.
4. Incorporation of an option to apply an arbitrary factor to the end effect for the exact model anywhere from zero (no end effect) to one (full end effect).
5. Incorporation of the option of using the Keith and John model for orifice discharge coefficient as a function of orifice Reynolds number or entering a constant value for the discharge coefficient.

Features maintained from the existing model were:

1. The empirical end effect that includes porosity and grazing flow effects is provided as an option to the exact model. With this option, the exact model is used *except* for the end effect, which is replaced with the empirical end effect model.
2. The Heidelberg model for the resistance due to grazing flow.
3. The standard cotangent function for the cavity reactance.
4. The iteration algorithm to determine the nonlinear resistance, which depends inherently on acoustic velocity and impedance.

The incorporation of the exact Crandall model adds frequency-dependent features to the linear resistance and mass reactance that are not included in the existing impedance model. It is still a fundamental assumption of the model that the nonlinear velocity-dependent quantities are functions of the rms velocity summed over all contributing frequency bands, rather than on the acoustic velocity in individual narrowbands.

When the Keith and John model is chosen to determine the discharge coefficient as a function of orifice Reynolds number, an iteration is performed similar to the iteration to determine nonlinear resistance. The iteration is based on the orifice overall rms acoustic velocity, which changes as the treatment impedance changes nonlinearly. The C_D iteration is coupled to the nonlinear resistance iteration.

A Users' Guide to the impedance model computer program PPZ4 is included as Appendix A.

38

4.2 Reynolds Number Effects on Orifice Flow

4.2.1 Problems in Developing a Model for Orifice Discharge Coefficient

Melling notes that the major difficulty in applying the nonlinear form for resistance is that the orifice discharge coefficient is not a constant, but is a function of orifice Reynolds number, orifice geometry, and porosity. In fact, most of the discrepancies among the predictions and measurements of both perforated plate impedance and DC flow resistance can probably be traced to uncertainties in the value of the discharge coefficient, although uncertainties in the end effect will also contribute. We shall examine some of these discrepancies at this point.

Melling obtained mixed results in comparing orifice discharge coefficients derived from acoustic measurements, DC flow measurements, and a single ideal orifice model[42]. Larger discrepancies were found for the 7.5% porosity samples than for the 22% porosity samples. Other than this initial work of Melling, there is little available in the open literature to shed further light on this problem.

The discharge coefficient of an orifice, C_D, is defined as the product of the coefficient of contraction and the coefficient of velocity. The coefficient of contraction is the ratio of the area of the *vena contracta* to the orifice area. The coefficient of velocity is the ratio of the ideal to actual velocity at the *vena contracta*. The *vena contracta* is the minimum flow area in a jet formed by contraction of the streamlines, at the point where the streamlines become parallel. At this point the flow velocity is at a maximum and the effective flow area is a minimum.

The Reynolds number for the orifice based on hole diameter is defined as

$$Re_d = \frac{v_h d}{v} \qquad (4\text{-}28)$$

where v_h is the flow velocity in the hole, d is the hole diameter, and v is the kinematic viscosity. In terms of the incident acoustic velocity, this is can be written as

$$Re_d = \frac{v_i d}{\sigma C_D v} \qquad (4\text{-}29)$$

where σ is the porosity. Note that in this formulation, the acoustic form, the Reynolds number depends on the discharge coefficient which in turn is a function of the Reynolds number.

It is useful to consider some typical ranges of orifice Reynolds number obtained in acoustic excitation of perforated sheets in aircraft engine environments. First, however, we must specify how to define the incident acoustic velocity. If the faceplate/cavity is excited by a pure tone, the rms acoustic velocity will be given by magnitude of the incident acoustic pressure

---

[42]   Melling, T. H., "The Acoustic Impedance of Perforates at Medium and High Sound Pressure Levels", J. Sound and Vibration, 29(1), 1973, pp. 54-55.

divided by the surface impedance. For illustrative purposes, we could assume an impedance of 41.5 cgs Rayls and obtain pressure for several SPL values from 130 to 150 dB.

If the resonator is excited by a broadband pressure signal, the method of determining the incident velocity becomes more problematic. The velocity in each narrowband is determined by the pressure and impedance in that narrowband, and both pressure and impedance will vary over the full frequency range. It seems reasonable to use the overall rms value of acoustic velocity (integrated over all frequencies) in the Reynolds number, in the same sense that the overall rms value appears to be the appropriate value to use in the nonlinear flow resistance term.

This would say that the velocity to use to calculate the Reynolds number to determine C_D would be the overall velocity. Although this would appear to make some sense for modeling C_D as a function of Re_d, there is no available experimental justification for doing so. An additional consequence would be that the Reynolds number would be likely to be in the higher ranges for SPL's above 130 dB or so, where C_D has achieve a constant value, so that there may be no problem with C_D variation with low Reynolds numbers. At this point, this must be considered to be an hypothesis.

Returning to our original objective of determining typical Reynolds number ranges for the acoustic process, Figure (4-2) shows a contour plot of lines of constant Re_d in the plane of SPL versus the parameter of hole diameter in cm. divided by porosity.
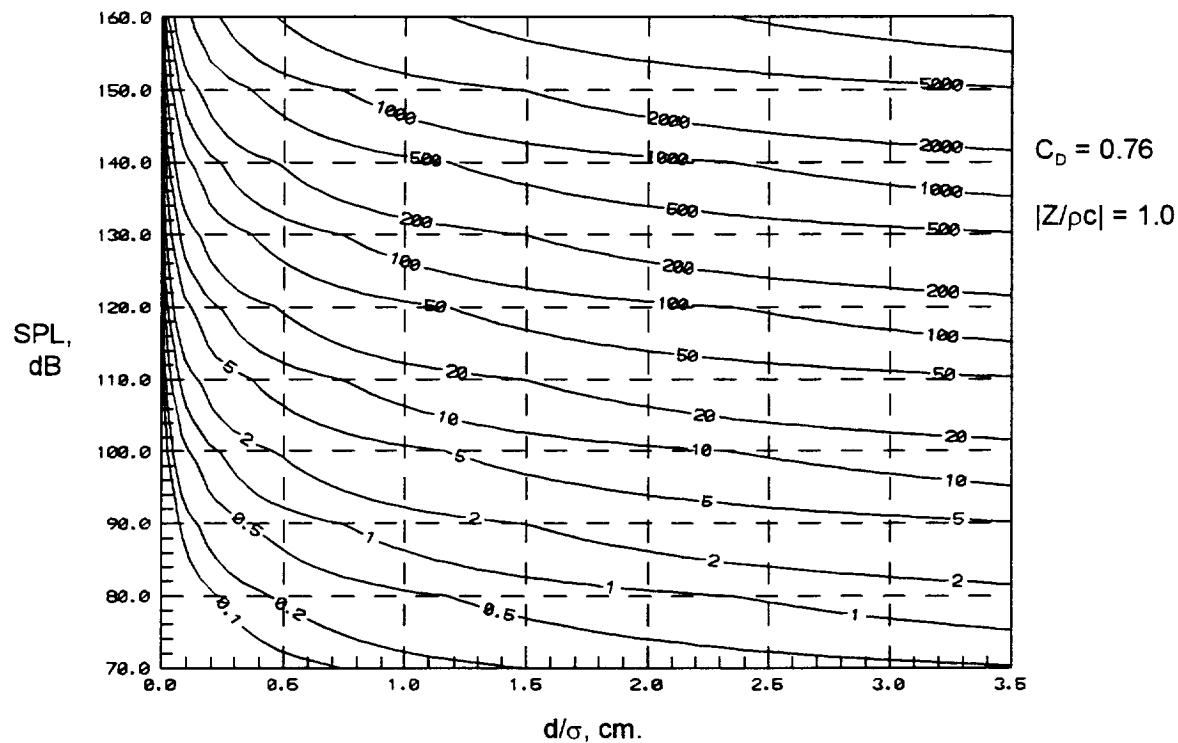
Figure (4-2)   **Contours of constant orifice Reynolds number as a function of incident SPL and d/σ for constant $C_D = 0.76$ and $|Z/\rho c| = 1.0$.**

To calculate these contours, the discharge coefficient was assumed to be constant at 0.76 and the impedance was held constant with a magnitude of 1.0. The resistance and reactance of the hypothetical resonator can take on any values, as long as $|Z/\rho c| = 1.0$. The SPL can be interpreted either as the pressure level in a tone at which the wall impedance is 1.0 or as the overall SPL, in which case the impedance of 1.0 would represent an overall average value. A typical value of d/σ, for a hole diameter of 0.05 inches and porosity of 10% would be 1.27.

To illustrate cases where the orifice Reynolds number is based on the overall rms acoustic velocity, Table (4-1) lists values obtained from impedance predictions for three different treatment configurations. The impedances from these predictions will be compared to measured values later in this report. Note that the fourth case is representative of a 1/4 scale treatment panel, has hole diameters in the range usually associated with "linear" perforates, and is measured over a higher frequency range.

41

Case #	σ	d, in	t, in	h, in.	SPL, dB	Freq Range	u_rms cm/sec	Re_d
1	0.06	0.062	0.026	0.75	139	750-6300	61.6	1264
2	0.06	0.062	0.026	0.75	149	750-6300	166.9	3489
3	0.08	0.02	0.012	0.5	144	750-6300	61.4	339
4	0.08	0.008	0.005	0.2	136	2600-13500	17.4	46.9

Table (4-1) **Table of orifice Reynolds number obtained for typical treatment panels under various SPL levels, using overall rms definition of Re_d.**

It should be reiterated that the orifice discharge coefficient in not solely a function of the orifice Reynolds number. It has been found to vary strongly with such effects as orifice thickness to diameter ratio, the longitudinal shape of the hole (particularly whether the inlet and outlet edges are sharp or rounded), and the porosity (a coupling effect among neighboring holes). These effects will influence both the resistance and mass reactance. There is not, as yet, to the author's knowledge, a unified model for the discharge coefficient of a perforated plate that incorporates all these parameters.

4.2.2 Keith and John Model for Orifice Discharge Coefficient

One attempt to develop a model for the variation of C_D with Re_d was made by Keith and John[43]. They used a computational fluid dynamics procedure involving vorticity-stream function system numerical integration to integrate the steady axisymmetric form of the Navier-Stokes equation. This was applied to an isolated orifice mounted in a tube, with the ratio of the orifice diameter to the tube diameter (square root of porosity) as a parameter. The study is also limited to thin orifices, which means it will not account for effects of t/d or orifice interaction. They compared their computations to the measurements previously made by several investigators, with very good agreement.

A curve fit was made to the Keith and John model for the case that corresponded to a porosity of 0.09. The model is divided into three regions, a linear low Re_d region, an intermediate transition region, and a constant high Re_d region. The algorithm follows:

[43] Keith, T. G. and John, J. E. A., "Calculated Orifice Plate Discharge Coefficients at Low Reynolds Numbers", Transactions of the ASME, J. of Fluids Engineering, June, 1977, pp.424-425.

Let $LGR = \log_{10}(Re_d)$

Let $LGCD = \log_{10}(C_D)$

For $Re_d < 3.33$

        $LGCD = 0.4985 \cdot LGR - 0.8477$

For $3.33 \leq Re_d \leq 300$

$$LGCD = -0.842817 + 0.528152 \cdot LGR - 0.0283395 \cdot LGR^2$$
$$- 0.04733 \cdot LGR^3 + 0.00828709 \cdot LGR^4$$

For $Re_d > 300$

        $LGCD = -0.119$

Then $C_D = 10^{LGCD}$

The constant value of C_D above $Re_d = 300$ is just 0.76, which is the nominal value of C_D used in the current impedance model, but this does not account for variations with hole geometry or porosity.

Figure (4-3) is a plot of the curve fit to Keith and John model for orifice discharge coefficient versus Reynolds number. This form of C_D versus Re_d will be used as an option for the Reynolds number variation of C_D in the advanced impedance model.

43
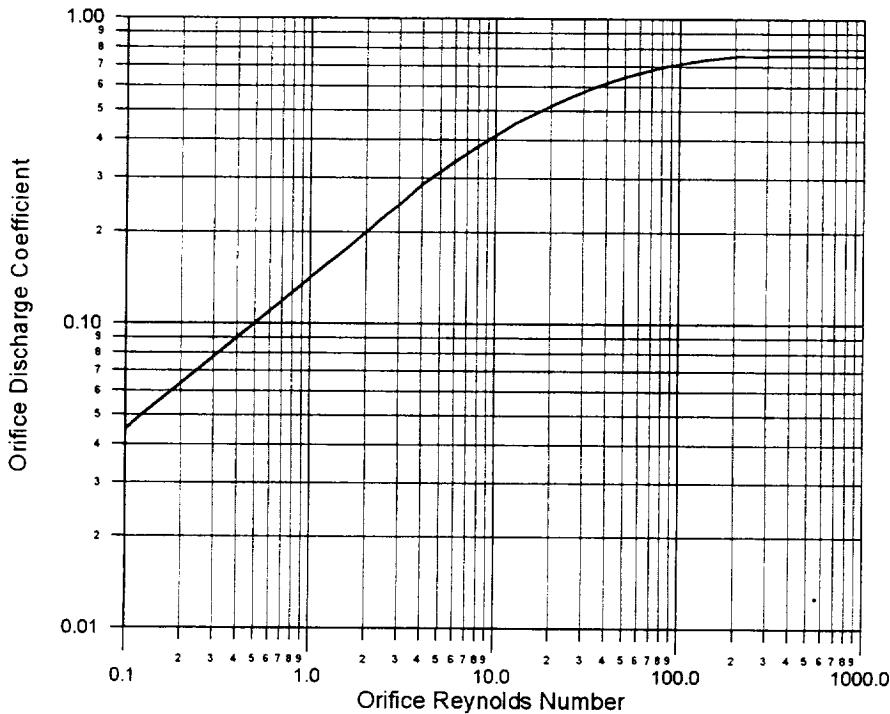
Figure (4-3)   Curve fit to the Keith and John model for orifice discharge coefficient as a function of orifice Reynolds number.

4.2.3 Discharge Coefficient Evaluation Using DC Flow Resistance Data

In the theoretical formulation, the discharge coefficient appears in both the linear and nonlinear terms of the DC flow resistance model:

$$\frac{R_{DC}}{\rho c} = \frac{32 v t}{c \sigma C_D d^2} + \frac{1 - \sigma^2}{2 c (\sigma C_D)^2} U_{inc} = A + B \cdot U_{inc} \tag{4-30}$$

where U_{inc} is the steady flow velocity incident on the faceplate. As shown, the first term on the right is the A-value, and the coefficient of U_{inc} is the B-value. Given a set of measurement values of R_{DC} versus U_{inc}, a value of C_D can be extracted for each flow value, which can then be used to compute Re_d.

To compare the predicted DC flow resistance to measured values for specific cases, two treatment configurations were chosen for which measured data were available. The cases are defined in Table (4-2). The first perforate is that typical of a full scale engine design at 8.5% porosity and the second is roughly a 1/5 scale representation of the full scale, with 8.0% porosity, very small hole size, and very thin. The measured DC flow resistance will be compared to the

44

predicted DC flow resistance using an assumed constant C_D of 0.76, an assumed constant C_D that is the average of the values that fit the model to the measured curve, and a variable C_D as given by the Keith and John model.

Case No.	Porosity, σ	Hole diameter, d, in.	Thickness, t, in.
1	0.085	0.062	0.024
2	0.08	0.008	0.005

Table (4-2)   **Definition of the perforated sheet cases for comparison of measured and predicted DC flow resistance.**

Figure (4-4) shows the comparison of predicted and measured DC flow resistance for Case 1, the standard full scale facesheet. Note that the value predicted using $C_D = 0.76$ underpredicts the flow resistance and also has a lower slope (B-value) than measured. The measured data averaged fit coefficient, $C_D = 0.711$, gives a much closer match to the measured throughout the range of flow velocity. It should be noted that $Re_d = 491$ at the lowest flow velocity, so that it is in the region where C_D should be constant at its maximum value. The Keith and John model, therefore, would give a constant C_D of 0.76, so that it would give the same curve as already plotted. The empirical maximum C_D value, however, is about 6.5% less than this 0.76 nominal value.
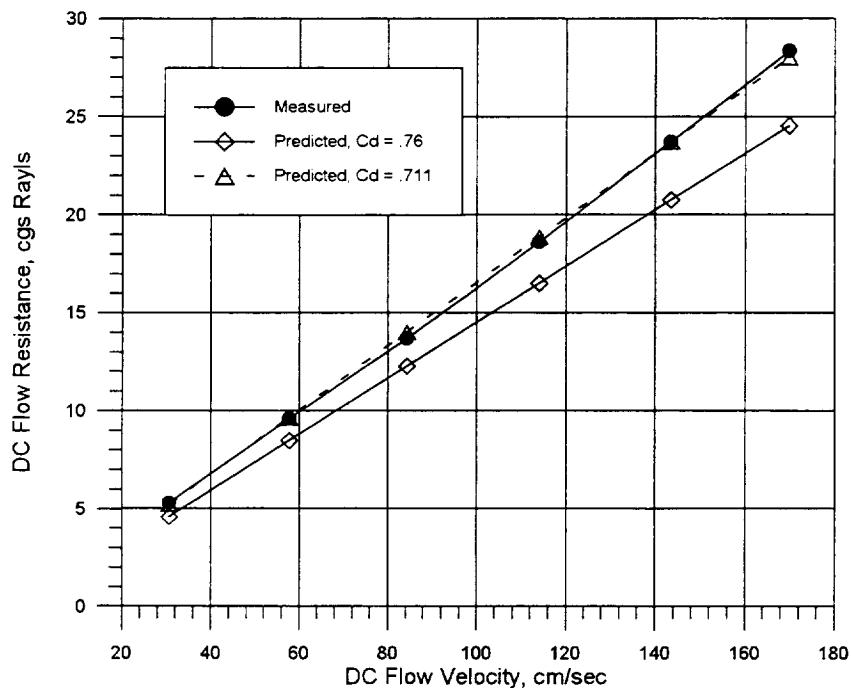

Figure (4-4)   **Predicted DC flow resistance compared to measured value for different assumptions regarding orifice discharge coefficient, Case 1, standard 8.5% facesheet.**

Figure (4-5) shows the comparison of predicted and measured DC flow resistance for Case 2, the 1/5 scale facesheet with small diameter holes. In this case, the average best fit C_D value that matches the prediction model to the measured data is greater than 1.0, so that it is set to 1.0. The lowest flow velocity does give a Reynolds number that is in the transition region of the Keith and John model, so that it predicts a decrease in C_D for the two lowest flow values as indicated in Table (4-3).

U, cm/sec	Re_d	C_D	A	B	K&J R_{DC}	Meas R_{DC}
30	73.0	0.686	3.258	0.1969	9.16	4.29
60	136.1	0.736	3.037	0.1711	13.30	7.23
105	230.7	0.76	2.942	0.1606	19.80	11.65
150	329.6	0.76	2.942	.1616	27.19	16.07
200	439.5	0.76	2.942	.1616	35.27	20.97

Table (4-3)   Orifice Reynolds number, Keith and Johnson discharge coefficient, predicted DC flow resistance A and B values, predicted DC flow resistance, and measured DC flow resistance for facesheet Case 2, 8.0% 1/5 scale.
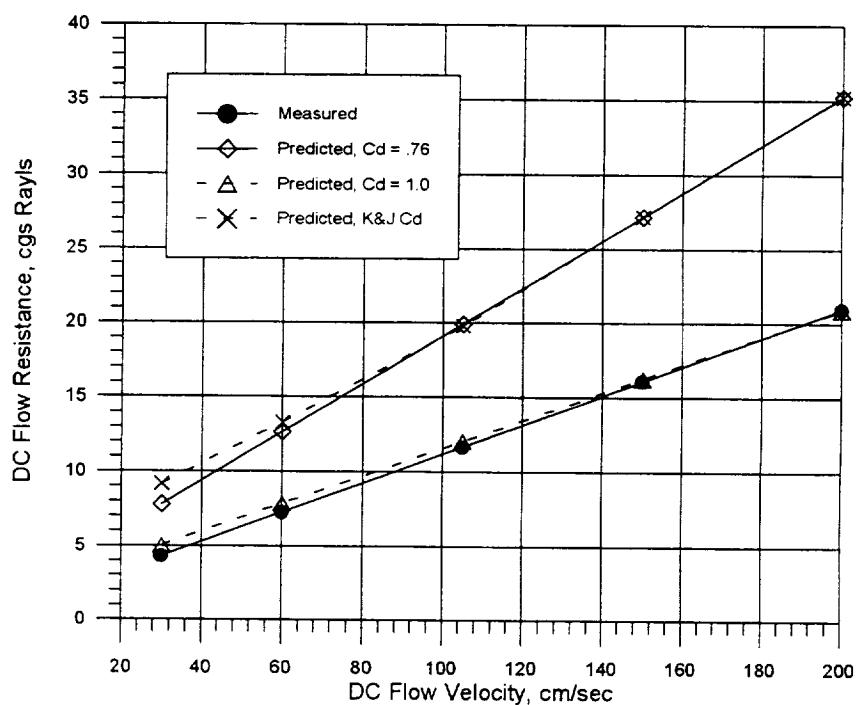

Figure (4-5)   Predicted DC flow resistance compared to measured value for different assumptions regarding orifice discharge coefficient, Case 1, 1/5 scale 8.0% facesheet.

46

Note that in this case, the predicted values using the nominal $C_D = 0.76$ give a worse match to the measured values than the previous case. In this case, both the predicted A value and B value are too large. Using the data fit averaged C_D gives a very close match, as expected, and implies that the discharge coefficient is 1.0. The Keith and John model for C_D is causing the predicted curve to move in the wrong direction at the lower flow velocity values, raising questions regarding its validity as applied to the present case.

Although it would be unwise to generalize these results to other perforated facesheets, they are typical of the type of results that will be obtained. Some facesheets will give a very close fit for $C_D = 0.76$, others will give discrepancies that will vary in the opposite direction from the examples provided here.

In conclusion, there is much left to do in achieving a complete understanding of the behavior of acoustic flow fluctuations through orifices. These results along with those previously derived by Melling have shown a disagreement among the discharge coefficient values found from ideal isolated orifices, the effective DC flow-derived values, and the acoustical values. The problem may be made even more difficult by the coupling of the variation in end effects with the same parameters that the discharge coefficient has been found to depend upon. This could effect both the linear resistance component and the mass reactance.

Advancements in understanding and modeling the discharge coefficient and end effects on impedance would bring improvements in both full scale and sub-scale impedance modeling. Achieving these advancements will require an extensive and exacting series of tests in which all the relevant facesheet parameters were varied over a useful range. Coupled with this should be CFD studies that calculate the unsteady flow of an acoustic wave through a perforated sheet for the laminar through the turbulent flow regimes.

5. Comparison of Predictions with Measured Data

5.1 Measured and Predicted Comparisons

In this section, we shall compare predicted and measured impedances for six treatment panel configurations. The measurements were made by Rohr, Inc., using both a 3.0 cm. low frequency normal incidence impedance tube and a 1.5 cm. high frequency impedance tube. Details of these tests and procedures will be documented in a separate final report volume. The predictions are made using two models, the existing model that is currently in use by industry and the advanced model that has been developed in this effort. Details of the parameters that define the test configurations are given in Table (5-1). Since the measurements were made in a normal incidence impedance tube, there are no grazing flow effects included.

Config No.	Test Panel Designation	Open Area Ratio σ	Hole Diam, d, in	Thkns, t, in	Cavity Depth, h, in	Frequency Range of Msrmnt	OASPL Meas Values, dB	C_D from DC flow
1	Panel 3.4	0.08	0.020	0.012	0.5	800-6200	144.3	0.812
2	Panel 3.4	0.08	0.020	0.012	0.5	2570-13500	130.7	0.812
3	Panel R001a	0.0665	0.062	0.026	0.75	750-6300	139	n/a
4	Panel R001a	0.0665	0.062	0.026	0.75	750-6300	149	n/a
5	Panel 3.6	0.08	0.008	0.005	0.2	800-6200	145.9	0.972
6	Panel 3.6	0.08	0.008	0.005	0.2	2570-13500	136.2	0.972

Table (5-1) **Definition of treatment panel configurations for which predicted and measured impedance is to be compared.**

Configuration 1

Configuration 1 is a half-scale perforated plate resonator panel with 8.0% porosity, measured over the full-scale frequency range with 144.3 dB overall SPL. The measurement was made in the 3.0 cm. normal incidence impedance tube, with broadband excitation, and the data were reduced with 20 Hz. frequency resolution. The predictions were made at the same narrowband frequencies as the measurement.

Figure (5-1) shows a comparison of the measured impedance and the impedance predicted using the current prediction model as described in Section 2. Figure (5-2) shows the SPL spectrum shape for this measurement. The prediction, in this case, represents both the nominal C_D value of 0.76 and the C_D derived from the DC flow resistance measurement, which was 0.812, since there is only a negligible difference between the two cases.

Note that the agreement between prediction and measurement is quite good, although the reactance is over-predicted above about 2500 Hz. This total reactance over-prediction is caused by an over-prediction of the mass reactance component. The deviation in resistance below 1500 Hz. is caused by measurement problems in the normal incidence impedance tube experienced when the magnitude of the impedance becomes large.

48
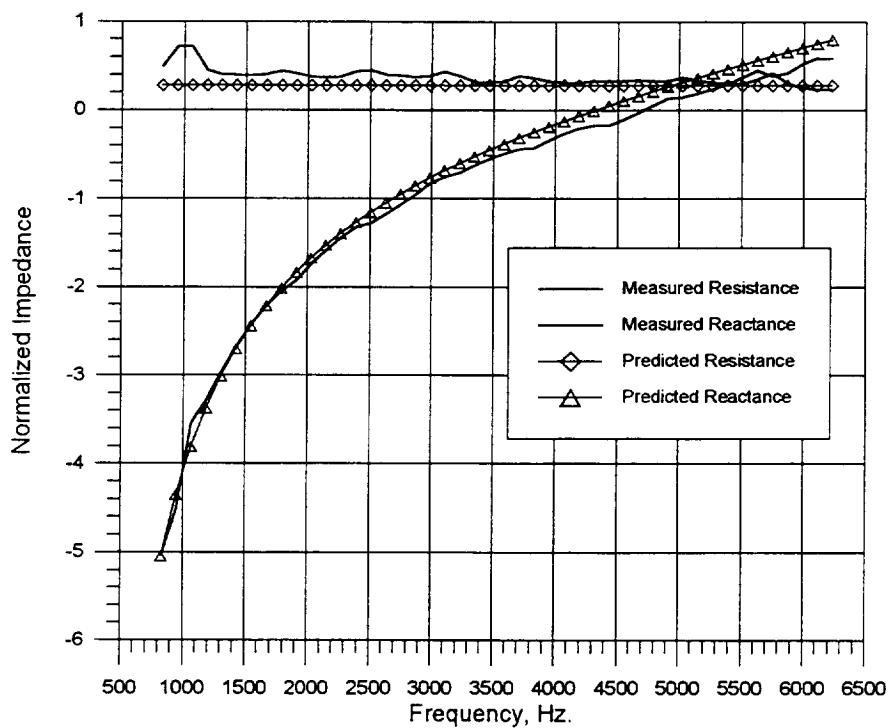
Figure (5-1) **Comparison of measured impedance to current model prediction for Configuration 1.**
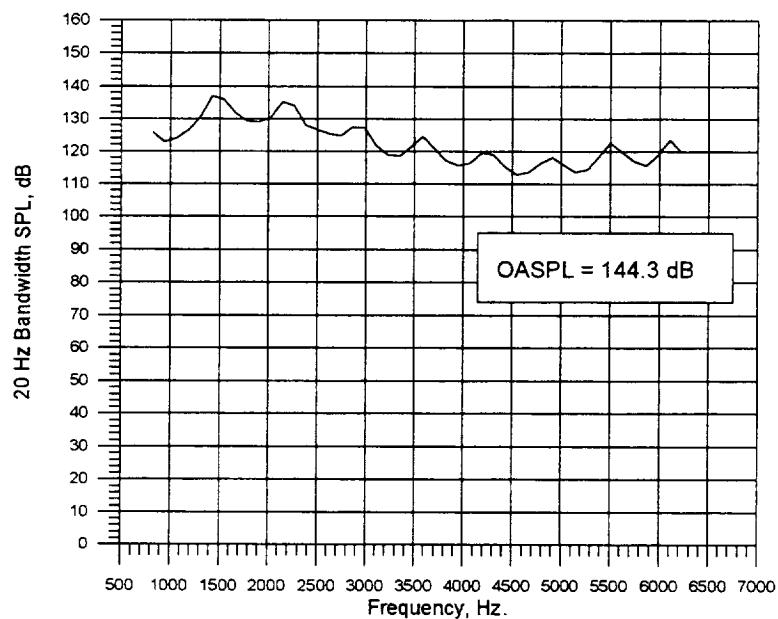

Figure (5-2) **SPL spectrum for Configuration 1.**

49

Figure (5-3) compares the same measured impedance for Configuration 1 to predictions using the exact impedance model as described in Section 3. The exact model prediction includes two cases, one in which the end correction factor was set equal to zero (no-end correction) and the other in which it was set equal to 1.0 (full end correction). For this prediction, the Keith and John correlation for C_D was used, although the resulting C_D becomes just 0.76, based on the overall rms acoustic velocity in both cases.

Note that the case with no end correction is remarkably close to the measured reactance over the full frequency range and is close to the measured resistance above about 3300 Hz. The full end correction, grossly over-predicts the mass reactance, giving large discrepancies above about 1000 Hz. The resistance with full end correction is too high, although it appears to fit better below 2500 Hz.
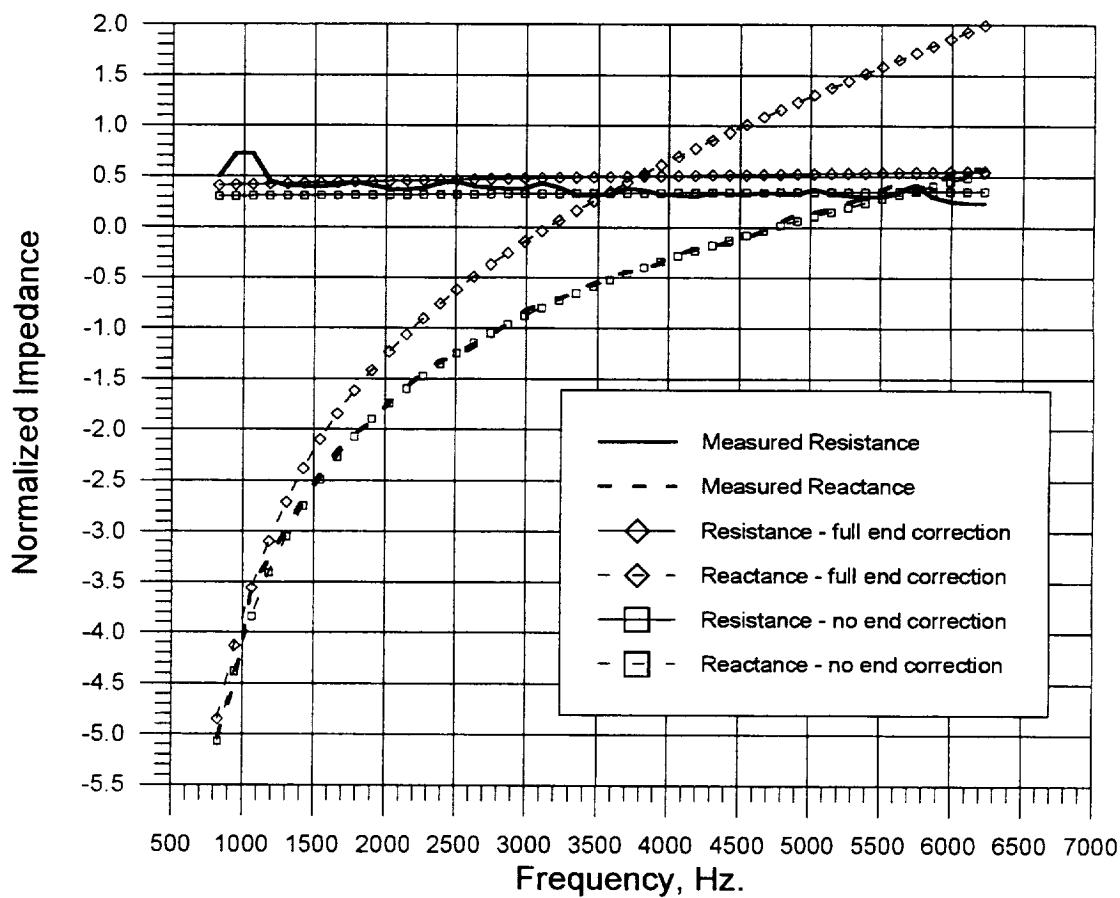

Figure (5-3)   Comparison of measured impedance to exact prediction with full and no end correction for Configuration 1.

Figure (5-4) compares the measured impedance to the exact model, using the empirical end correction and a C_D of 0.812, and to the current model, also using a C_D of 0.812. This C_D value is the best fit to the measured DC flow resistance data. Both prediction cases use the same empirical end correction and the same C_D, so that the only difference in the prediction model cases is the exact model resistance and mass reactance versus that for the current model. The exact model gives slightly higher resistance and mass reactance. For this case, the DC flow resistance best fit to the C_D value does not give appreciably better agreement with the measured impedance than the nominal value of 0.76.
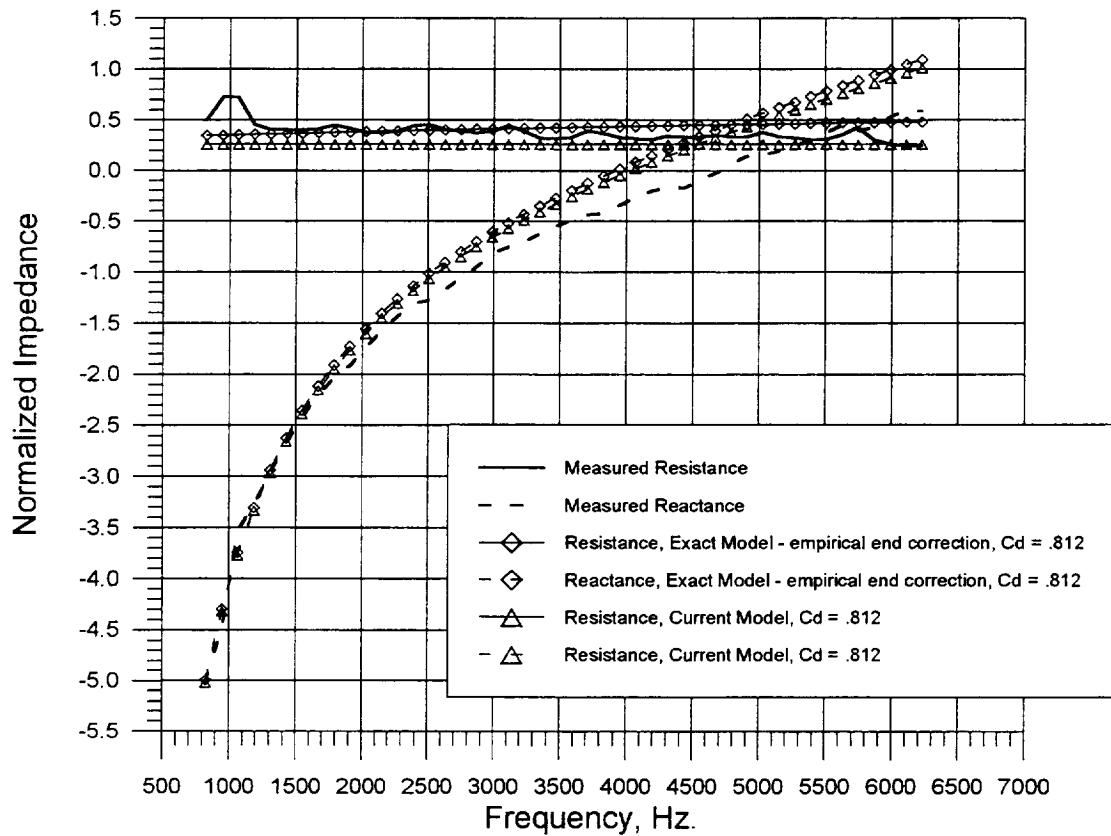
Figure (5-4)   **Comparison of measured impedance to exact prediction model and current model both using discharge coefficient of 0.812 for Configuration 1.**

Configuration 2

Configuration 2 is the high frequency measurement of Configuration 1 treatment panel, made in the 1.5 cm. normal incidence impedance tube. The measurement was made with broadband excitation and the data reduced in 40 Hz. bandwidths. The predictions are made at the same frequencies as the measurement.

51

The overall SPL is 130.7 dB in this case. Figure (5-5) compares the measured impedance with the prediction for the current model, using a C_D of 0.76. The agreement is very good up to about 9000 Hz., where the measurement is experiencing problems from the high magnitude of the impedance. Figure (5-6) shows the SPL spectrum for this case.
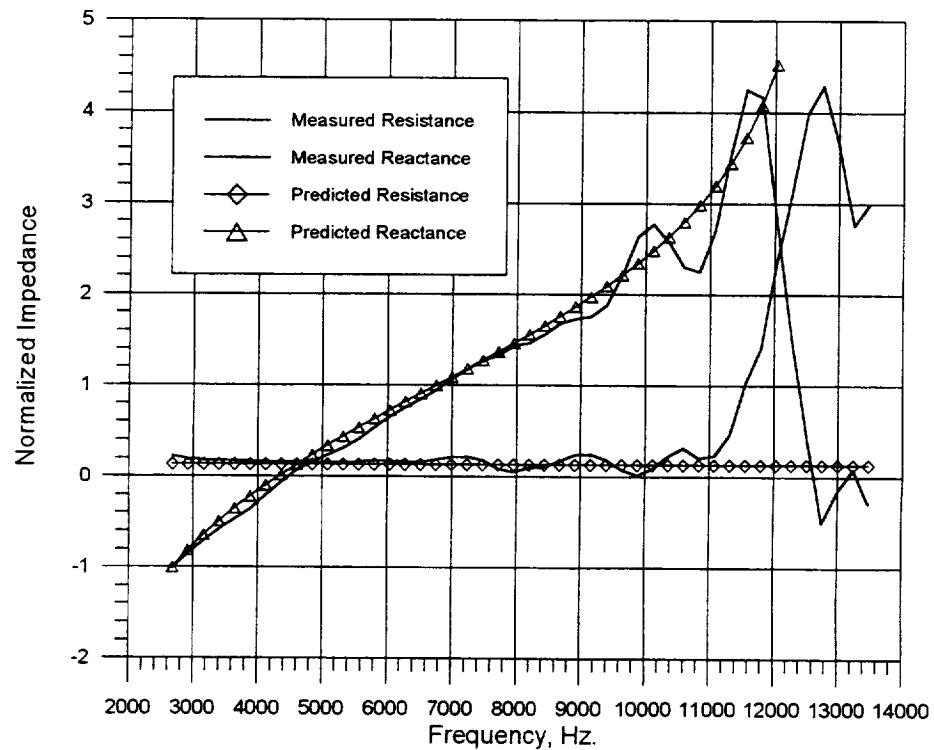

Figure (5-5)   **Comparison of measured impedance to current prediction model for Configuration 2.**
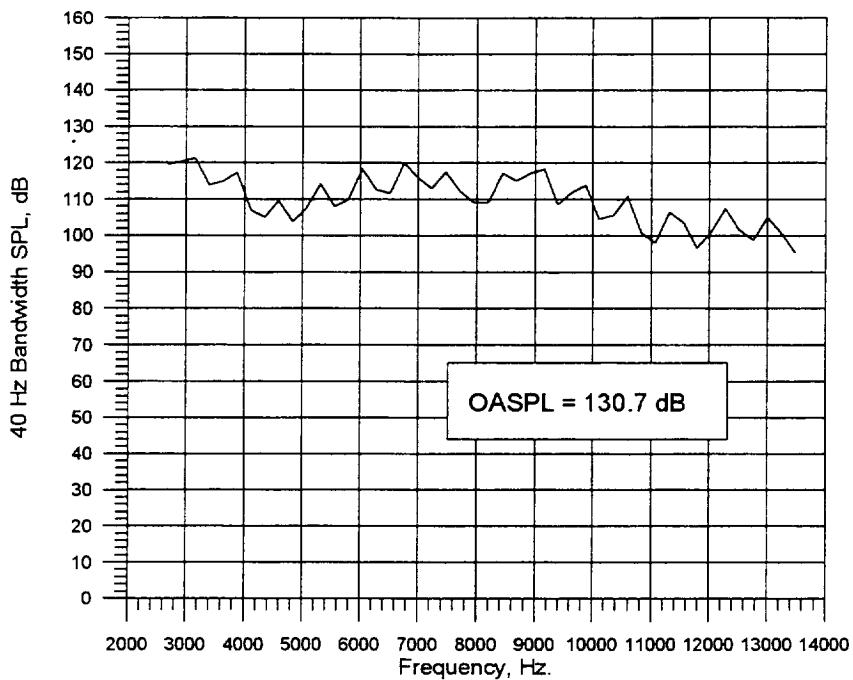
Figure (5-6) **SPL spectrum for Configuration 2.**

Figure (5-7) compares the measured impedance to the prediction using the exact model with the Keith and John C_D , with the full end correction and with no end correction. The C_D in this case does not achieve the nominal 0.76, becoming 0.740 with full end correction and 0.737 with no end correction.

Note that the no end correction case gives better agreement, as it did at the low frequencies, but that the mass reactance is slightly under-predicted. Choosing a small number for the end correction factor, say between 0.1 and 0.2, would have given a much better match to the measured reactance. The full end correction gives an extreme over-prediction of the mass reactance at the high frequencies. With the full end correction, the resistance prediction is too high, not much in absolute value but fairly high in percent difference, given the low value of measured resistance.
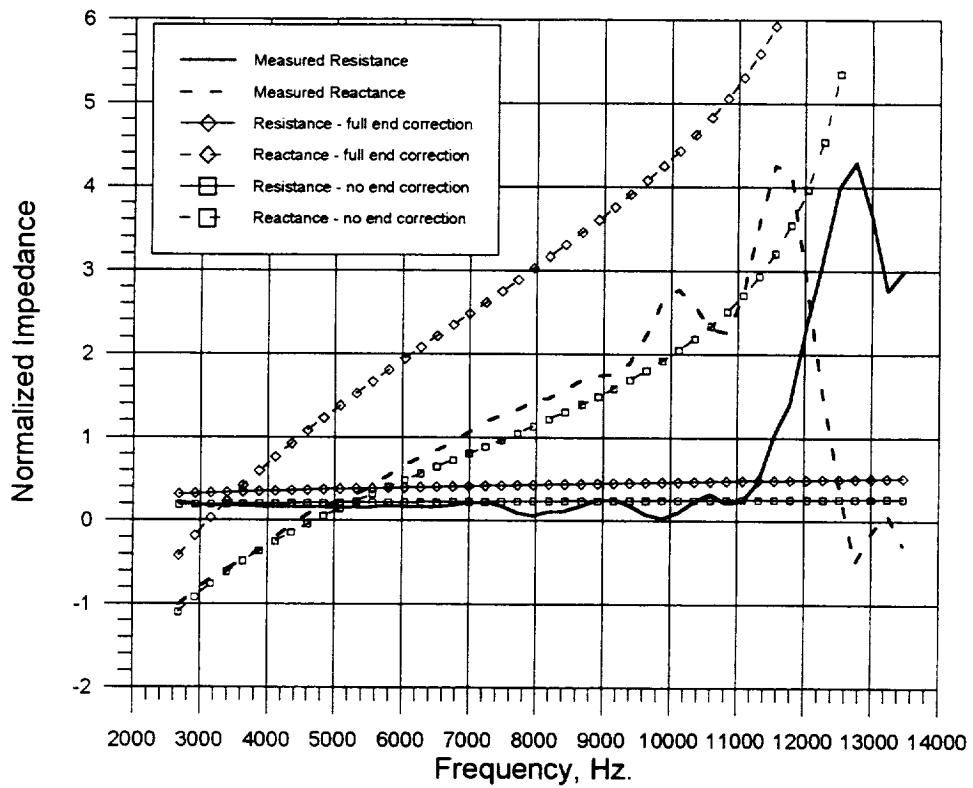
Figure (5-7) **Comparison of measured impedance to exact prediction model with full and no end correction for Configuration 2.**

Configurations 3 and 4

The panel used for Configurations 3 and 4 is a full-scale design with a porosity of 6.65%, which might be a bit lower than would be used in practice. The hole size and facesheet thickness are representative of full-scale designs. The impedance for Configuration 3 was measured in the 3.0 cm. impedance tube at low frequencies, with a broadband excitation of 139 dB SPL. The only difference for Configuration 4 is the overall excitation SPL is 10 dB higher at 149 dB. The data were reduced in 8 Hz. narrowbands, and the prediction is also made every 8 Hz.

Figure (5-8) compares the measured impedance with the impedance predicted using the current impedance model with a C_D of 0.76 for Configuration 3. The predicted and measured resistance agree quite closely, but the reactance prediction is too high, indicative of an over-predicted mass reactance. The measurement deviations from a smooth curve at both the low and high frequency ends is likely to be caused by measurement error. Figure (5-9) shows the excitation pressure spectrum for both Configurations 3 and 4.
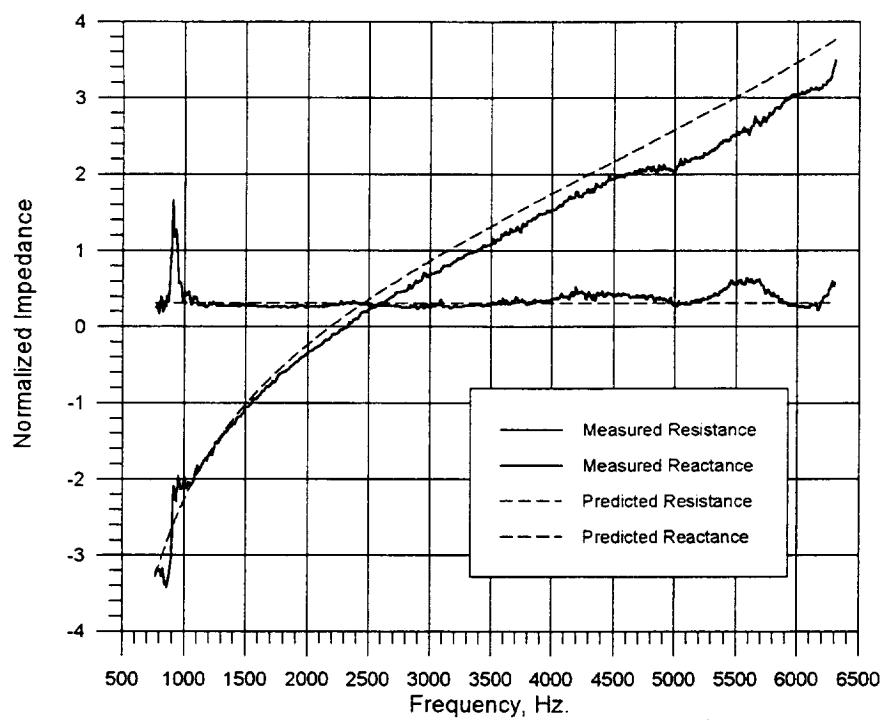
**Figure (5-8)**   **Comparison of measured impedance and current prediction model for Configuration 3.**
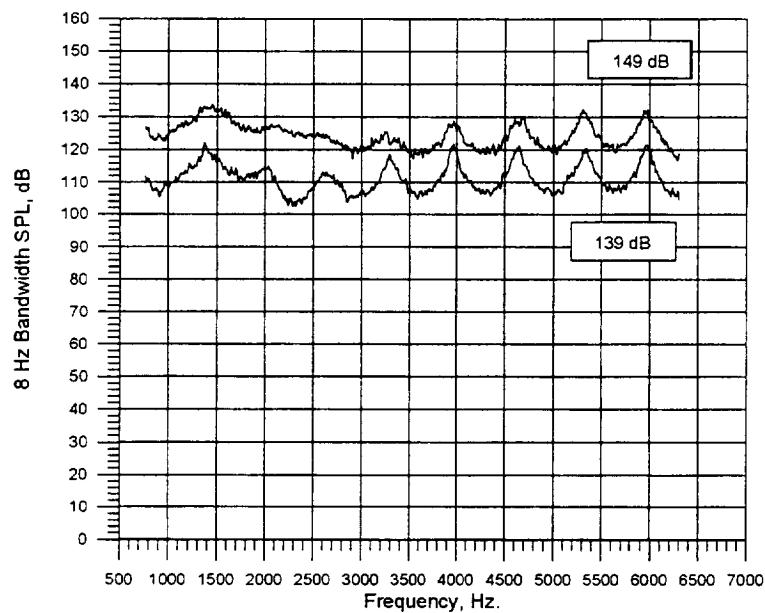
Figure (5-9)   **SPL spectra for Configuration 3 (149 dB overall) and Configuration 4 (139 dB overall).**

Figure (5-10) compares the measured impedance for Configuration 3 to the exact model with the Keith and John impedance model, with and without end correction. The effective C_D is 0.76 for both end correction cases. Note that the end correction makes little difference in the resistance prediction, but that the mass reactance predictions bracket the measured reactance. An end correction factor could be chosen to match the reactance curve quite closely, if desired.
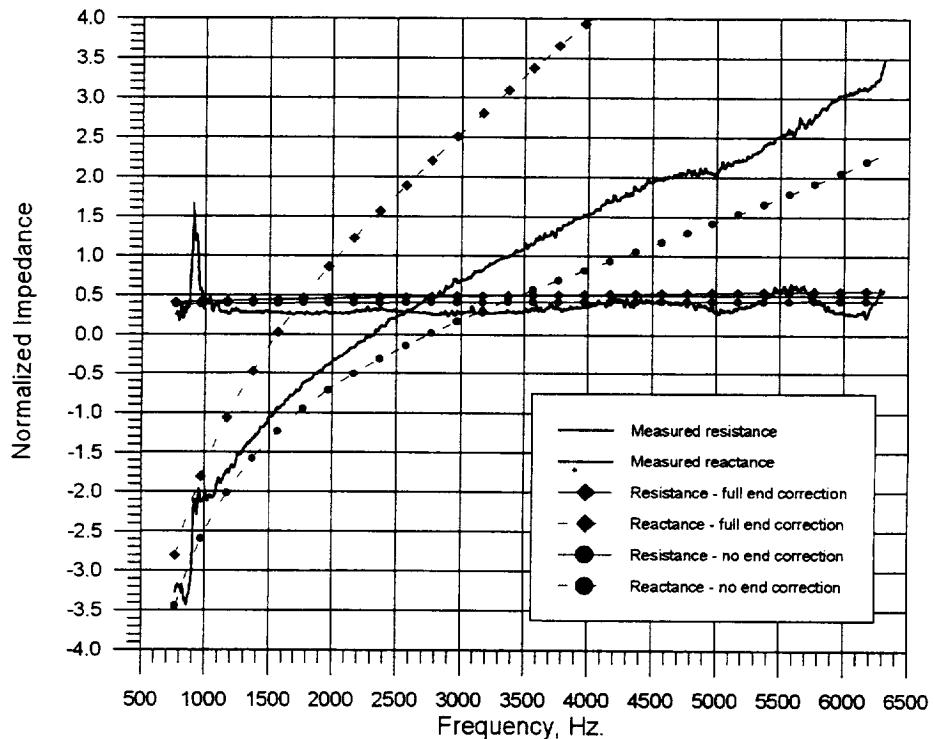
Figure (5-10)   **Comparison of measured impedance to exact prediction model with full and no end correction for Configuration 3.**

Figure (5-11) compares the measured impedance for Configuration 4 with the prediction from the current impedance model. The resistance is predicted quite well, indicating the model is accurately accounting for nonlinear resistance effects. The mass reactance has a higher over-prediction than the lower SPL case, a possible indication of nonlinear effects on mass reactance, which are not included in this model.
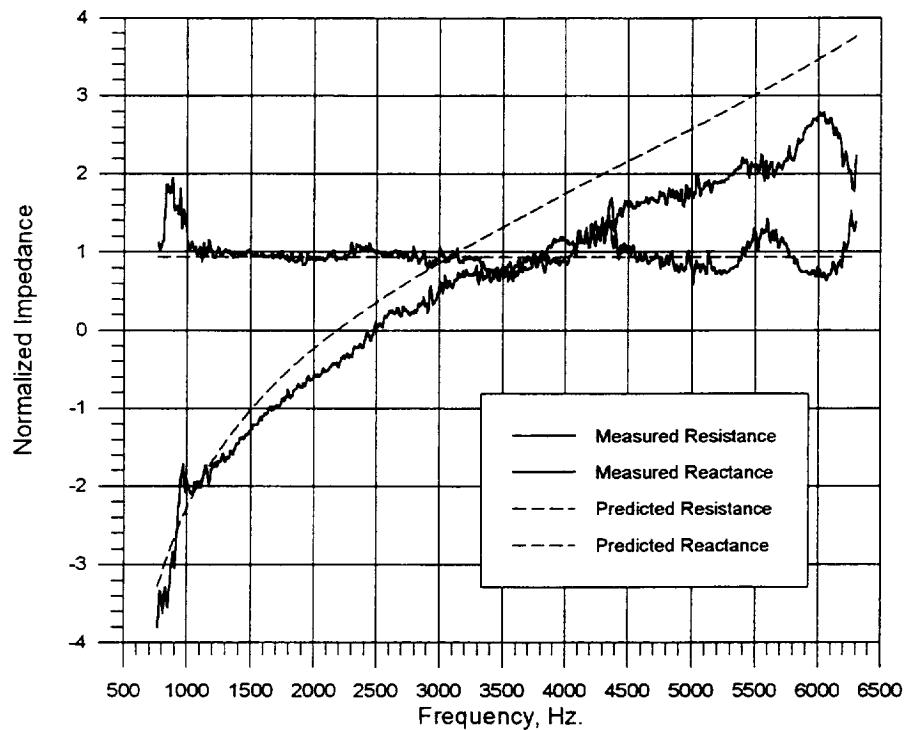
Figure (5-11)   **Comparison of measured impedance to current prediction for Configuration 4.**

The exact model with and without end corrections is compared to the measured data in Figure (5-12) for Configuration 4. The effective C_D is 0.76 for both end correction cases. The resistance prediction is very similar to the current model prediction, and matches the measurement quite well. The reactance with no end correction is just slightly below the measured reactance, indicating that the 149 dB SPL high intensity effects may extinguish the end correction almost entirely.
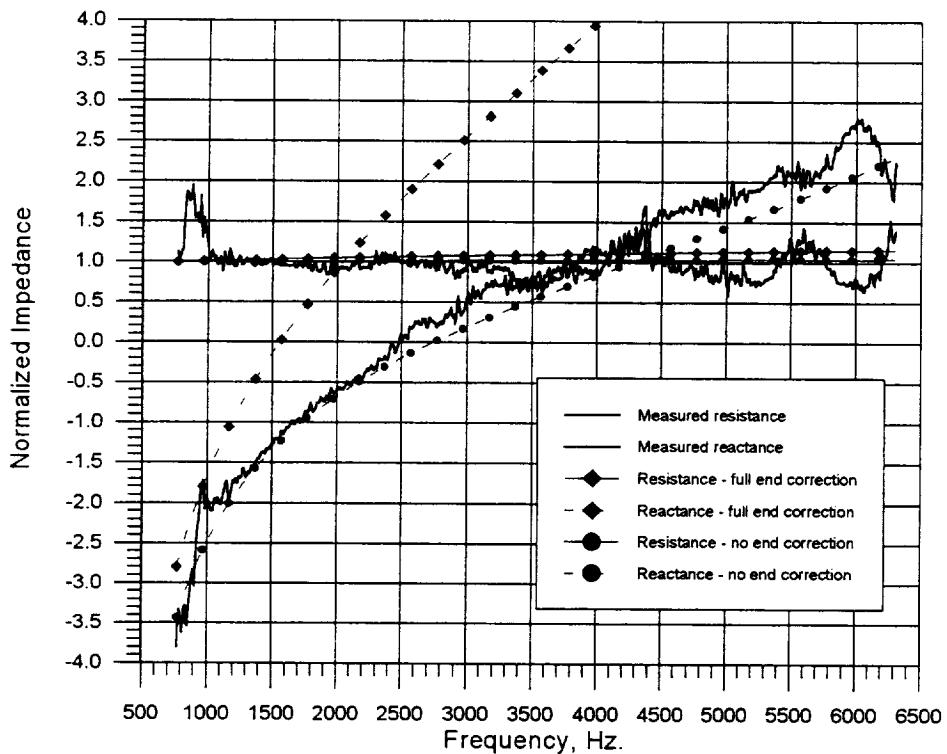
Figure (5-12)   **Comparison of measured impedance to exact prediction model with full and no end correction for Configuration 4.**

Configurations 5 and 6

Configurations 5 and 6 represent a 1/5 scale model panel design, with 8% porosity but with hole size and facesheet thickness reduced by the scale factor. The hole diameter in this case is representative of "micro-porous" linear facesheets, but the primary difference is that the microporous sheets would not have a reduced facesheet thickness, giving small holes with high thickness-over-diameter aspect ratio. The measurement for Configuration 5 was made in the 3.0 cm. normal incidence impedance tube, with broadband excitation of 145.9 dB overall SPL, and the data were reduced with 20 Hz. frequency resolution. The predictions were made at the same narrowband frequencies as the measurement.

Figure (5-13) compares the measured impedance with the prediction from the current model for Configuration 5 for the low frequency range. The prediction matches the measurement fairly well. Deviation at the low frequency end may be due to measurement problems. Figure (5-14) shows the SPL excitation spectrum for this case.
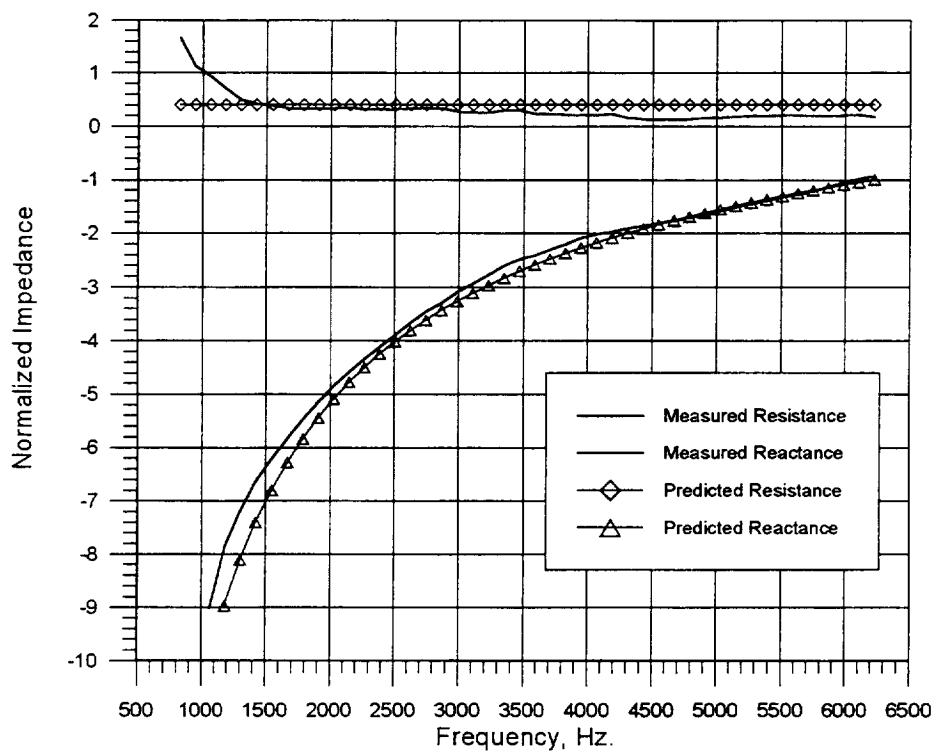
Figure (5-13)   **Comparison of measured impedance to current prediction model for Configuration 5.**
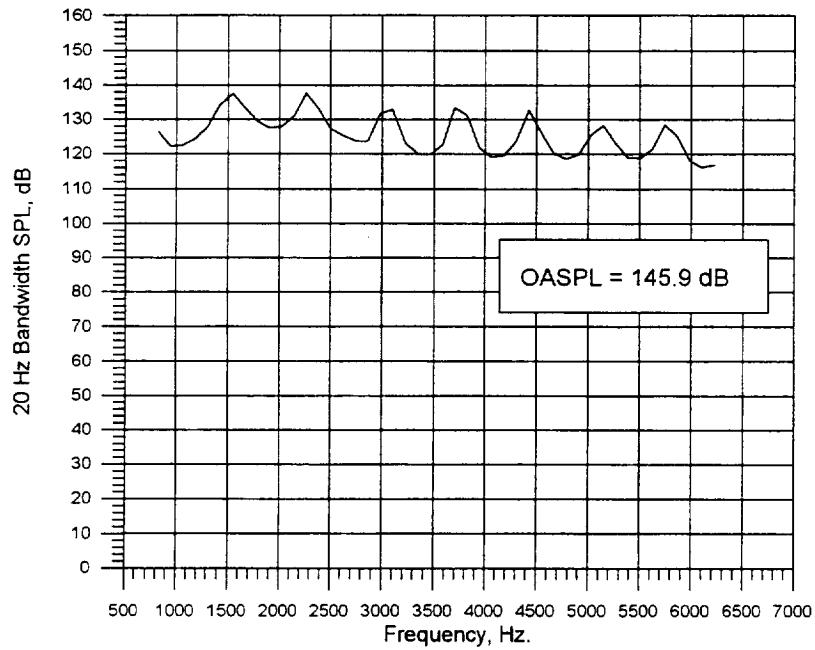
Figure (5-14) SPL spectrum for Configuration 5.

The measured impedance and the prediction for the exact models with and without end corrections are shown for Configuration 5 in Figure (5-15). The effective C_D for both end correction cases is 0.76. The upper and lower end correction bands for the predicted impedance in this case bracket the reactance curve much more closely than previous cases. The resistance is predicted most closely by the no end correction case. Deviation at the very low frequencies may be due to measurement error. As we tend toward the upper frequency limit, the no end correction case is giving better agreement to the measured reactance.
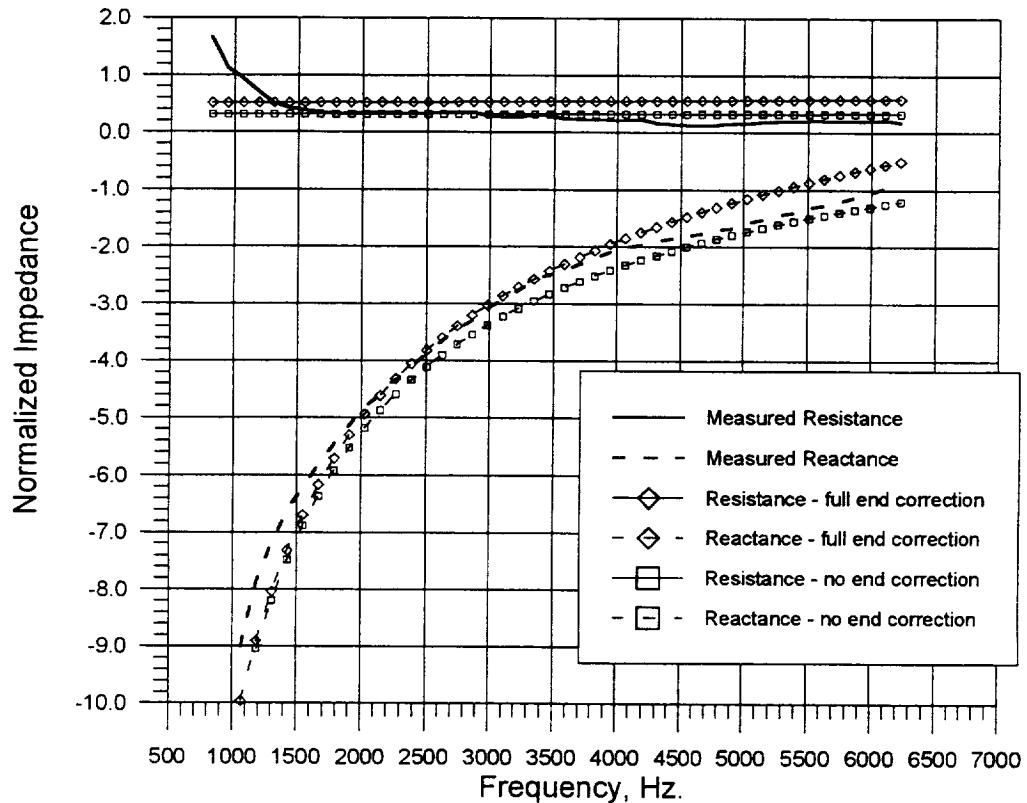
**Figure (5-15)**   **Comparison of measured impedance to exact prediction model with full and no end correction for Configuration 5.**

Figure (5-16) compares the measured impedance with the prediction from the current model for Configuration 6 for the high frequency range, where the frequency resolution is now 40 Hz. The prediction is made with two different C_D values, the nominal 0.76 and the DC flow resistance best fit value of $C_D = 0.972$. The prediction matches the measurement fairly well for $C_D = 0.76$ and extremely well for $C_D = 0.972$. Deviation at the low frequency end may be due to measurement problems. Figure (5-17) shows the SPL excitation spectrum for this case.
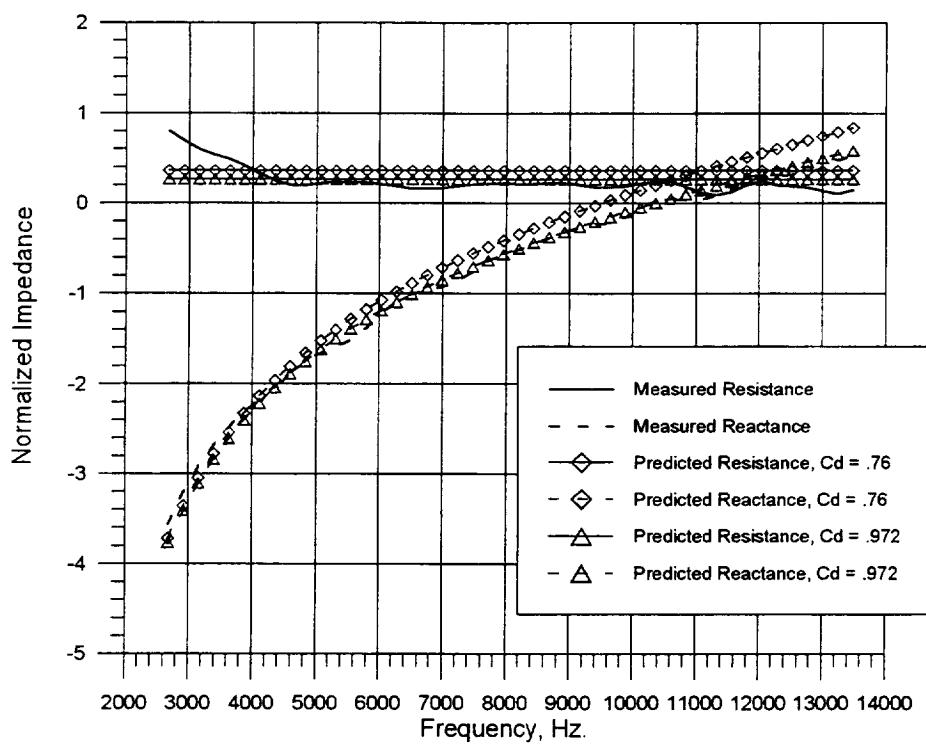
Figure (5-16)   **Comparison of measured impedance to current prediction model using two different discharge coefficient values for Configuration 6.**
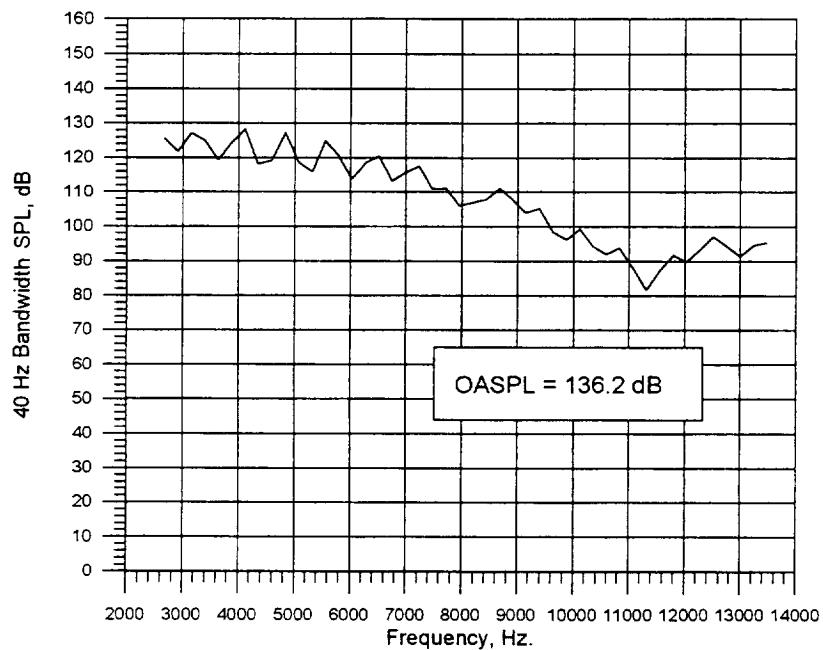

Figure (5-17) SPL spectrum for Configuration 6.

The measured impedance and the prediction for the exact models with and without end corrections are shown for Configuration 6 in Figure (5-18). The effective C_D for both end correction cases is 0.76. The resistance and reactance are both predicted most closely by the no end correction case, where the agreement is excellent.
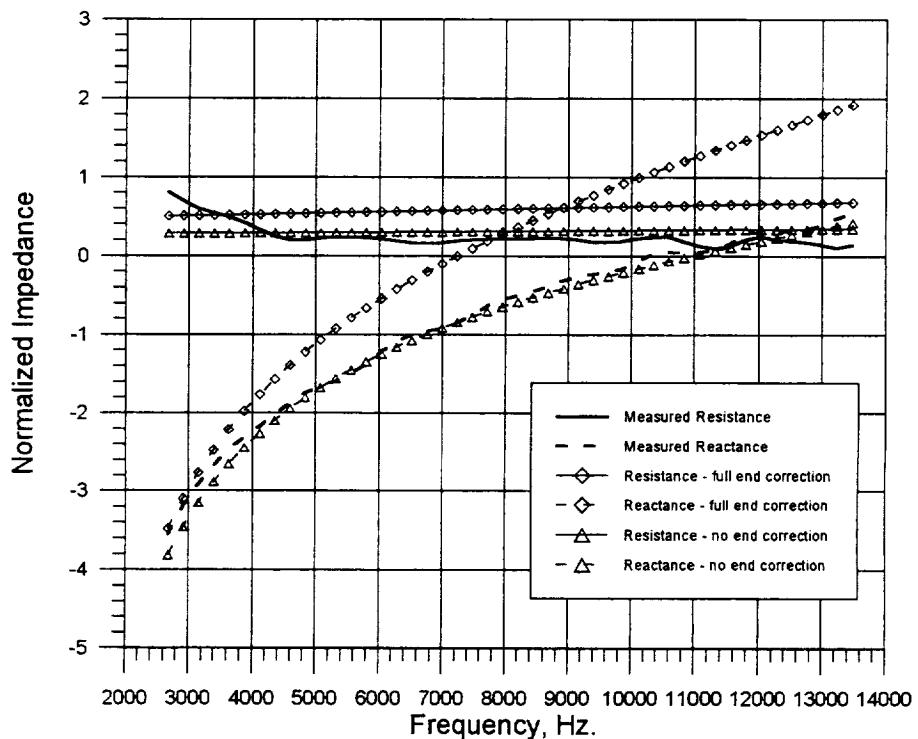

Figure (5-18)   Comparison of measured impedance and exact prediction model with full and no end correction for Configuration 6.

5.2 Observations

The potential for excellent agreement between measured and predicted impedance is seen for almost all cases. The main problem is that the fit requires the choice of a mass reactance end correction factor which is not known a priori and for which no universally-accepted general model is available. The determination of the proper end correction factor would, in general, require an extensive parametric study in which the porosity and hole geometry were varied, and in which the discharge coefficient were a topic of investigation as well.

The data were too limited to draw conclusions about whether the DC flow best fit C_D value gave any improvement in the fit, although it did work well in one case. The empirical mass reactance end correction is not too bad an approximation, giving roughly the same curve one would have gotten by choosing the proper end correction factor for the exact model.

No unexpected high frequency effects were found in the measured data up to the highest measurement frequency of 13,400 Hz., which is twice the highest frequency studied previously. This gives encouragement that the frequency effects will behave as expected under another doubling of upper frequency. It appears to be fortunate that the end correction effects on mass reactance up to the highest frequencies seem to be minimal, so that the mass reactance does not increase with frequency as rapidly as it might. In many cases, the best fit to the measured data required elimination of the end correction entirely. The effects of grazing flow should further reduce the end correction.

5.3 Application to Linear Facesheet Liners

5.3.1 Linear Facesheet Impedance Models

The standard method for handling the prediction of impedance for linear facesheet liners is to assume that the resistance of the facesheet can be determined from the DC flow resistance measurement and that the mass reactance is either zero or a nominally small amount (typically about 0.15 ρc). Fundamental assumptions for using the DC flow resistance are that the A- and B-values measured under steady flow conditions can be used with the rms overall acoustic velocity replacing the steady flow velocity and that A and B are not themselves functions of frequency.

There are several different types of so-called "linear" facesheet liners. One type is fabricated from compressed and sintered randomly oriented metallic fibers, usually bonded to a high open area (that is, from 25% to 35% porosity) perforated support sheet. Another is the "microporous" or "millipore" design, in which extremely small holes, usually less than 0.010 inches in diameter, are laser drilled or etched into an otherwise standard thickness sheet. The small hole size and relatively long hole length makes the linear viscous contribution to the resistance high compared to the nonlinear component.

The type of linear facesheet with which we will be exclusively concerned in this study is the fine-weave wiremesh sheet, either bonded to a perforated plate support or used in isolation. Typical wire diameters for the wiremesh sheets range from a maximum of about 6 mils (0.006 inches) down to 10 microns (about 0.4 mils or 0.0004 inches). Such liners have been in service in aircraft engines for many years, those built by Rohr, Inc. having the designation "DynaRohr".

A further advantage of linear liners is that they are known to be relatively unaffected by grazing flow. Perfectly linear liners to not exist: they are usually characterized by nonlinear factors (say $NLF_{150/20}$) on the order of 1.2 to 3.0, whereas perforates typically have nonlinear factors greater than 5.0.

Little published work has been done on the behavior of linear wiremesh liners. Two notable exceptions are the work of Rice[1] and of Hersh and Walker[2]. Both authors conclude, based on theory and corroborating experiment, that the grazing flow effects are negligible and that the DC flow resistance model applied to the acoustic case gives no problems up through the full scale frequency range.

Rice give a criterion for conditions under which frequency effects may begin to become important for wiremesh sheets, in terms of the wire diameter. This is

[1]   Rice, Edward J., "A Model for the Acoustic Impedance of Linear Suppressor Materials Bonded on Perforated Plate", NASA TM 82716, also AIAA 81-1999, October, 1981.

[2]   Hersh, A. S., and Walker B., "Effects of Grazing Flow on the Steady-State Flow Resistance and Acoustic Impedance of Thin Porous-Faced Liners", AIAA 77-1335, October, 1977.

$$f >> \frac{v}{2\pi d_w^2}$$

(5-1)

where v is the kinematic viscosity and d_w is the wire diameter. Figure (5-19) shows how this critical frequency varies with wire diameter in microns.
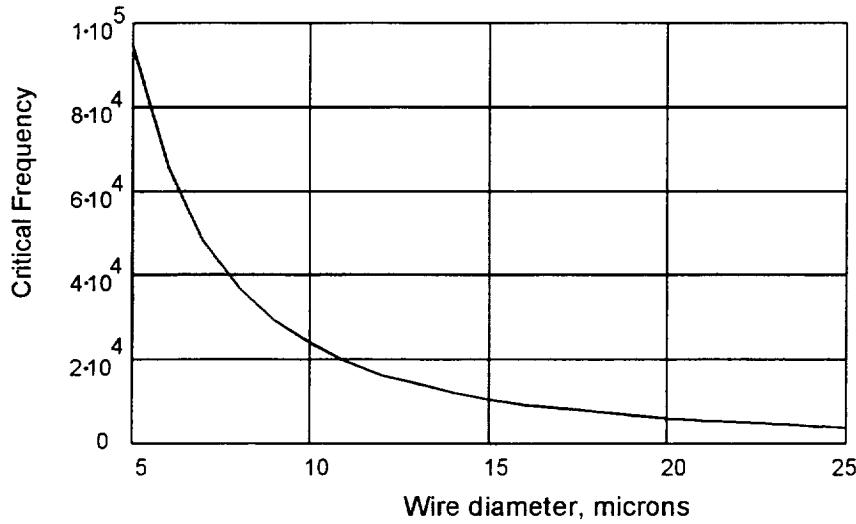
Figure (5-19)   **Critical frequency above which impedance of wiremesh facesheet may become frequency-dependent, as a function of wire diameter.**

Application of Rice's model for wiremesh faceplate impedance requires knowledge of the wire diameter and spacing of the screen, which is usually available from the manufacturer. The expression for resistance is

$$\frac{R}{\rho c} = \frac{R_{lin}}{\sigma_p \rho c} + \frac{1 - \sigma_{se}}{2c\sigma_p^2}\left(\frac{1}{\sigma_{se}^2} - 1\right)v_i + \frac{1 - \sigma_p}{2c\sigma_p^2}\left(1 - \sigma_p^2\right)v_i$$

(5-2)

where σ_p is the porosity of the perforated support sheet. The linear part of the resistance is given by

$$\frac{R_{lin}}{\rho c} = \frac{272.6\mu\left(1 - \sqrt{\sigma_{se}}\right)^2}{\rho c d_w},$$

(5-3)

where d_w is the wire diameter. The effective screen porosity, σ_{se}, is given by

$$\sigma_{se} = \left(0.95 + 36.56 d_w\right)\sigma_{sd}$$

(5-4)

where the reference porosity, σ_{sd}, is given by

$$\sigma_{sd} = \left(1 - \frac{d_w}{S_w}\right)\left[\sqrt{1 + \left(\frac{d_w}{S_w}\right)^2} - \frac{d_w}{S_w}\right] \tag{5-5}$$

where S_w is the wire spacing in the screen weave (projected on a plane parallel to the screen).

The various numerical constants were empirically-determined in the study by Hersh and Walker, from whom much of the model originated, as Rice points out. The resistance expression contains three terms; the linear viscous resistance due to the screen, the nonlinear resistance due to the screen and the nonlinear resistance due to the perforate. The small viscous resistance contribution from the perforate is neglected. The absence of a supporting perforated plate is equivalent to setting $\sigma_p = 1$. Note that the effect of the perforate on the resistance of the wiremesh alone is to increase it by the factor $1/\sigma_p$. This formulation should give A and B values quite close to those obtained from a DC flow resistance measurement.

An expression for the mass reactance, due primarily to Hersh and Walker, is

$$\frac{X_m}{\rho c} = \frac{k}{\sigma_p}\left[t_p + 0.43d_p + \frac{t + 0.52S_w\sqrt{\sigma_{se}}}{\sigma_{se}}\right] \tag{5-6}$$

where t_p is the thickness of the perforated support plate and d_p is the perforate hole diameter. The effect of the wiremesh covering the holes, Rice surmises, is to reduce the orifice end correction by half, explaining the 0.43 value. The 0.52 is an empirical result based on the studies of Hersh and Walker.

The mass reactance due to the screen alone is typically very small for fine screens at full scale operating frequencies. Figure (5-20) shows the predicted mass reactance as a function of frequency for a 400-mesh screen with wire diameter of 0.0025 cm, wire spacing of 0.0064 cm., and an effective porosity of 0.424 (this was one of the sample cases in Rice). At 10,000 Hz., there is only a contribution of 0.031 ρc to the reactance. The contribution goes up rapidly, however, as wire diameter increases, and it is also magnified by a factor of 3 to 4 if the wiremesh is supported by a perforated plate.

66
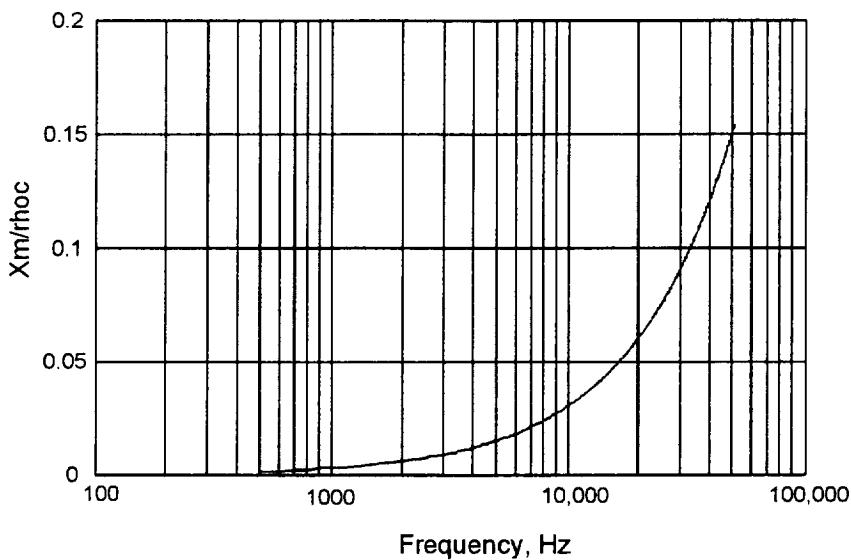
Figure (5-20) **Mass reactance of a 400 mesh wiremesh sheet predicted by Rice/Hersh/Walker model versus frequency.**

For further detail on the development of the models and their correlation with limited available experimental data, the reader is referred to the paper by Rice[1]. The Rice study gives a good idea of the parameters that are important to the impedance of the wiremesh and gives a feeling for the magnitude of the impedance as a function of frequency. For the current study, however, the resistance prediction was based on the DC flow measurement data, since this was readily available but the screen wire parameters were not. The simple empirical assumption of adding a constant mass reactance of 0.15 was also used. The Rice/Hersh/Walker model for wiremesh screen impedance would form an excellent foundation for further investigation, particularly a more comprehensive set of wiremesh screen DC flow resistance and normal incidence impedance measurements.

5.3.2 Comparison of Predicted and Measured Impedance

Four wiremesh liner configurations were tested as part of this program. There were two sets of two configurations each. Each set had a full scale design and a 1/5 scale design. The 1/5 scale design was aimed at being equivalent to the full scale design. The first set was designed to achieve a resistance (R_{100}) of about 80 cgs Rayls, the second set was designed to the lower R_{100} of about 50 rayls.

The full scale designs were for 1.0 inch deep treatment panels, and the wiremesh was supported by a 34% porosity perforated sheet. The 1/5 scale designs were 0.2 inches deep and had no supporting facesheet. Table (5-2) gives a complete set of parameters for the treatment designs. Table (5-3) presents the results of their DC flow resistance measurements.

Panel Designation	Faceplate Porosity	Faceplate Hole Diameter, in.	Faceplate Thickness, in.	Cavity Depth, in.
TP 4.3	0.34	0.05	0.025	1.0
TP-4.5	n/a	n/a	n/a	0.2
TP-5.3	0.34	0.05	0.025	1.0
TP-5.5	n/a	n/a	n/a	0.2

Table (5-2)   Geometric parameter definition for wiremesh test panels.

Panel Designation	R_{100} cgs Rayls	Nonlinear Factor, $NLF_{150/20}$	DC Flow A-Value	DC-Flow B-Value
TP 4.3	83.74	1.291	67.86	0.1588
TP-4.5	83.11	1.106	76.77	0.06342
TP-5.3	56.20	1.346	43.85	0.1234
TP-5.5	48.42	1.150	43.32	0.0510

Table (5-3)   Results of DC flow resistance measurements for wiremesh test panels.

The DC flow resistance measurements for the four wiremesh test panels is plotted in Figure (5-21), along with the best-fit linear curves from which the A- and B-values are derived. These measurements were made by Rohr, Inc, as part of this program.
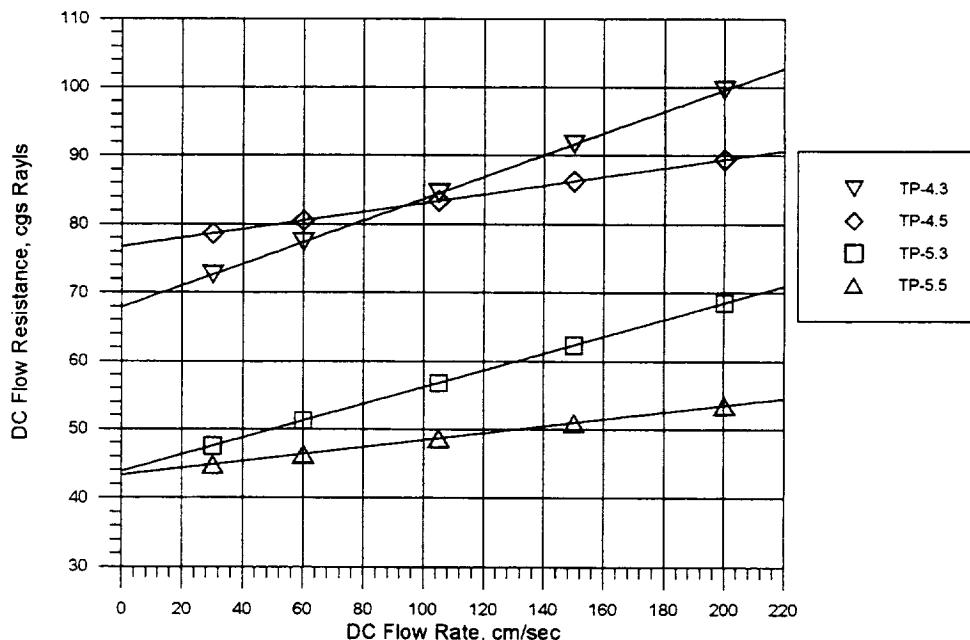
Figure (5-21)   DC flow resistance measurement results for four wiremesh facesheets, with linear best-fit curve.

Figure (5-22) compares the measured impedance for full scale TP-4.3 to the values predicted using the current model for wiremesh facesheet single-degree-of-freedom treatment panels. The measure impedance values are those measured in the 3.0 cm. normal incidence

impedance tube by Rohr over the low frequency range. The prediction is based on the values of A and B determined from the DC flow resistance measurement. The overall SPL for the broadband excitation for the normal incidence impedance measurement was 145.7 dB in this case. The prediction can be seen to be quite good up to about 5600 Hz, above which the measurement is encountering problems.
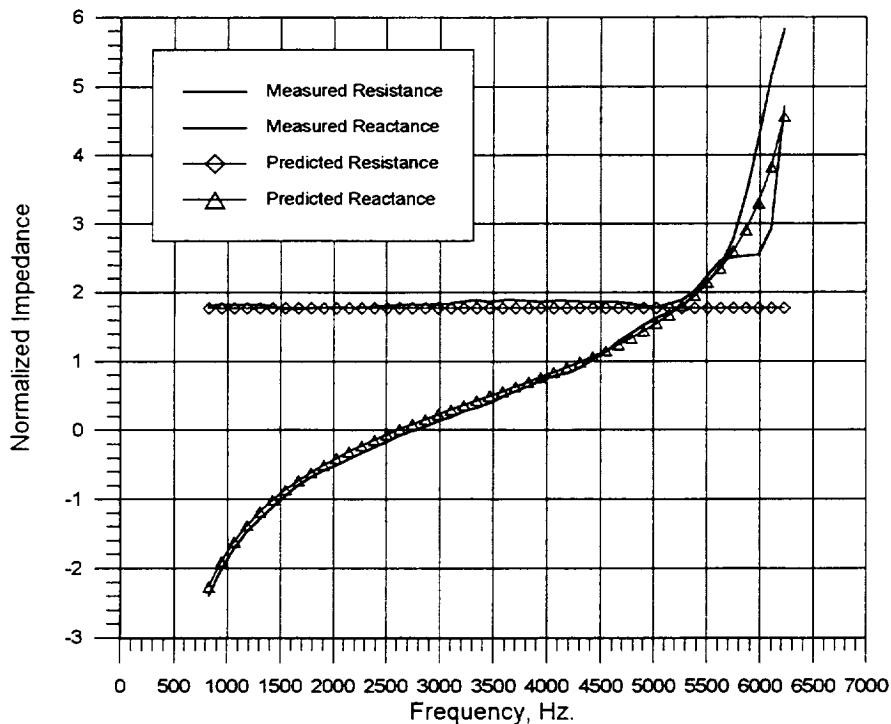
Figure (5-22)   **Comparison of measured impedance with current model prediction for TP-4.3.**

Figure (5-23) compares the prediction for 1/5 scale model TP 4.5 to the measured impedance data for the high frequency range. The current prediction model was used, and the measurement was made by Rohr over the high frequency range in the 1.5 cm. normal incidence impedance tube. The overall SPL in this case was 147.4 dB. The predicted reactance is quite close to the measured value up to about 10,000 Hz, where the measured reactance suddenly increases rapidly. The predicted resistance is flat, as expected, but the measured resistance seems to have a fairly wide variation. The predicted resistance is a good match to the average of the measured resistance. No explanation is offered for the variations in the measured impedance values, since the impedances are not sufficiently large near the deviations for them to be ascribed to measurement problems.

69
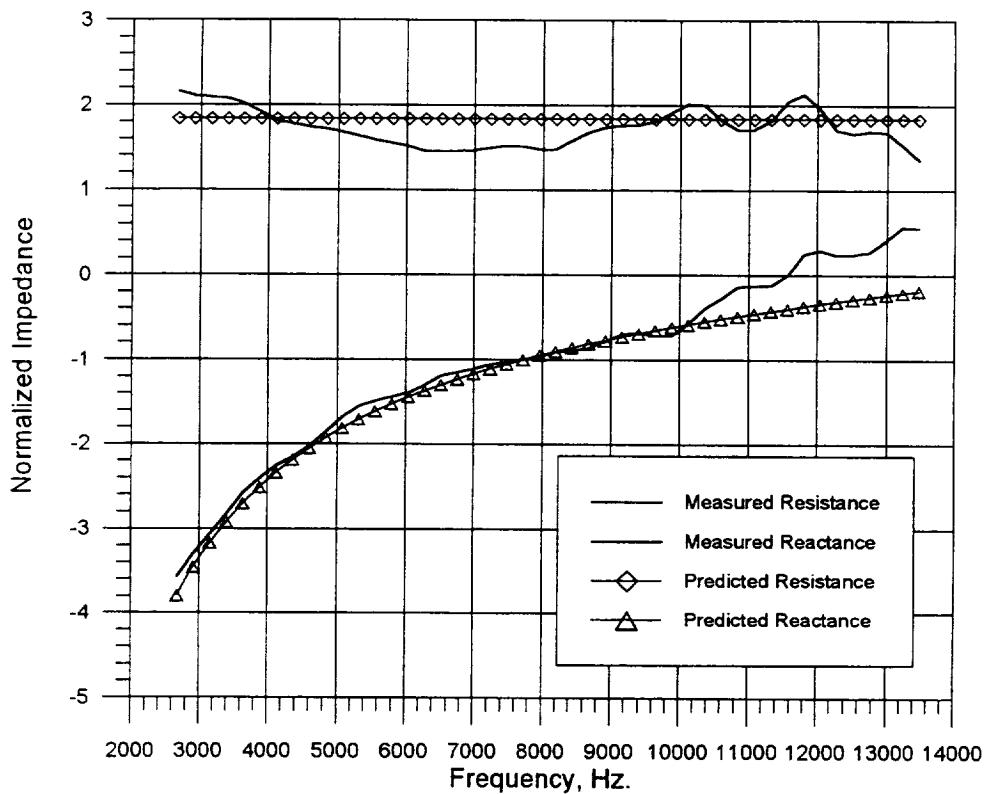
Figure (5-23)   Comparison of predicted and measured impedance for TP-4.5.

Figure (5-24) compares the measured impedance for full scale TP-5.3 to the values predicted using the current model for wiremesh facesheet single-degree-of-freedom treatment panels. The measure impedance values are those measured in the 3.0 cm. normal incidence impedance tube by Rohr over the low frequency range. The overall SPL for the broadband excitation for the normal incidence impedance measurement was 145.3 dB in this case. The prediction can be seen to be quite good up to about 5200 Hz, above which the measurement is encountering problems.

70
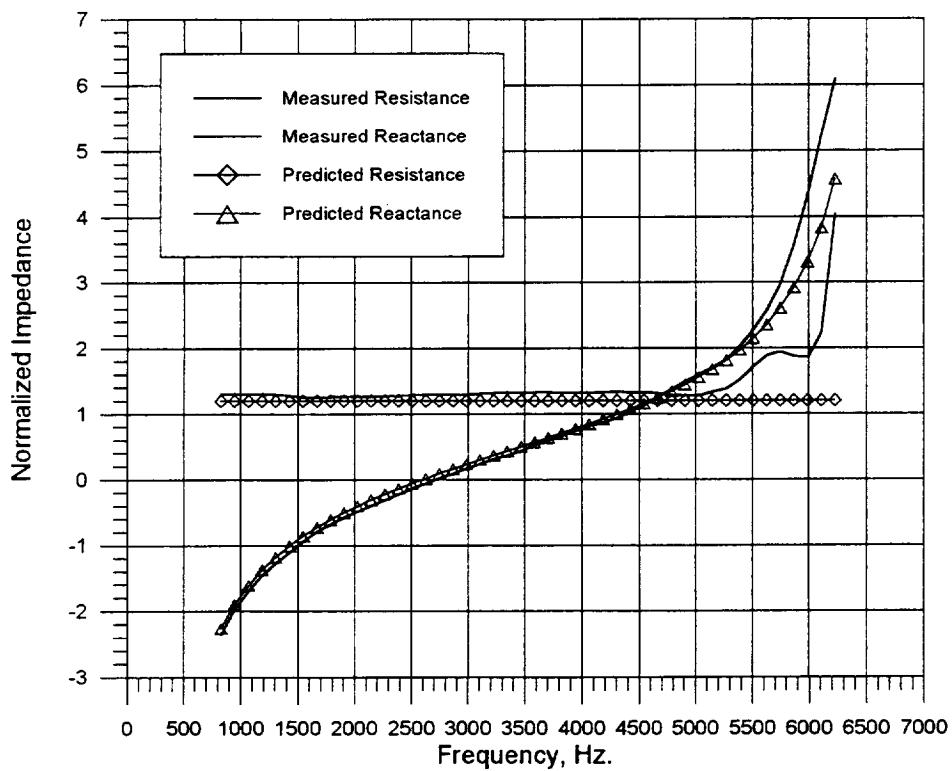
Figure (5-24)   **Comparison of predicted and measured impedance for TP 5.3.**

Figure (5-25) compares the prediction for 1/5 scale model TP 5.5 to the measured impedance data for the high frequency range. The current prediction model was used, and the measurement was made by Rohr over the high frequency range in the 1.5 cm. normal incidence impedance tube. The overall SPL in this case was 146.9 dB. The predicted reactance seems to under-predict the measurement. The measured reactance values seem to jump above 10,000 Hz., as they did in the TP 4.5 case. The predicted reactance is flat, as expected, but the measured resistance seems to have a fairly wide variation, as it did for TP 4.5. Again, the predicted resistance is a good match to the average of the measured resistance.
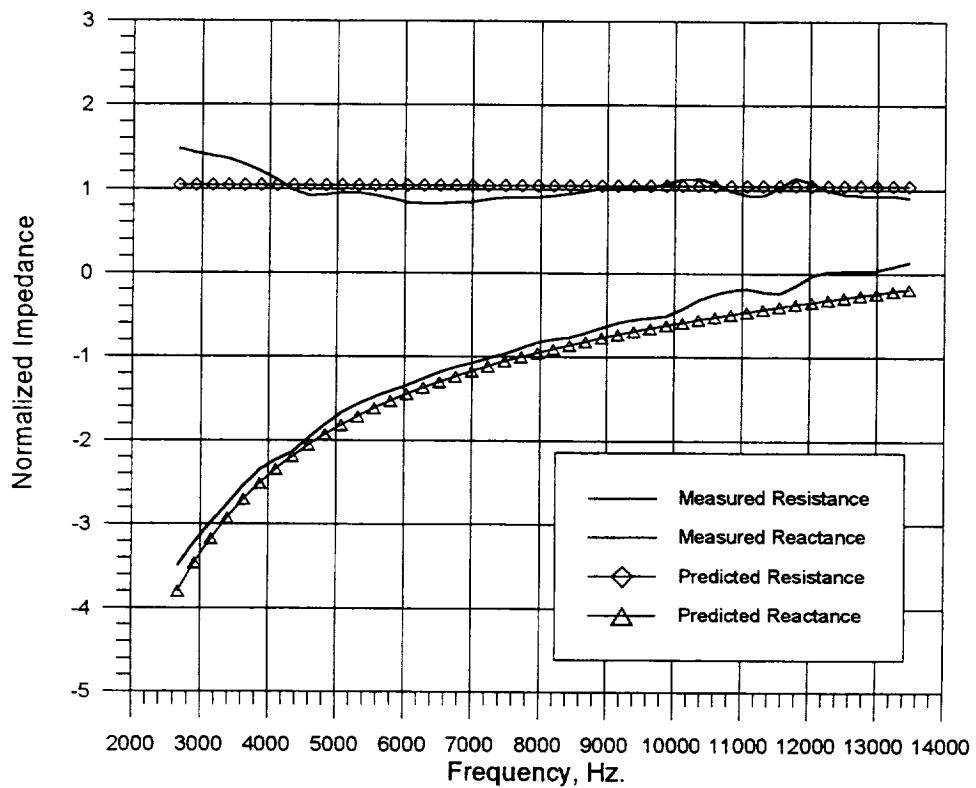
Figure (5-25)   **Comparison of predicted and measured impedance for TP-5.5.**

The SPL spectra for TP 4.5 and TP 5.5 are shown in Figure (5-26). The spectra closely resemble the spectra for the high frequency perforated plate cases considered previously, and give no indication of why the measured resistance for the 1/5 scale wire mesh cases might undergo such wide variation. One possibility might be a mechanical vibration of the wiremesh sheet without the perforated plate support over each open cell in the impedance tube.
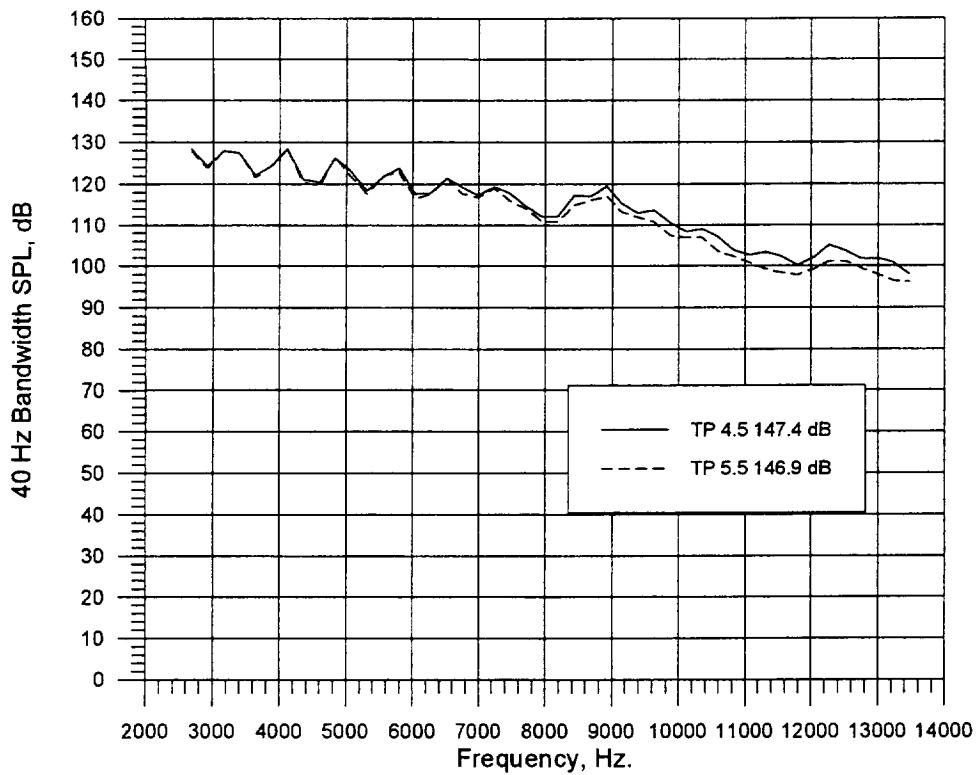
Figure (5-26)   **SPL spectra for TP 4.5 and TP 5.5.**

5.3.3 Conclusions

The comparisons of prediction and measurement indicate that the linear wiremesh facesheets are behaving close to predicted up to the highest frequencies. Some deviations are noted at the upper frequencies, but it is not clear at this point whether they are due to treatment behavior or measurement problems.

The impedance prediction model of Rice, Hersh, and Walker provides some insight to the behavior of linear wiremesh facesheets, but this model was not pursued to the fullest extent possible in this study. A more comprehensive examination of this model is warranted, but it would require an extensive concurrent test program to compare the prediction to measurement over a wide range of parameter variation and provide improvements to the empirical aspects.

The behavior of the wiremesh facesheet is more accurately predictable at high frequencies than the perforate, at least up to the maximum frequency studied of about 13,000 Hz. This is due to the small mass reactance contribution and the relative immunity to grazing flow effects. For this reason, it would make the best choice for scaled treatment design. From the results of Rice, however, it appears that it would be wise to scale the wire diameter, using a finer diameter wire for sub-scale designs, to minimize the effects of frequency on resistance mass reactance in frequency regions where they are not fully understood.

73

5.4 Advanced Impedance Model Prediction for High Frequencies

A sample computation was made in which the impedance of a conventional full scale perforate over honeycomb treatment panel was compared to the impedance of an equivalent 1/5 scale panel, with the scaled panel frequency range shifted to the full scale values. The full scale panel impedance was predicted up to 10,000 Hz. and the 1/5 scale panel impedance was predicted up to 50,000 Hz. The parameters used for the two panels, along with those for an "adjusted" 1/5 scale panel are listed in Table (5-4).

Parameter	Full Scale	1/5 Scale	1/5 Scale "Adjusted"
Porosity	0.08	0.08	0.95
Hole Diameter, in.	0.04	0.008	0.008
Thickness, in.	0.025	0.005	0.005
Cavity Depth, in.	1.0	0.2	0.2

Table (5-4)   Parameters for full scale and 1/5 scale treatment designs.

Figure (5-27) shows the comparison of the full scale impedance prediction and the 1/5 scale impedance prediction shifted to full scale frequencies. The predictions were made assuming an end correction factor of zero, that is, the end correction is eliminated. If the scaling were perfect, the curves would overlay. Note that the resistance and reactance of the 1/5 scale design are slightly higher than the full scale, indicating a frequency effect predicted by the model. The comparison is encouraging; however, the deviation would have been larger if an end correction were included.
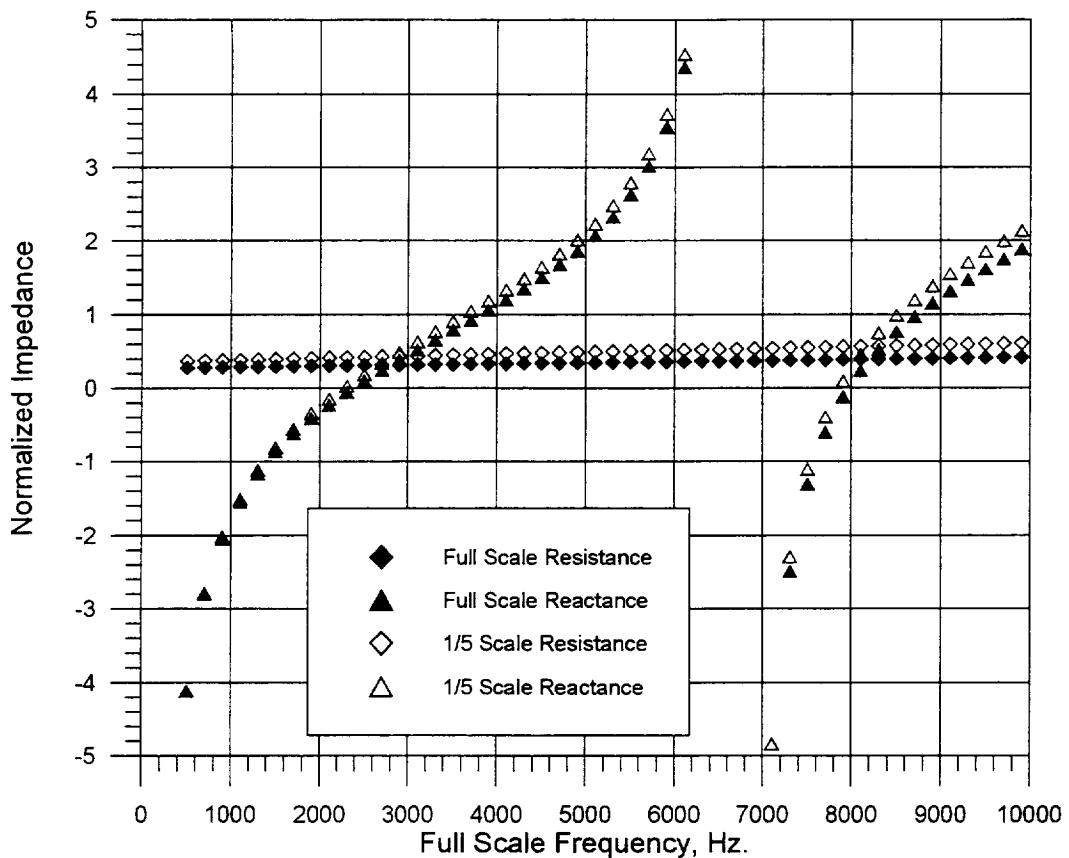
Figure (5-27)   Comparison of impedance predictions for full scale liner and 1/5 scale with frequency shifted to full scale.

Both the resistance and reactance can be decreased by increasing the porosity of the facesheet. The impedance of the 1/5 scale liner was re-predicted with the porosity adjusted by increasing it from 8.0% to the value of 9.5%. Figure (5-28) shows the comparison of the full scale liner to the adjusted 1/5 scale design. Note that the resistance is still slightly high but that the reactance is slightly low, and both are much closer than the previous case. This says that the reactance can be matched by appropriate adjustment of the faceplate porosity.

The resistance is closer, but in the final case, the match of resistance must also include the effects of grazing flow, for which the resistance will decrease with increasing porosity. The final match may require some adjustment in both porosity and cavity depth of the scaled panel to give the best match for a perforate plate resonator.

75
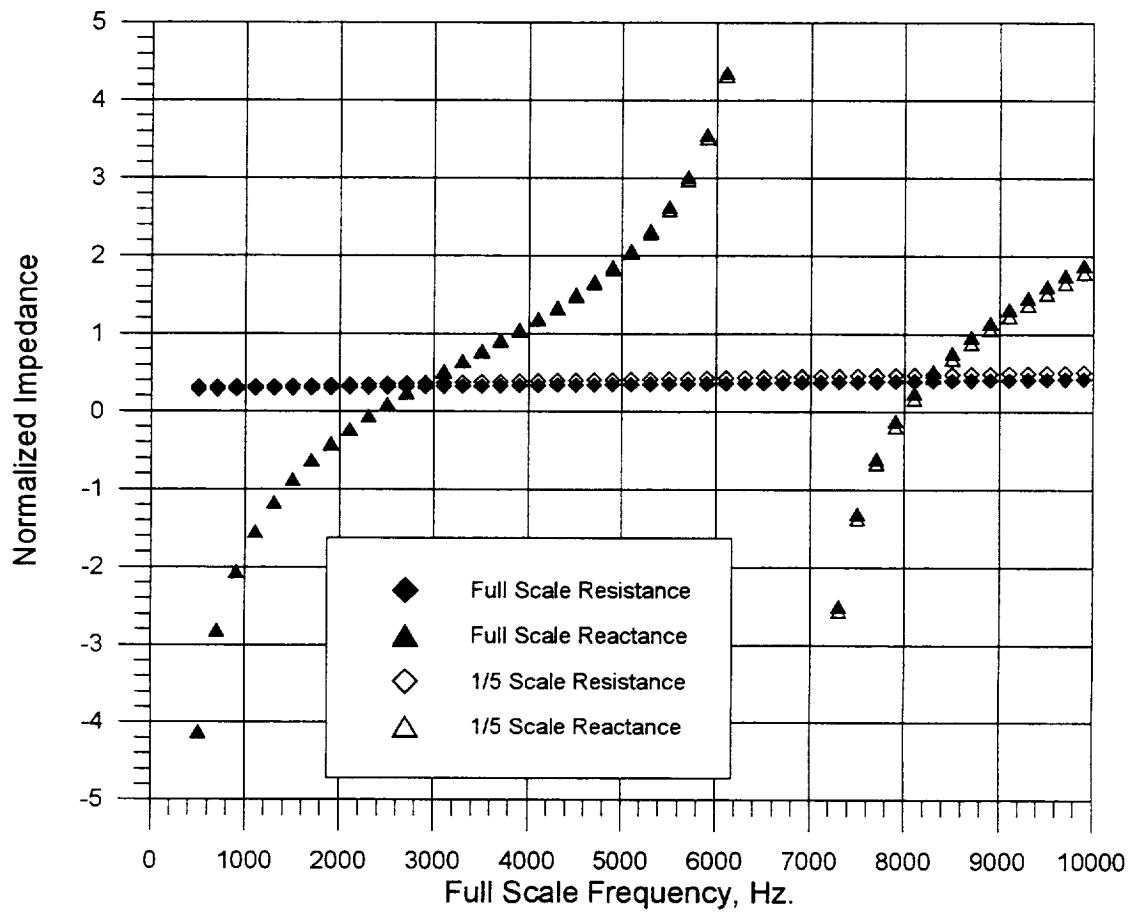
Figure (5-28)   Comparison of predicted full scale treatment impedance with adjusted scale model impedance shifted to full scale frequencies.

6. Conclusions and Recommendations

An advanced impedance prediction model has been developed that accounts for some of the known effects at high frequency that have previously been ignored as a small source of error for full scale frequency ranges. The model has been implemented in a computer program and used to compare with predicted data from the currently-used impedance model and with measured data for a number of treatment configurations of various scale.

Due to problems with measurements, it was not possible to obtain reliable measured data on the effects of grazing flow on impedance, so that this study has been limited to the case of no grazing flow only. Available studies of grazing flow impedance indicate that the frequency dependence of the grazing flow impedance component are minimal, but no data measured above about 5000 Hz. are available to corroborate this conjecture.

For broadband pressure excitation at high SPL levels such as will be experienced in an aircraft engine duct, the nonlinear effect on resistance tends to give a flat resistance spectrum over the full range of excitation frequencies. This appears to be verified by measurement for both full scale and sub-scale perforated plate treatment panels up to about 13,000 Hz.

The biggest problem encountered was accounting for the effects of the end correction on resistance and mass reactance. No comprehensive model was found that fit all cases, as the end correction has been found to vary in a complex manner with orifice Reynolds number, orifice geometry, and porosity. An extensive set of parametric measurements and concurrent theoretical investigations is needed if it is desired to develop a more universally-applicable model. The work of Rice and of Hersh and Walker have provided an excellent foundation on which to build the theoretical development.

Good agreement between predicted and measured impedance was found in the linear facesheet case when the DC flow resistance values are used to determine resistance, at least up to 13,000 Hz. The mass reactance issue is not so clear, but the mass reactance of a wiremesh facesheet is small. Further work to verify the model of Rice would be useful.

Based on this study, the outlook on ability to use scaled perforate facesheet single-degree-of-freedom resonator liners to represent full scale is encouraging. Care must be taken to make the proper adjustments in porosity and cavity depth of the scaled liner to best fit the full scale impedance.

A safer solution at this point is probably to use a linear wiremesh facesheet bonded directly to the honeycomb with no supporting perforate. Predicted and measured impedance for the linear single-degree-of-freedom panels agree quite well up to 13,000 Hz. The use of the wiremesh with no perforate support requires a small honeycomb cell size and may present bonding problems. The results of Rice indicate that it is important to scale the wire diameter when using wiremesh facesheets for scaled liners.

77

The conclusions in this study are restricted by the upper limit to the measurement frequency of 13,000 Hz. Extending to higher frequencies will require advanced measurement techniques both with and without grazing flow that are not yet available. It is highly recommended that any further effort include development of advanced impedance measurement methods.

7. Appendix A   Acoustic Impedance Prediction Program - PPZ4

A FORTRAN computer program was written to incorporate the elements of the advanced model described in Section 4. This section provides a Users' Guide, a sample input case, and a sample output case to illustrate the use of the program.

Input Data File Guide for Program PPZ4

DATA INPUT THROUGH ASCII DATA FILE PPZ4.DAT
USES FREE FORMAT AS FOLLOWS:

TDF	Temp, degF
SP	Porosity, sigma
DHIN	Hole diameter, inches
THKIN	Faceplate thickness, inches
HCAVIN	Cavity depth, inches
FMACH	Mach number
BLTIN	Boundary layer displacement thickness, inches
NUMFRQ	Number of frequencies
FRQ(J),SPL(J)	Frequency, SPL data
. . . . .	
. . . . .	Repeat NUMFRQ times

USER WILL BE ASKED TO INTERACTIVELY INPUT FOLLOWING DATA:

'FLNM'	Output data path/filename (max 30 char, put in single quotes)
IENDC	Option for mass reactance end correction model (=1 to use exact model) (=2 to use empirical model)
RECF,XMECF	Resistance and mass reactance end correction factors (0 to 1) (=1 for full end correction, = 0 for no end correction)
ICD	Index for C_D calculation option. (=1 to use internal Keith and John model) (=2 to input externally as a constant value)
CDINP	Value of C_D when ICD = 2

79

The input data must be stored in the ASCII file ppz4.dat in the same directory as the executable file ppz4.exe prior to each run. To save particular input data files, they must be saved under a separate name before modification.

A listing for a sample data case stored in ppz4.dat follows. The data is based on Test Panel 3.4 as measured by Rohr over the low frequency range.

```
70.
0.08
0.02
0.012
0.5
0.4
0.05
46
824,125.834
944,122.925
1064,123.975
1184,126.484
1304,130.644
1424,136.971
1544,135.971
1664,131.857
1784,129.459
1904,129.094
2024,130.403
2144,135.184
2264,134.177
2384,128.174
2504,126.563
2624,125.286
2744,124.826
2864,127.515
2984,127.354
3104,121.868
3224,118.916
3344,118.555
3464,121.384
3584,124.6
3704,120.94
3824,117.268
3944,115.699
4064,116.38
4184,119.565
4304,119.024
4424,115.358
4544,112.89
4664,113.604
4784,116.457
4904,118.153
5024,115.759
5144,113.636
```

```
5264,114.565
5384,118.426
5504,122.641
5624,119.858
5744,116.987
5864,115.722
5984,119.026
6104,123.642
6224,119.725
```

The output data for this case follows. The output was stored in the file named sample.out.

```
PROGRAM PPZ4
  IMPEDANCE OF PERFORATED PLATE SDOF LINER

  USES EXACT CRANDALL MODEL FOR LINEAR IMPEDANCE
  USES KIETH & JOHN MODEL FOR VARIABLE Cd
  USES OVERALL rms ACOUSTIC VELOCITY IN RESISTANCE


  POROSITY =        .0800
  FACEPLATE THICKNESS =        .0120 in       .0305 cm
  HOLE DIAM =        .0200 in        .0508 cm
  DEPTH =        .5000 in      1.2700 cm

  MACH # =        .4000
  B.L. DISPL THICKNESS =        .050000 in       .127000 cm
  TEMP =      70.0000 deg F    294.2611 degK

  SPEED OF SOUND =     34393.8500 cm/sec
  AMBIENT PRESSURE =     14.7000 psi
  AIR DENSITY =        .00119958 g/cm^3
  RHO*C =       41.2583 cgs Rayls

  INITIAL Cd =        .7600
  ABSOLUTE VISCOSITY =        .000181 poise
  KINEMATIC VISCOSITY =        .151076 cm^2/SEC
  EFFECTIVE KINEMATIC VISCOSITY =        .329346 cm^2/SEC

  OUTPUT FILE = sample.out


  USING EXACT MODEL FOR MASS REACTANCE END CORRECTION
  RESISTANCE END CORRECTION FACTOR =        .250
  REACTANCE END CORRECTION FACTOR =        .250

  GRAZING FLOW RESISTANCE/RHOC =        .9728
```

FREQ	SPL	RESIS	REACT	VELOC	Red	Cd
824.0	125.83	1.115	-4.937	1.874963	1.8797E+01	.5105
944.0	122.93	1.121	-4.221	1.554515	1.6709E+01	.4928
1064.0	123.97	1.120	-3.678	1.992273	1.9543E+01	.5164
1184.0	126.48	1.119	-3.250	2.975610	2.5536E+01	.5557
1304.0	130.64	1.120	-2.908	5.298336	3.8731E+01	.6132
1424.0	136.97	1.135	-2.629	11.941670	7.4230E+01	.6881
1544.0	135.97	1.137	-2.361	11.631460	7.2600E+01	.6859

IMPEDANCE BASED ON NARROWBAND SPL VALUES

1664.0	131.86	1.132	-2.111	7.927899	5.2988E+01	.6519
1784.0	129.46	1.132	-1.893	6.533078	4.5480E+01	.6336
1904.0	129.09	1.135	-1.709	6.735298	4.6575E+01	.6365
2024.0	130.40	1.140	-1.554	8.333391	5.5154E+01	.6565
2144.0	135.18	1.158	-1.433	15.103490	9.0795E+01	.7066
2264.0	134.18	1.158	-1.293	14.276960	8.6472E+01	.7024
2384.0	128.17	1.146	-1.129	7.722819	5.1890E+01	.6495
2504.0	126.56	1.147	-1.000	6.783287	4.6834E+01	.6372
2624.0	125.29	1.149	-.880	6.157930	4.3442E+01	.6279
2744.0	124.83	1.151	-.774	6.093249	4.3089E+01	.6269
2864.0	127.51	1.156	-.703	8.508214	5.6086E+01	.6585
2984.0	127.35	1.158	-.611	8.631233	5.6741E+01	.6598
3104.0	121.87	1.158	-.466	4.814629	3.6050E+01	.6037
3224.0	118.92	1.163	-.342	3.528707	2.8768E+01	.5727
3344.0	118.56	1.166	-.255	3.438740	2.8247E+01	.5702
3464.0	121.38	1.165	-.217	4.797457	3.5954E+01	.6034
3584.0	124.60	1.166	-.185	6.970667	4.7846E+01	.6398
3704.0	120.94	1.169	-.062	4.612730	3.4923E+01	.5995
3824.0	117.27	1.177	.073	3.000811	2.5685E+01	.5566
3944.0	115.70	1.183	.177	2.469299	2.2500E+01	.5373
4064.0	116.38	1.184	.235	2.647301	2.3578E+01	.5442
4184.0	119.57	1.180	.241	3.829983	3.0498E+01	.5809
4304.0	119.02	1.183	.319	3.536964	2.8815E+01	.5730
4424.0	115.36	1.195	.470	2.212574	2.0922E+01	.5265
4544.0	112.89	1.207	.606	1.583519	1.6901E+01	.4945
4664.0	113.60	1.207	.656	1.689655	1.7599E+01	.5006
4784.0	116.46	1.200	.646	2.366266	2.1870E+01	.5331
4904.0	118.15	1.197	.667	2.859355	2.4847E+01	.5518
5024.0	115.76	1.208	.799	2.054720	1.9936E+01	.5194
5144.0	113.64	1.220	.933	1.517942	1.6465E+01	.4906
5264.0	114.57	1.219	.970	1.665215	1.7439E+01	.4993
5384.0	118.43	1.207	.915	2.670427	2.3717E+01	.5450
5504.0	122.64	1.199	.863	4.447734	3.3998E+01	.5959
5624.0	119.86	1.208	.998	3.044653	2.5944E+01	.5580
5744.0	116.99	1.220	1.151	2.043254	1.9864E+01	.5188
5864.0	115.72	1.229	1.260	1.683529	1.7559E+01	.5003
5984.0	119.03	1.218	1.208	2.526214	2.2846E+01	.5395
6104.0	123.64	1.208	1.129	4.460852	3.4071E+01	.5961
6224.0	119.72	1.221	1.308	2.625728	2.3448E+01	.5433

```
URMS =   3.8435E+01 cm/sec
ACOUSTIC REYNOLDS # =   2.1276E+02
DISCHARGE COEFF =        .7575
```

IMPEDANCE VS. FREQUENCY USING OVERALL rms VELOCITY

FREQ	RESIS	REACT
824.0	1.209	-5.012
944.0	1.211	-4.316
1064.0	1.213	-3.771
1184.0	1.215	-3.330
1304.0	1.218	-2.964
1424.0	1.220	-2.656
1544.0	1.222	-2.391
1664.0	1.224	-2.159
1784.0	1.227	-1.955
1904.0	1.229	-1.773
2024.0	1.231	-1.610
2144.0	1.233	-1.461
2264.0	1.235	-1.325
2384.0	1.237	-1.199
2504.0	1.239	-1.083
2624.0	1.241	-.975
2744.0	1.243	-.874
2864.0	1.245	-.778
2984.0	1.246	-.688

```
3104.0    1.248    -.603
3224.0    1.250    -.521
3344.0    1.252    -.444
3464.0    1.254    -.369
3584.0    1.255    -.298
3704.0    1.257    -.229
3824.0    1.259    -.162
3944.0    1.260    -.098
4064.0    1.262    -.036
4184.0    1.263     .025
4304.0    1.265     .084
4424.0    1.267     .142
4544.0    1.268     .198
4664.0    1.270     .253
4784.0    1.271     .308
4904.0    1.273     .361
5024.0    1.274     .413
5144.0    1.276     .464
5264.0    1.277     .515
5384.0    1.279     .565
5504.0    1.280     .614
5624.0    1.282     .663
5744.0    1.283     .712
5864.0    1.285     .760
5984.0    1.286     .808
6104.0    1.288     .855
6224.0    1.289     .902
```

REACTANCE COMPONENTS

FREQ	WNK	Xm	-cot	Xtot
824.0	.151	.15496	-5.16694	-5.01198
944.0	.172	.17645	-4.49265	-4.31620
1064.0	.194	.19769	-3.96832	-3.77063
1184.0	.216	.21871	-3.54834	-3.32963
1304.0	.238	.23952	-3.20390	-2.96438
1424.0	.260	.26015	-2.91589	-2.65574
1544.0	.282	.28061	-2.67114	-2.39052
1664.0	.304	.30092	-2.46028	-2.15935
1784.0	.326	.32110	-2.27646	-1.95536
1904.0	.348	.34115	-2.11456	-1.77341
2024.0	.370	.36110	-1.97067	-1.60957
2144.0	.392	.38094	-1.84174	-1.46081
2264.0	.414	.40069	-1.72540	-1.32471
2384.0	.436	.42036	-1.61973	-1.19936
2504.0	.457	.43996	-1.52317	-1.08321
2624.0	.479	.45949	-1.43448	-.97499
2744.0	.501	.47897	-1.35260	-.87363
2864.0	.523	.49838	-1.27666	-.77828
2984.0	.545	.51775	-1.20594	-.68819
3104.0	.567	.53707	-1.13981	-.60275
3224.0	.589	.55634	-1.07775	-.52141
3344.0	.611	.57558	-1.01931	-.44374
3464.0	.633	.59477	-.96410	-.36932
3584.0	.655	.61394	-.91177	-.29783
3704.0	.677	.63307	-.86203	-.22897
3824.0	.699	.65217	-.81463	-.16246
3944.0	.721	.67124	-.76933	-.09809
4064.0	.742	.69028	-.72593	-.03564
4184.0	.764	.70930	-.68425	.02505
4304.0	.786	.72830	-.64413	.08417
4424.0	.808	.74726	-.60542	.14185
4544.0	.830	.76621	-.56799	.19822
4664.0	.852	.78514	-.53173	.25340
4784.0	.874	.80404	-.49653	.30751
4904.0	.896	.82293	-.46229	.36063
5024.0	.918	.84179	-.42892	.41287

5144.0	.940	.86064	-.39634	.46430
5264.0	.962	.87947	-.36447	.51500
5384.0	.984	.89829	-.33324	.56505
5504.0	1.005	.91708	-.30258	.61450
5624.0	1.027	.93586	-.27244	.66342
5744.0	1.049	.95463	-.24275	.71188
5864.0	1.071	.97338	-.21346	.75992
5984.0	1.093	.99212	-.18451	.80760
6104.0	1.115	1.01084	-.15586	.85498
6224.0	1.137	1.02955	-.12746	.90209

RESISTANCE COMPONENTS

FREQ	U	RRAD	A	B	RESIS
824.0	1.8405E+00	9.1342E-05	8.4745E-02	3.9441E-03	1.208808
944.0	1.5143E+00	1.2093E-04	8.6874E-02	3.9441E-03	1.210966
1064.0	1.9340E+00	1.5209E-04	8.9053E-02	3.9441E-03	1.213176
1184.0	2.8851E+00	1.8859E-04	9.1258E-02	3.9441E-03	1.215418
1304.0	5.1514E+00	2.2895E-04	9.3469E-02	3.9441E-03	1.217669
1424.0	1.1703E+01	2.7220E-04	9.5673E-02	3.9441E-03	1.219916
1544.0	1.1354E+01	3.2092E-04	9.7858E-02	3.9441E-03	1.222150
1664.0	7.6474E+00	3.7241E-04	1.0002E-01	3.9441E-03	1.224360
1784.0	6.2401E+00	4.2893E-04	1.0214E-01	3.9441E-03	1.226544
1904.0	6.4014E+00	4.8886E-04	1.0423E-01	3.9441E-03	1.228694
2024.0	7.9246E+00	5.5160E-04	1.0629E-01	3.9441E-03	1.230808
2144.0	1.4566E+01	6.1903E-04	1.0830E-01	3.9441E-03	1.232887
2264.0	1.3691E+01	6.8927E-04	1.1027E-01	3.9441E-03	1.234928
2384.0	7.2103E+00	7.6508E-04	1.1220E-01	3.9441E-03	1.236934
2504.0	6.2708E+00	8.4364E-04	1.1409E-01	3.9441E-03	1.238903
2624.0	5.6454E+00	9.2648E-04	1.1594E-01	3.9441E-03	1.240838
2744.0	5.5620E+00	1.0131E-03	1.1775E-01	3.9441E-03	1.242738
2864.0	7.8445E+00	1.1046E-03	1.1953E-01	3.9441E-03	1.244609
2984.0	7.9390E+00	1.1989E-03	1.2128E-01	3.9441E-03	1.246447
3104.0	4.3361E+00	1.2965E-03	1.2299E-01	3.9441E-03	1.248256
3224.0	3.1591E+00	1.3984E-03	1.2467E-01	3.9441E-03	1.250038
3344.0	3.0905E+00	1.5050E-03	1.2632E-01	3.9441E-03	1.251795
3464.0	4.3502E+00	1.6151E-03	1.2794E-01	3.9441E-03	1.253528
3584.0	6.3812E+00	1.7290E-03	1.2954E-01	3.9441E-03	1.255237
3704.0	4.2279E+00	1.8464E-03	1.3111E-01	3.9441E-03	1.256924
3824.0	2.7890E+00	1.9669E-03	1.3265E-01	3.9441E-03	1.258590
3944.0	2.3372E+00	2.0928E-03	1.3417E-01	3.9441E-03	1.260238
4064.0	2.5312E+00	2.2224E-03	1.3567E-01	3.9441E-03	1.261868
4184.0	3.6485E+00	2.3566E-03	1.3715E-01	3.9441E-03	1.263481
4304.0	3.4170E+00	2.4925E-03	1.3861E-01	3.9441E-03	1.265076
4424.0	2.2287E+00	2.6336E-03	1.4005E-01	3.9441E-03	1.266656
4544.0	1.6656E+00	2.7783E-03	1.4147E-01	3.9441E-03	1.268222
4664.0	1.7927E+00	2.9263E-03	1.4288E-01	3.9441E-03	1.269773
4784.0	2.4647E+00	3.0794E-03	1.4426E-01	3.9441E-03	1.271312
4904.0	2.9623E+00	3.2364E-03	1.4563E-01	3.9441E-03	1.272839
5024.0	2.2208E+00	3.3958E-03	1.4698E-01	3.9441E-03	1.274352
5144.0	1.7160E+00	3.5604E-03	1.4832E-01	3.9441E-03	1.275855
5264.0	1.8826E+00	3.7309E-03	1.4965E-01	3.9441E-03	1.277349
5384.0	2.8926E+00	3.9003E-03	1.5096E-01	3.9441E-03	1.278828
5504.0	4.6264E+00	4.0760E-03	1.5225E-01	3.9441E-03	1.280299
5624.0	3.3042E+00	4.2558E-03	1.5353E-01	3.9441E-03	1.281761
5744.0	2.3351E+00	4.4386E-03	1.5480E-01	3.9441E-03	1.283213
5864.0	1.9846E+00	4.6258E-03	1.5606E-01	3.9441E-03	1.284657
5984.0	2.8534E+00	4.8173E-03	1.5730E-01	3.9441E-03	1.286093
6104.0	4.7702E+00	5.0128E-03	1.5854E-01	3.9441E-03	1.287521
6224.0	2.9852E+00	5.2128E-03	1.5976E-01	3.9441E-03	1.288942

The first tabulation of output data give the impedance for the narrowband frequencies assuming the nonlinear resistance and reactance depends only on the SPL value in the

narrowband, not on the overall rms value. These impedances are used as initial values for the overall rms velocity nonlinear iteration, which follows. The second table of data is the final resistance and reactance at each frequency, suitable for pasting into a spreadsheet or plotting program.

The third data set is the details of the reactance computation, broken down into mass reactance and cavity compliance components. The final data set presents the components of the resistance computation, including acoustic velocity in the narrowband, the radiation resistance, and the A and B coefficients of the linear and nonlinear resistance.

8. Appendix B   Acoustic Treatment Scaling Chronological Bibliography

1930

1. Johansen, F. C., "Flow Through Pipe Orifices at Low Reynolds Numbers", Proc. Royal Society, Series A, 126, 1930, pp. 231-245.

1935

1. Sivian, L. J., "Acoustic Impedance of Small Orifices", J. Acoustical Soc America, Vol. 7, October 1935.

1949

2. Zwikker, C., and Kosten, C. W., *Sound Absorbing Materials*, Elsevier Publishing Company, 1949.

1950

3. Ingard, U., and Labate, S., "Acoustic Circulation Effects and the Nonlinear Impedance of Orifices", J. Acoustical Soc America, Vol. 22, No. 2, March 1950

1953

4. Ingard, Uno and Lyon, Richard, "The Impedance of a Resistance Loaded Helmholtz Resonator", J. Acoustical Soc America, Vol. 25, No. 5, 1953.

5. Ingard, Uno, "The Near Field of a Helmholtz Resonator Exposed to a Plane Wave", J. Acoustical Soc America, Vol. 25, No. 6, November 1953.

6. Ingard, Uno, "On the Theory and Design of Acoustic Resonators", J. Acoustical Soc America, Vol. 25, No. 6, November, 1953.

7. Lambert, Robert F., "A Study of the Factors Influencing the Damping of an Acoustical Cavity Resonator", J. Acoustic Society of America, Volume 25, No. 6, November, 1953.

1957

8. Bies, David A., and Wilson, O. B., "Acoustic Impedance of a Helmholtz Resonator at Very High Amplitude", J. Acoustical Soc America, Vol. 29, No. 6, June, 1957.

9. Kolodzie, P. A. and Van Winkle, Matthew, "Discharge Coefficients Through Perforated Plates", AIChE Journal, Vol. 3, No. 3, 1957.

10. Thurston, George B., Hargrove, Logan E., and Cook, Bill D., "Nonlinear Properties of Circular Orifices", J. Acoustical Soc America, Vol 29, No. 9, September 1957.

1958

11. Smith, P. L. and Van Winkle, Matthew, "Discharge Coefficients Through Perforated Plates at Reynolds Numbers of 400 to 3,000", AiChE Journal, Vol. 4, No. 3, 1958.

1967

12. Ingard, Uno, "Acoustic Nonlinearity of an Orifice", J. Acoustical Soc America, vol 42, No. 1, 1967.

1968

13. Ingard, Uno, " Absorption Characteristics of Nonlinear Acoustic Resonators", J. Acoustical Soc America, Vol.44, No. 4, 1968

14. Zorumski, William E. and Parrott, Tony L., "Nonlinear Acoustic Theory for Thin Porous Sheets", NASA SP-189, October, 1968.

1969

15. Groeneweg, John F., "Current Understanding of Helmholtz Resonator Arrays as Duct Boundary Conditions", NASA SP-207, 1969.

1970

16. Zinn, B. T., "A Theoretical Study of Non-Linear Damping by Helmholtz Resonators", J. Sound and Vibration, 13(3), 1970.

1971

17. De Mestre, N. J. and Guiney, D. C., "Low Reynolds Number Oscillatory Flow Through a Hole in a Wall", J. Fluid Mech, Vol. 47, part 4, 1971.

18. Rice, Edward J., "A Model for the Acoustic Impedance of a Perforated Plate Liner with Multiple Frequency Excitation", NASA TM X-67950, October, 1971.

1972

19. Ronneberger, D., "The Acoustical Impedance of Holes in the Wall of Flow Ducts", J. Sound and Vibration, 24(1), 1972.

1973

20. Leppington, F. G. and Levine, H., "Reflexion and Transmission at a Plane Screen with Periodically Arranged Circular or Elliptical Apertures", J. Fluid Mech., Vol. 61, part 1, 1973.

21. Melling, T. H., "The Acoustic Impedance of Perforates at Medium and High Sound Pressure Levels", J. Sound and Vibration, 29(1), 1973.

22. Reethof, G. and McDaniel, O.H., "Acoustically Absorbent Materials for Complex Incidence at High Sound Intensities and with Air Flow", Interagency Symposium on University Research in Transportation Noise, Proceedings, Vol. III, Stanford Univ., Mar 28-30, 1973.

23. Rice, Edward J., "A Model for the Pressure Excitation Spectrum and Acoustic Impedance of Sound Absorbers in the Presence of Grazing Flow", AIAA 73-995, October 1973.

1975

24. Guess, A. W., "Calculation of Perforated Plate Liner Parameters from Specified Acoustic Resistance and Reactance", J. Sound and Vibration, 40(1), 1975.

25. Hersh, A. S. and Rogers, T., "Fluid Mechanical Model of the Acoustic Impedance of Small Orifices", AIAA 75-495, March, 1975.

26. Mungur, P. and Whitesides, J. L., "Influence of Grazing Flow on Duct Wall Normal Impedances", AIAA 75-494, March 1975.

27. Rogers, T. and Hersh, A. S., "The Effect of Grazing Flow on the Steady State Resistance of Square-Edged Orifices", AIAA 75-493, March, 1975.

28. Tijdeman, H., "On the Propagation of Sound Waves in Cylindrical Tubes", J. Sound & Vibration, 39(1), 1975, pp. 1-33.

1976

29. Bauer, Andrew, "Impedance Theory and Measurements of Single- and Multi-Layer Liners in a Duct with Flow", AIAA 76-539, July, 1976.

30. Baumeister, Kenneth J., and Rice, Edward J., "Flow Visualization in Long Neck Helmholtz Resonators with Grazing Flow", AIAA 76-537, July, 1976.

31. Hersh, A. S. and Walker, B., "The Acoustic Behavior of Helmholtz Resonators Exposed to High Speed Grazing Flows", AIAA 76-536, July, 1976.

32. Zorumski, William E. and Tester, Brian J., "Prediction of the Acoustic Impedance of Duct Liners", NASA TM X-73951, September, 1976.

1977

33. Keith, T. G. and John, J. E. A., "Calculated Orifice Plate Discharge Coefficients at Low Reynolds Numbers", Transactions of the ASME, J. of Fluids Engineering, June, 1977.

34. Hersh, Alan S. and Walker, Bruce, "Fluid Mechanical Model of the Helmholtz Resonator", NASA CR-2904, September, 1977.

35. Hersh, A. S., and Walker B., "Effects of Grazing Flow on the Steady-State Flow Resistance and Acoustic Impedance of Thin Porous-Faced Liners", AIAA 77-1335, October, 1977.

36. Hersh, A. S. and Walker, B., "Effect of Grazing Flow on the Acoustic Impedance of Interacting Cavity-Backed Orifices", AIAA 77-1336, October, 1977.

37. Mattingly, G. E. and Davis, R. W., "Numerical Solutions for Laminar Orifice Flow", ASME, 77-WA/FE-13, November, 1977.

1978

38. Hersh, A. S., Walker, B., and Bucka, M., "Effect of Grazing Flow on the Acoustic Impedance of Helmholtz Resonators Consisting of Single and Clustered Orifices", AIAA 78-1124, July, 1978.

39. Hersh, A. S., and Walker, B., "Effects of Grazing Flow on the Steady-State Flow Resistance and Acoustic Impedance of Thin Porous-Faced Liners", NASA CR-2951, 1978.

1979

40. Howe, M. S., "On the Theory of Unsteady High Reynolds Number Flow Through a Circular Aperture", Proc. R. Soc. London, A. 366, 1979.

1980

41. Heidelberg, Laurence J., Rice, Edward J., and Homyak, Leonard, "Experimental Evaluation of a Spinning-Mode Acoustic-Treatment Design Concept for Aircraft Inlets", NASA Technical Paper 1613, 1980.

42. Howe, M. S., "The Influence of Vortex Shedding on the Diffraction of Sound by a Perforated Sheet", J. Fluid Mech., Vol 97, part 4, 1980.

43. Kompenhans, J., Ronneberger, D., "The Acoustic Impedance of Orifices in the Wall of a Flow Duct with a Laminar or Turbulent Flow Boundary Layer", AIAA 80-0990, June, 1980.

1981

44. Cummings, A., "High Amplitude Acoustic Power Losses in Perforated Materials", ASME, 81-WA/NCA-10, August, 1981.

45. Zandbergen, T., "On the Practical Use of Three-Microphone Technique for In-Situ Acoustic Impedance Measurements on Double Layer Flow Duct Liners", AIAA 81-2000, October 1981.

46. Kooi, J. W., and Sarin, S. L., "An Experimental Study of the Acoustic Impedance of Helmholtz Resonator Arrays Under a Turbulent Boundary Layer", AIAA 81-1998, October, 1981.

47. Rice, Edward J., "A Model for the Acoustic Impedance of Linear Suppressor Materials Bonded on Perforated Plate", NASA TM 82716, also AIAA 81-1999, October, 1981.

1982

48. Walker, B. E., Charwat, A. F., "Correlation of the Effects of Grazing Flow on the Impedance of Helmholtz Resonators", J. Acoustical Soc America, 72(2), August, 1982.

1983

49. Cummings, A. and Eversman, W., "High Amplitude Acoustic Transmission Through Duct Terminations: Theory", J. Sound and Vibration, 91(4), 1983.

50. Motsinger, R. E., "The Measurement of the Steady Flow Resistance of Porous Materials", AIAA-83-0779, April, 1983.

1984

51. Craggs, A., and Hildebrandt, J. G., "Effective Densities and Resistivities for Acoustic Propagation in Narrow Tubes", J. Sound and Vibration, 92(3), 1984.

52. Cummings, A., "Acoustic Nonlinearities and Power Losses at Orifices", AIAA Journal, Vol. 22, No. 6, June 1984.

53. Cummings, A., "Transient and Multiple Frequency Sound Transmission Through Perforated Plates at High Amplitude", AIAA 84-2311, October 1984.

1986

54. Craggs, A., and Hildebrandt, J. G., "The Normal Incidence Absorption Coefficient of a Matrix of Narrow Tubes with Constant Cross-Section", J. Sound and Vibration, 105(1), 1986

1987

55. Zandbergen, T., "Acoustic and Aerodynamic Characteristics of Perfolin, the Linear Perforated Plate Acoustic Liner", AIAA 87-2740, Oct, 1987.

1988

56. Botros, K. K., Jungowski, W. M., and Studzinski, W., "On the Transfer Matrix of Orifice Plate with Flow", Proceedings, Noise-Con 88, June 20-22, 1988.

1989

57. Innes, D. and Crighton, D. G., "On a Non-Linear Differential Equation Modelling Helmholtz Resonator Response", J. Sound and Vibration, 131(2), 1989.

58. Dowling, A. P. and Hughes, I. J., "Sound Absorption by Perforated Plates", Proceedings, Inter-Noise, December 4-6, 1989.

59. Ingard, Uno, Kirschner, Francis, Koch, John, Poldino, Michael, "Sound Absorption by Porous Flexible Materials", Proceedings, Inter-Noise, December 4-6, 1989.

1990

60. Hersh, A. S., "Nonlinear Behavior of Helmholtz Resonators", AIAA 90-4020, October 1990.

1991

61. Motsinger, R. E. and Kraft, R. E., "Design and Performance of Duct Acoustic Treatment", Chapter 14 in Hubbard, H. H., ed., Aeroacoustics of Flight Vehicles: Theory and Practice, Volume 2: Noise Control, NASA RP 1258, Vol. 2, August, 1991.

1993

62. Allard, J. F., Propagation of Sound in Porous Media: Modelling Sound Absorbing Materials, Elsevier Applied Science, 1993.

REPORT DOCUMENTATION PAGE

Public reporting burden for this collection of information is estimated to average 1 hour per response, including the time for reviewing instructions, searching existing data sources, gathering and maintaining the data needed, and completing and reviewing the collection of information. Send comments regarding this burden estimate or any other aspect of this collection of information, including suggestions for reducing this burden, to Washington Headquarters Services, Directorate for Information Operations and Reports, 1215 Jefferson Davis Highway, Suite 1204, Arlington, VA 22202-4302, and to the Office of Management and Budget, Paperwork Reduction Project (0704-0188), Washington, DC 20503.

1. AGENCY USE ONLY (Leave blank)	2. REPORT DATE April 1999	3. REPORT TYPE AND DATES COVERED Contractor Report

4. TITLE AND SUBTITLE
Acoustic Treatment Design Scaling Methods
Volume 2: Advanced Treatment Impedance Models for High Frequency Ranges

5. FUNDING NUMBERS
C-NAS3-26617
TA 25

6. AUTHOR(S)
R. E. Kraft, J. Yu, and H. W. Kwan

WU 538-03-12-02

7. PERFORMING ORGANIZATION NAME(S) AND ADDRESS(ES)
General Electric Aircraft Engines (GEAE)   Rohr, Inc.
P.O. Box 156301   Chula Vista, CA
Cincinnati, OH 45215-6301

8. PERFORMING ORGANIZATION REPORT NUMBER

9. SPONSORING/MONITORING AGENCY NAME(S) AND ADDRESS(ES)
National Aeronautics and Space Administration
Langley Research Center
Hampton, Virginia 23681-2199

10. SPONSORING/MONITORING AGENCY REPORT NUMBER
NASA/CR-1999-209120/VOL2

11. SUPPLEMENTARY NOTES
Lewis Project Manager: Christoper E. Hughes   J. Yu and H. W. Kwan: Rohr, Inc.
Langley Technical Monitors: Tony L. Parrott, Lorenzo R. Clark   R. E. Kraft: GEAE
Prepared for Langley Research Center under Contract NAS3-26617, Task 25.

12a. DISTRIBUTION/AVAILABILITY STATEMENT
Unclassified-Unlimited
Subject Category 71   Distribution: Standard
Availability: NASA CASI (301) 621-0390

12b. DISTRIBUTION CODE

13. ABSTRACT (Maximum 200 words)
The primary purpose of this study is to develop improved models for the acoustic impedance of treatment panels at high frequencies, for application to subscale treatment designs. Effects that cause significant deviation of the impedance from simple geometric scaling are examined in detail, an improved high-frequency impedance model is developed, and the improved model is correlated with high-frequency impedance measurements. Only single-degree-of-freedom honeycomb sandwich resonator panels with either perforated sheet or "linear" wiremesh faceplates are considered. The objective is to understand those effects that cause the simple single-degree-of-freedom resonator panels to deviate at the higher-scaled frequency from the impedance that would be obtained at the corresponding full-scale frequency. This will allow the subscale panel to be designed to achieve a specified impedance spectrum over at least a limited range of frequencies. An advanced impedance prediction model has been developed that accounts for some of the known effects at high frequency that have previously been ignored as a small source of error for full-scale frequency ranges.

14. SUBJECT TERMS
Aircraft noise; acoustic treatment; fan noise suppression; scale models; acoustic impedance

15. NUMBER OF PAGES
99

16. PRICE CODE
A05

17. SECURITY CLASSIFICATION OF REPORT	18. SECURITY CLASSIFICATION OF THIS PAGE	19. SECURITY CLASSIFICATION OF ABSTRACT	20. LIMITATION OF ABSTRACT
Unclassified	Unclassified	Unclassified	UL